From Source to Stream:

Measuring and Modelling Sediment Shape Evolution in Mountain Catchments

Alessandro Cattapan

FROM SOURCE TO STREAM: MEASURING AND MODELLING SEDIMENT SHAPE EVOLUTION IN MOUNTAIN CATCHMENTS

Alessandro Cattapan

FROM SOURCE TO STREAM: MEASURING AND MODELLING SEDIMENT SHAPE EVOLUTION IN MOUNTAIN CATCHMENTS

DISSERTATION

for the purpose of obtaining the degree of doctor
at Delft University of Technology
by the authority of the Rector Magnificus Prof.dr.ir. H. Bijl,
chair of the Board for Doctorates
and
in fulfilment of the requirement of the Vice Rector of IHE Delft
Institute for Water Education, Prof.dr. G.P.W. Jewitt,
to be defended in public on
Thursday, 30 April 2026 at 17:30 hours

by

Alessandro CATTAPAN

This dissertation has been approved by the (co)promotors.

Composition of the doctoral committee:

Rector Magnificus TU Delft	chairperson
Vice Rector IHE Delft	vice-chairperson
Prof.dr. M.E. McClain	TU Delft / IHE Delft, promotor
Prof.dr. M.J. Franca	Karlsruher Institut für Technologie, Germany, promotor
Dr. K. Katsanou	IHE Delft, copromotor
Independent members:	
Prof.dr.ir.W.S.J. Uijttewaal	TU Delft
Prof.dr. V. Ruiz-Villanueva	University of Bern, Switzerland
Prof.dr. C.V. Camporeale	Politecnico di Torino, Italy
Prof.dr. R.J. Batalla	Universidad de Lleida, Spain
Prof.dr.ir. J.A. Roelvink	TU Delft / IHE Delft, reserve member

This research was conducted under the auspices of the Graduate School for Socio-Economic and Natural Sciences of the Environment (SENSE)

Published by IHE Delft Institute for Water Education
www.un-ihe.org
ISBN 978-90-73445-82-6

To my father, Mario Cattapan.

ACKNOWLEDGEMENTS

This work is the result of a long journey, during which many things changed around and within me. While I am aware that this is just a symbolic moment and that the journey continues, I would like to take this opportunity to express my gratitude to a few people who made it possible.

I would like to start by simply saying “Thank you!” to my promotor, Mário Franca. His commitment to me as a person and to the work we were doing has been exemplary. Over the years, we spent hundreds of hours brainstorming about the problems tackled in this thesis, and I will forever cherish those memories. Our meetings used to start with personal life updates, and then descent into rabbit holes of stochastic sediment transport models, the mechanical properties of sediments and what controls them, averages of nonlinear transformations, optimisation algorithms and much more, and for me it was great. It was great to discuss with him because his open mind and his sensitivity made me feel free to express my ideas without fear of judgment, knowing that we were working together toward a common goal. Beyond providing essential scientific, methodological and formal input, Mário’s contribution to me as a person has also been essential: he was someone I could trust for his expert opinion, he believed in me and in my ideas; he did his best to push me to focus when I was dispersing my energy; he gave me a second, a third and an n^{th} chance when I became blocked along the way; and he remained consistently engaged even after moving to another university and another country. Overall, he supported me through the process, and I am deeply grateful for that. If today we are here, and hopefully tomorrow we will have a couple more papers published, it is because of Mário’s dedication to his work, his human qualities, and his moral strength.

The second person I would like to thank is my promotor, Michel McClain. When I started my PhD, the chair group I was part of did not have a full professor who could take on this role, and Michael gave me that opportunity. In our meetings, he often asked questions that made me reconsider assumptions or look at things from a different perspective. I truly admire his ability to combine different fields of expertise and address problems from an interdisciplinary perspective. During this long process, he remained attentive to my progress (or lack thereof), and when I was facing difficulties, he made sure to receive regular updates. Even though my rather informal and unstructured way might not always have been easy to deal with, I knew that I could always knock on his door with a quick question, a check, or an update, and that, if he was available, he would listen and do what he could to help.

I am writing these acknowledgements, looking at Konstantina's aquarium. It is a rare sunny Saturday in the Netherlands. People are outside shopping at weekly markets, enjoying the light, a few beers, and finger food. I am here because I have a thesis deadline approaching, and she invited me over to work from her place, knowing how overwhelming the last stretch had become and wanting to help as much as possible until the end. This small gesture already says more about her character than many words could. Over the years, I have realised that one of the things I like the most about life is that one should just listen to what people say: sooner or later, their nature reveals itself; it is almost unavoidable. "Facts matter more than words", "People need to feel that they belong", "We should, at least, treat people fairly"… these are just a few sentences that continuously come out of her mouth. But as I said, her actions say even more. When few people believed I could do it, not even myself, she saw the potential that I could not see. At one point, when the PhD seemed to be going nowhere, and I was contemplating giving up, I told her she should probably distance herself from the situation. She answered firmly that she was not willing to step down, and that if I chose to give up, I would also have to accept that I would be failing her. When I was sick, she brought me throat lozenges and something warm to eat. When I felt hopeless, there was always someone who was willing to listen. Kindness and care are no longer words for her, but actions. Now I will stop these somewhat tearful words because I could go on with countless memories and sentences, from "The only rule is ouzo!" to "Somehow these things speak to me!", which she said, referring to her skills fixing laptops, but I will try to be kind as well and keep the rest to myself. For your guidance as a co-promotor and for the person you have been throughout this journey, thank you, Konstantina.

I read Hervé's papers with fascination. His work on pebbles was among the first I encountered, and as I expanded my research, I realised the breadth of his work and his ability to look at rivers as systems with multiple dimensions (or, from an interdisciplinary perspective, as contemporary scientific vocabulary would prescribe). When I received his positive feedback on my PhD proposal, I was over the moon: it was clear that we shared a similar fascination for studying sediment shape to contribute to solving practical issues, not just for the sake of science. Later on, I went through long periods during which I did not contact him, mostly out of shame for my lack of progress. In the summer of 2025, I attended a summer school where he was among the guest speakers, and regardless of my long silence, he was still there, willing to look at my work and give me another chance. We spent a couple of hours discussing what I had done and the future steps in my research. We then submitted a paper together, which he went above and beyond to review in time, and I look forward to future scientific adventures together. Thank you, Hervé, for the chances you have given me and for your example.

I would also like to sincerely thank the following professors, who acted as independent members of my doctoral committee: Wim Uijttewaal, Virginia Ruiz-Villanueva, Carlo Camporeale, and Ramon Batalla. Their encouraging comments have been deeply appreciated, and their thoughtful suggestions showed attention to this work and helped improve the document in both structure and content.

I would like to thank Paolo Paron, who was my PhD supervisor when I started this journey. He introduced me to fieldwork, to the possibility of using drones for data collection, and to image processing. He was the person who introduced me at IHE and involved me in projects: thanks to him, I was able to travel to Mozambique and help build a hydrodynamic model of the Limpopo River. Although he was living in Africa, during one of his trips back to Europe, he joined me for fieldwork to help with the identification of outcrops. He showed his commitment through actions and did the best he could to contribute to this project.

Manuel Conedera is the geologist who first accompanied me to the Sarzana Stream to teach me how to recognise arenites and metabasalts. He did so out of genuine kindness and passion for those places. Thank you so much Manuel. Without your initial guidance, I would not have been able to move forward.

Among the many people who have been helping me towards the end of this journey, one who deserves acknowledgement is Anique Karsten. She went above and beyond her role to make sure that I was following the required procedures, but also supported me on a human level. Her kind presence and attention made me feel cared for. Thank you, Anique.

Jochen Wenninger is a hydrologist; our work has linkages, but he had no obligation to involve me in the work he was doing on surface water and groundwater interactions with Konstantina. Nonetheless, he gave me a chance, and this provided me with more exposure to fieldwork and other data collection techniques. More importantly, I experienced the feeling of working within a group where different expertise combines toward a shared objective. Even more importantly, he made me feel that he cared for me. When I had to perform salt dilution measurements, he helped prepare the equipment, provided manuals, and was always available for a last-minute phone call to check how much salt to use or to review my measurements. I am sure he did even more than I could see and checked on me when I was not aware of it. After those first experiences, Jochen was always attentive to me and to my PhD progress. In his role as head of the Water Resources and Ecosystems Department, he allowed me to take all my holiday leave to write my thesis and to attend courses. Similarly, I am also thankful to Graham Jewitt for his support and willingness to help while serving as Head of the department.

Raymond Venneker is the person with whom I went on my first mission, and some colleagues still tell me how lucky I was. Raymond is one of the funniest people I know, but his sense of humour hides sharp intelligence and a natural dislike for nonsense and charlatans. If one is lucky enough to take part in some of the after-work beers that turn into early weekend beers, one can appreciate the care he has for people, his attention to others' feelings, and his talent for blending with ease into any setting. He can attend with the same ease a meeting with ministries as well as a punk rock concert. Raymond showed me the example of someone who keeps working for an ideal, to improve the use of water resources in the Global South, even if the system is flawed, even if resources are not used optimally, and even if not everyone is well-intentioned. Unlike what people might think of him, he is an example of someone who looks at the full side of the glass and tries to add a little bit more, one precious drop at a time. You can also find his contribution in this thesis; his comments really helped to improve my earlier versions of the summary, and he has been so kind and patient in going through multiple reviews and finally translating it into Dutch. Thank you, Raymond!

Together with Konstantina, Jochen, and Raymond, we spend quite some time working on surface and groundwater interactions. We installed devices, collected data, shared good (rare) and bad (common, if not awful) weather, picked each other out of wetlands, and offered each other a warm hand when ours was too frozen to open a sampling bottle. We faced temporary defeats that taught us valuable lessons, such as remembering to bring all sets of cables to perform geophysics, or how to splice an optical fibre cable in cold conditions. We did all that because we worked as a team. We believed that where my limits would have appeared, someone else's strength would have shown up. We achieved something, but there are still fruits of our efforts waiting to ripen. Thank you all, guys, for the opportunity to live such experiences.

László Hayde is my hydraulic engineering buddy. During my University Teaching Qualification, he came to attend one of my classes. It was the first time I was teaching hydraulics at a master's level. Even if my lecture was full of mistakes in terms of educational strategy, László gave me kind and proactive suggestions. Later on, we worked together, coordinating and teaching a module on hydraulics and another on hydraulic structures. Seen from the outside, László might appear as a classical engineer, but if you have ever attended one of his classes, you would know one thing for certain: students adore him. Why? Because when he is teaching, he becomes another person. He is light on his feet; he moves and dances like water flowing down a morning glory spillway, or through a mountain stream. He engages with students, and hydraulics stops being a set of equations and becomes something alive, something to perceive with all senses. Plus, he is full of sayings that highlight concrete wisdom and common sense (such a rare quality nowadays); the Wienerschnitzel changing price while you are eating it is just brilliant!

Other moments when László showed what mattered to him were formal events, where it was clear to me that he had his priorities very well defined: his family is the most important thing, and, as in other topics, he lets his actions speak for themselves. Thank you, László!

Ken Irvine is my favourite person to debate with. We have spent an unreasonable amount of time discussing all sorts of topics, most of the time concluding that we agreed to disagree, so much so that the rare occasions when we do agree leave both of us surprised. Nonetheless, disagreeing with Ken is often more pleasurable than agreeing with most people, and now that he has become an emeritus professor, I realise that I miss the times we stayed after lunch a little longer just talking. When it comes to his work, Ken is extremely dedicated, and he expects people around him to show a similar devotion. When working with him, performance is not everything; intentions matter, and this is one of the things we agree on. But Ken is not just hardworking; above all, he is a sensitive and well-intended person. He has shown real care for me in many ways and offered his support, honest opinion, and feedback whenever I needed it. One day, I asked him to rate my communication skills. He replied, "No comment!", which was just another example of him speaking his mind while keeping his good manners. Thank you, Ken!

I would like to thank my colleagues from the former Hydraulic Engineering and River Basin Development chair group. Micha, with his messy desk but sharp focus on his work, who gave me so much of his time to answer my "stupid questions". Alessandra, who introduced me to river morphodynamics and to so many great people in this field. Francesco, who has been a great companion throughout these years; people can probably hear our laughs in the corridor. It is nice to see that our office has become a place where people come to have a chat, a coffee, and feel heard. Daniel Valero, who has been such an example and an inspiration while we worked together. Fredrik, who did his best to give me time to work on my PhD by taking on part of my teaching load. And finally, I would like to particularly thank Miroslav, because he embodies, in my opinion, the ideal career trajectory of an engineer who gained solid scientific and technical expertise, applied it in multiple projects around the world, and decided to share it with young students. He involved me in projects, we went on missions together, we developed short courses, mentored students, and contributed to modules. Over the years, I came to appreciate his ability to turn difficult situations into something positive, a skill that I am sure benefited him and his clients. More importantly, I witnessed his kindness and calm demeanour, which can quickly turn enthusiastic and funny in a group situation, especially in front of a beer.

I would also like to thank my students for their patience and kindness toward me and my limitations, and for all they taught me. I learn a great deal from their questions: having to clarify ideas has been an excellent exercise and an opportunity to see things from different perspectives.

This is particularly true for IHE students: coming from so many different backgrounds, they made me realise how sometimes my priorities were completely off, and what truly matters. Listening to their stories and understanding what studying in Europe meant for them made me realise the value of, and the responsibility we have toward, them. A full list of names would be excessive, and, knowing myself, I would certainly miss many who deserve to be mentioned. If you read this, know that you probably meant something to me, and thank you for the time we spent together. I look forward to possibly working together again in the future.

There have been a lot of people with whom I shared moments through this long journey. They are listed here in alphabetical order, with many important names surely missing, but you know me by now: if we shared any part of it, then you have a place in this list and in my heart. Thank you Abhishek, Adele, Alessandro, Alessandro, Alessio, Alex, Amani, Andrea, Andres, Anna, Berend, Carlo, Chiara, Claudia, Daniel, Débora, Elisa, Fabio, Filippo, Francesco, Giulia, Hamid, Ilaria, Irene, Jessica, Laddaporn, Lisa, Marco, Margherita, Marta, Matteo, Maurizio, Samantha, Sandro, Sara, Sofia, Stefan, Thaine, and Yared.

I would like to deeply thank Lucia Marziano. She has been by my side for a significant part of my PhD journey, supporting me and contributing in many ways: she did not let me stop working when I was frustrated, she believed in me, she joined me in parts of the fieldwork, and the vast majority of the sediment images used in this work were taken with her camera. Lucia, thank you so much for everything.

Dear childhood friends, I know that you are scanning this document searching for your names. You will probably find them here, not because you are less important, but because I tried (probably failing) not to involve or burden you too much with my PhD over the years. Nonetheless, I know that you cared for me and were probably waiting for this moment for a long time. The other day, I realised that during my PhD I faced the loss of a parent, an important breakup, job insecurity, and a pandemic… I really hope I will not have to add a war to this list. Thank you, Alberto and Laura, Davide and Alessia, Marco and Laura, and Marco and Elvira, for being there with me through all of these, and for all the memories.

And finally, I owe my deepest gratitude to my family: my mother Delfina, my brother Matteo, and his partner Stefania, who have supported me throughout my life with patience and care. And finally, finally, thanks to my nephews Leonardo and Niccoló, who are a constant source of joy and discovery, and the main reason I find myself flying back to Italy so often these days.

SUMMARY

If one is lucky enough to have the opportunity to follow a river from the source to the sea, one could witness its sediments changing in size and shape.

The objective of this work is motivated by a somewhat naïve, almost childish, question: *"Is it possible to pick up a stone from a river and determine, just by measuring its shape, how far it has travelled?"* Being able to answer this question reliably and accurately would create valuable opportunities to improve our understanding of river systems, to enhance restoration practices, infrastructure planning, and management, and to reduce natural hazards. Accurately identifying sediment pathways based on an easily measurable property would, for example, allow us to select which reaches in a network should be left free to flow, since they convey most of the sediments, or which should be more protected from erosion, since they represent major sediment sources.

This research provides three contributions to this overarching objective.

The first contribution concerns the measurement of sediment shape in the field. This is often done by analysing images that are collected, placing the sediments sampled on a contrasting background with their maximum projected area facing upwards. Field conditions do not, however, allow control of the lighting, and shadows are often present. In such conditions, the segmentation of individual pebbles is challenging using existing automatic tools. Machine learning tools are available, but, to the best of our knowledge, they still require the operator to manually refine the segmentation, making the process operator-dependent. In this respect, an alternative fully automated method for pebble segmentation was developed, which makes the data collection operation repeatable, even in field lighting conditions, including shadows. The proposed algorithm allowed the accurate segmentation of around 91% of the sampled particles, which had a minimum intermediate dimension of 12 mm. Two models were used to estimate the shape parameters of the obtained 2D outlines. The results show that the impact of such models on the overall error of shape estimates is comparable to that of the segmentation method proposed, confirming its applicability to real datasets.

The second contribution involves the collection of shape data of sediments originating from two tracer lithologies (arenites and metabasalts), starting from their respective outcrops and progressing downstream along a small Alpine stream in Northeast Italy. A conceptual, physically based model was developed and applied to describe sediment circularity as a function of the distance from the outcrop, resulting in Mean Absolute Percentage Errors (MAPE) of 0.34% and 0.64% for arenites and metabasalts, respectively. Moreover, the analysis of the shape of fragments produced by the outcrops suggests that the shape is a lithology-specific property, which can be considered constant among outcrops with similar weathering mechanisms.

Additionally, field data support the hypothesis that the shape of a sediment depends not only on the distance travelled but also on its initial shape. Finally, the model was also applied to describe the average circularity of pebbles from multiple arenite outcrops along the stream, with a Root Mean Square Error of 0.017. The results suggest that the relative contribution of a source decreases as its distance from the measuring location increases. This effect can be explained by the diffusion of bedload particles and can be successfully modelled with an exponential distribution.

The third contribution concerns the estimation of the distance travelled by sediment. The proposed deterministic model for sediment circularity as a function of travel distance was inverted to assess the accuracy and precision of shape-derived estimates of average travel distance. The results show that the accuracy of such estimates varies depending on the lithology, with softer lithologies (e.g. arenites) producing more accurate results (MAPE 31%), albeit for the shorter distances. The opposite happens for harder lithologies (e.g. metabasalts, MAPE 63.5%). The precision of the estimates, measured by the coefficient of variation of travel distances, was equal to 2.4 and 4.3 for arenites and metabasalts, respectively, also suggesting that softer lithologies are likely to provide more precise results. Since the data suggest that the shape of a particle depends on both travel distance and initial shape, an approach was developed in which the estimated travel distance probability is based on the fragment shape probability. The proposed approach is cast in a Bayesian framework that requires the definition of a prior probability of travel distances. Through choosing different priors, if uncorrelated with sediment shape, it is possible to include additional information, such as the position of the outcrops for the lithology of interest.

Several opportunities for further research are possible within this general theme. In terms of data collection, the combination of technologies like Unmanned Aerial Vehicles (UAVs) and Radio Frequency Identification tags (RFID) could allow the collection of significantly larger datasets in a shorter time compared to manual sampling methods. Moreover, recent developments in point-cloud segmentation and object identification could allow the characterisation of the 3D shape of sediment particles, providing more detailed information on their shape and with the potential of improving our understanding of different forms of attrition.

With respect to the physics of attrition, a series of questions remains. Although recent studies identified the governing parameter relating the energy of particle impacts to the amount of mass lost during the impact, the coefficient describing the type of impact remains uncertain. In terms of the relationship between the mass lost due to attrition and the change of shape of particles, the dependency on the initial shape found in our field data has not been tested in laboratory experiments yet. Moreover, the effect of mechanical sediment properties on the relationship between shape and mass loss has not yet been quantified.

Finally, multiple authors suggest that the transport of bedload particles is characterised by dispersion, partly attributed to the fat-tailed distributions of resting times. Since the estimation of travel distances using the shape of sediments from multiple sources requires knowledge of the relative source contributions, further research on sediment dispersion is needed to improve the accuracy of the travel distance inference.

Overall, this research has both scientific and societal relevance. With respect to the former, it contributes to better measuring and understanding sediment attrition in mountain catchments, providing a relatively simple and novel model for use in both laboratory and field studies on sediment attrition. Moreover, it provides for the first time estimates of the accuracy and precision of travel distance based on particle morphometry, and it describes two possible setups for future field campaigns using sediment shape as a tracing property. With respect to the societal relevance of this research, accurate estimations of sediment travel distance provide information on sediment fluxes and contribute to evidence-based decision-making. Examples of applications that could benefit from a better and simpler estimation of sediment sources and fluxes are: the calibration and validation of sediment connectivity models, the geomorphological mapping of erosion-transport-accumulation zones, the prioritisation of land conservation efforts, and the assessment of impacts of infrastructure development.

SAMENVATTING

Wie de mooie gelegenheid heeft om een rivier van de bron tot aan de zee te volgen, zou observeren dat de samenstelling van het rivier sediment verandert in grootte en vorm.

Het doel van deze studie is ingegeven door een op het eerste gezicht eenvoudige vraag: “Is het mogelijk een steen uit een rivier op te pakken en door het simpelweg meten van de vorm te bepalen van hoe ver deze gekomen is?” Indien men deze vraag betrouwbaar en accuraat zou kunnen beantwoorden zou dit waardevolle mogelijkheden bieden om ons begrip van riviersystemen te verdiepen, de rivierherstel praktijk, infrastructuur plannen en rivierbeheer te verbeteren, en de natuurlijke gevaren te weerstaan. Nauwkeurige identificatie van sediment trajecten op basis van een gemakkelijk meetbare eigenschap zou het bijvoorbeeld mogelijk maken om te bepalen welke takken in een rivier netwerk vrij gelaten kunnen worden om het sediment verder te transporteren en welke takken verdere bescherming tegen erosie behoeven omdat deze de grootste sedimentbronnen zijn.

Deze studie bevat drie bijdragen aan dit algehele doel.

De eerste bijdrage betreft de veldmetingen van de vorm van het sediment. Dit gebeurt vaak middels analyse van fotobeelden welke gemaakt zijn tegen een contrasterende achtergrond en waarbij het materiaal met de grootste geprojecteerde oppervlakte naar het beeld wijst. Echter, veldcondities laten geen controle over de belichting toe en daarom zijn er vaak schaduwen aanwezig. Segmentatie van de individuele stenen onder deze omstandigheden is uitdagend voor bestaande automatische hulpmiddelen. Zelflerende hulpmiddelen bestaan hiervoor, maar voor zover bekend zijn deze nog steeds afhankelijk van de gebruikers om de segmentatie handmatig bij te sturen. Hiertoe is een volledig automatische kiezel segmentatie methode ontwikkeld, welke het verzamelen van data onder belichtings- en schaduw condities in het veld herhaalbaar maakt. Het voorgestelde model voorzag in een accurate segmentatie van 91% van de verzamelde bestanddelen, met een minimum intermediaire dimensie van 12 mm. Twee modellen zijn gebruikt voor schattingen van vorm parameters uit de verkregen tweedimensionale contouren. De resultaten laten tevens zien dat het effect van dergelijke modellen op de algehele fout in de vormbepalingen vergelijkbaar is met die in de hier voorgestelde segmentatie methode, hetgeen de toepasbaarheid hiervan op werkelijke dataverzamelingen bevestigd.

De tweede bijdrage omvat het verzamelen van sedimentvorm gegevens uit twee traceer lithologiën (arenieten en meta-basalten), beginnende bij hun respectievelijke ontsluitingen en vervolgens stroomafwaarts langs een kleine Alpine bergstroom in noordoost Italië. Een conceptueel, fysisch gebaseerd model werd ontwikkeld en toegepast om de circulariteit van het sediment materiaal als functie van de afstand tot de ontsluiting te beschrijven, resulterend in gemiddelde absolute foutpercentages (GAF) van respectievelijk 0,34% en 0,64% voor de arenieten en de meta-basalten.

Tevens suggereert analyse van de fragmenten uit de ontsluitingen dat de vorm een lithologie-specifieke eigenschap is welke gezien kan worden als constante voor ontsluitingen met soortgelijke verwerings-mechanismen. Daarboven ondersteunen de veldgegevens de hypothese dat de vorm van het sediment niet alleen afhangt van de afgelegde afstand maar ook van de initiële vorm. Tenslotte werd het model ook toegepast om de gemiddelde circulariteit van kiezels afkomstig uit meerdere areniet ontsluitingen langs de stroom te beschrijven, met een wortelgemiddelde kwadraatfout van 0,017. De resultaten suggereren dat de relatieve bijdrage van een sedimentbron afneemt als de afstand naar de meetlocatie toeneemt. Dit effect kan verklaart worden uit de diffusie van bedding materiaal en kan met succes door een exponentiële verdeling worden gemodelleerd.

De derde bijdrage betreft de schatting van de door het sediment afgelegde afstand. Het voorgestelde deterministische model van de circulariteit als functie van de afgelegde afstand werd hiervoor geïnverteerd ten einde de nauwkeurigheid en de precisie van de gemiddelde op de vorm gebaseerde afstand schattingen te beoordelen. De resultaten laten zien dat de nauwkeurigheid van deze schattingen varieert met de lithologie, waarbij de resultaten voor ‘zachtere’ gesteenten (bijv. arenieten) nauwkeuriger zijn (GAF 31%), althans voor de kortere afstanden. Het tegenovergestelde is het geval voor ‘hardere’ gesteenten (bijv. meta-basalten, GAF 63,5%). De precisie van de schattingen, gemeten als de variatiecoëfficiënt van de afgelegde afstanden, was gelijk aan 2,4 voor de arenieten en 4,3 voor de meta-basalten, hetgeen ook suggereert dat de resultaten preciezer zijn voor ‘zachtere’ gesteenten. Omdat de gegevens suggereren dat de sedimentvorm zowel van de afstand als de initiële vorm afhangt, is een benadering ontwikkeld waarbij de waarschijnlijkheid van de afstand wordt geschat uit de waarschijnlijkheid van de vorm. De hier voorgestelde benadering is een Bayesiaans raamwerk welke de bepaling van een a priori waarschijnlijkheid van de afgelegde afstand nodig heeft. Door verscheidene priors te kiezen welke niet gecorreleerd zijn met de vorm is het mogelijk additionele informatie toe te voegen, zoals de positie van de ontsluitingen voor de betreffende lithologie.

In het kader van het hier algemene thema zijn er verscheidene mogelijkheden voor verder onderzoek. De combinatie van technieken zoals onbemande luchtvaartuigen (unmanned aerial vehicles, UAVs) en radio frequency identification (RFID) tags zouden het mogelijk kunnen maken om significant meer gegevens te verzamelen in kortere tijd ten opzichte van handmatige data verzameltechnieken. Daarnaast kunnen recente ontwikkelingen in puntenwolk segmentatie en object identificatie de driedimensionale vormbeschrijving mogelijk maken welke meer gedetailleerde informatie omtrent de vorm zal geven, wat dan zou kunnen leiden tot beter begrip van de verschillende soorten erosie tijdens transport.

Er resten een aantal vragen met betrekking tot de fysica van transport erosie. Alhoewel recente studies de parameter welke de impact energie relateert aan het verlies van massa tijdens impact hebben geïdentificeerd, blijft de coëfficiënt welke het impact type beschrijft onzeker. Met betrekking tot de relatie tussen massaverlies tijdens transport erosie en vormverandering, is de afhankelijkheid van de initiële vorm blijkend uit de veldgegevens vooralsnog niet getest in laboratorium experimenten. Bovendien is het effect van de mechanische sediment eigenschappen op de relatie tussen vorm en massaverlies vooralsnog niet gekwantificeerd.

Tot slot wordt door meerdere onderzoekers gesuggereerd dat het transport van bedding materiaal wordt gekarakteriseerd door dispersie, hetgeen gedeeltelijk toegeschreven wordt aan de breed uitlopende verdelingen van de rust-tijden. Omdat schatting van de afgelegde afstanden uit de vorm van sedimenten afkomstig uit meerdere bronnen kennis vereist van de relatieve bijdragen uit deze bronnen, is verder onderzoek naar sediment dispersie nodig om de nauwkeurigheid van de afgelegde afstand inferenties te verbeteren.

Dit onderzoek heeft in het algemeen zowel wetenschappelijke als maatschappelijke relevantie. Met betrekking tot het eerste draagt het bij aan beter meten en begrijpen van sediment transport erosie in gebergte- stroomgebieden, waarbij het voorziet in een relatief eenvoudig, nieuw model voor laboratorium- en veld- studies van transport erosie. Daarnaast bevat het voor het eerst schattingen van de nauwkeurigheid en precisie van op morfometrie gebaseerde afgelegde afstandsbepalingen van sediment bestanddelen, en worden twee opzetten beschreven voor toekomstige veldcampagnes welke gebruik maken van sediment vorm als traceer eigenschap. Met betrekking tot de maatschappelijke relevantie voorzien nauwkeurige schattingen van de afgelegde weg van sediment informatie over sediment fluxen en leveren een bijdrage aan bewijs- gebaseerde besluitvorming. Voorbeelden van toepassingen welke kunnen profiteren van betere en eenvoudigere schattingen van sediment- bronnen en fluxen zijn calibratie en validatie van sedimentconnectiviteits- modellen, geomorfologische kartering van erosie-transport-accumulatie zones, prioritering van landconservatie- inspanningen en het beoordelen van de impact van infrastructuur ontwikkelingen.

CONTENTS

1

INTRODUCTION

This chapter provides the theoretical and practical background of this work, a description of the methodology applied, and the main results. Moreover, it provides an outline of the whole research work.

1.1 Background and Context

Rivers are complex systems whose behaviour results from interactions among physical (water, rocks, sediments, and soils), biological (flora and fauna), and anthropic (infrastructures) factors (Rhoads, 2016; Tarolli and Sofia, 2016; Atkinson et al., 2017). Changes in any of these factors can potentially affect the services rivers provide to humans and ecosystems (Bregoli et al., 2019; Beveridge et al., 2020; Scorpio and Piégay, 2020). Despite this complexity, and even without a full understanding of these interactions, humans have made use of rivers for millennia (Viollet, 2017).

For example, the oldest known dam, built on the Wadi Rajil, Jordan, in the IV^{th} millennium BC, controlled winter floods, the main source of water available in that arid region. It had a height of around 4.5 m and a length of 80 m and was part of a complex system of canals and reservoirs that supplied water to Jawa, a city of 2000 and 3000 inhabitants at the time. Yet, interventions based on limited or flawed knowledge have sometimes had unintended negative effects. The Sunsari-Morang Irrigation Project (SMIP) in Nepal diverts water from the Koshi River to irrigate an area of about 68,000 ha. Construction of the system began in 1977 and was completed in 1985. In 2015, bridge construction approximately 100 m upstream of the SMIP intake left a cofferdam partially in place, worsening sediment deposition patterns in front of the intake (Shrestha et al., 2020) and reducing water supply to agricultural fields that support crops for thousands of people. This case illustrates how a seemingly minor oversight in a local intervention can cause impacts kilometres downstream.

Even when potential risks are known or can be forecasted by theoretical knowledge, projects have proceeded to strengthen control over key resources (Janku, 2016; Pacific Institute, 2024). For example, the Mekong Delta in Vietnam, home to approximately 18 million people, maintains its elevation relative to sea level through sediment deposition and accumulation of organic matter. It is well established that dams reduce downstream sediment loads, yet a series of dams have been built or are planned in the Mekong system, drastically reducing sediment delivery to the delta (Schmitt et al., 2019). Combined with ongoing subsidence and sea level rise, this significantly increases flood risk and exacerbates saltwater intrusion and riverbank erosion (Binh et al., 2021; Chong et al., 2021; Nguyen et al., 2021).

Because of the network-like structure of fluvial systems, local interventions such as dams or diversions can have catchment-wide effects. Nevertheless, development requires investment, infrastructure development, and resource management, all of which involve trade-offs between stakeholders (McClain et al., 2013; Wheeler et al., 2018; Shrestha et al., 2022). Quantitatively assessing the small- and large-scale impacts of different solutions (Tangi et al., 2023) supports informed decision-making and provides a shared basis for negotiations.

In striving to assess cause-and-effect relationships between interventions and consequences, remarkable improvements have been made in modelling the liquid phase. Significant advances have also been achieved in modelling sediment transport and its effects on river morphology, although the accuracy of such estimates remains comparatively limited (Recking, 2010). Like other Earth-surface processes, sediment transport is characterised by nonlinear responses to external forcings and by the presence of intrinsic thresholds (Schumm, 1979; Phillips, 2006; Recking, 2013).

The process is nonlinear because the specific sediment flux (q_s), defined as the mass of sediment passing through a river cross-section per unit time and per unit width, can be approximated by a power law relationship with the specific water discharge, q, with an exponent greater than 2. Moreover, as water flux can only entrain particles below a certain size, sediment transport is also governed by a threshold for motion. This threshold is determined by near-instantaneous flow velocities that occur close to the riverbed, where velocity variability is greatest within the water column (Feehan et al., 2023).

In addition, riverbeds are rarely flat and are typically characterised by bedforms that further influence local flow conditions and the threshold for motion (Dhont and Ancey, 2018). As a result, sediment transport rates exhibit strong spatial and temporal variability, making consistent and accurate monitoring extremely challenging.

Given the complexity of the sediment transport process, particle-scale modelling is not feasible. Upscaling methods are therefore applied depending on the simulation's scale and purpose. For whole river networks, simplified approaches have been developed to assess the impacts of alternative scenarios, such as changes in sediment inputs or infrastructure development, on sediment fluxes (Czuba, 2018; Czuba and Foufoula-Georgiou, 2014; Schmitt et al., 2017, 2018a). These network-based frameworks quantify the contribution of a river reach, i, to the sediment flux passing at a downstream reach, j. This metric is used to estimate the "connectivity" between the reaches i and j. Models that allow this type of analysis are therefore referred to as connectivity models. In addition, these models enable the comparison of a pre-intervention scenario with alternative scenarios in which infrastructure is developed on different river reaches. The CASCADE model (Schmitt et al., 2016), and its most recent dynamic version, the D-CASCADE model (Tangi, 2023), are examples of such models.

In these frameworks, the river network is subdivided into a series of reaches, defined as sections of the river that can be assumed to share common attributes (e.g., width, depth, slope, roughness, active layer thickness, etc.). For each reach, a time series of discharge values is also required. Because precise quantification of sediment inputs, in terms of both volumes and grain-size distributions, remains an open question in the scientific literature (Sklar et al., 2016), these inputs are often estimated a posteriori (Tangi et al., 2023).

The outputs of these models include estimates of the relative contribution of each upstream reach to the sediment flux at a downstream location, as well as the provenance of the riverbed material. Validation is typically carried out by comparing simulated sediment fluxes with measurements. These models represent a major advance compared with what was possible only a decade ago and now provide opportunities to compare, at least qualitatively, different management solutions or scenarios.

Nonetheless, their calibration and validation remain limiting factors for quantitative acceptance. Although their central aim is to reproduce connectivity between reaches, calibration and validation are generally performed using sediment fluxes. However, multiple connectivity patterns can produce the same flux, a principle known in systems theory as equifinality (Nicholas and Quine, 2010; van Westen et al., 2025).

Calibrating connectivity models with connectivity metrics requires characterising sediment fluxes or bed material by source. Since the late 1970s, fingerprinting techniques have advanced considerably (Walling, 2013) using a multitude of physical and chemical properties, cosmogenic and fallout radionuclides, and stable isotopes. These have focused mostly on fine sediments and on source types, e.g., channel erosion, gully erosion, sheet or rill erosion, rather than on their spatial organisation. Although useful for initial screening of sources, no property currently allows tracing individual sediment particles back to their transport history. Ideally, such a property would reveal either provenance or travel distance. If available, it could be used to calibrate and validate connectivity models and help predict intervention impacts across scales.

This thesis contributes to the overarching scientific question of assessing whether sediment shape can be such a property.

1.2 MOTIVATION

This research is driven by scientific questions, which, in turn, may enable practical applications. The latter were outlined in the previous chapter, while the theoretical background underpinning the scientific questions is presented below.

Humans have long been fascinated by the shape of pebbles. To the best of the author's knowledge, the earliest theory attempting to explain why pebbles become rounder as they move downstream can be traced back to Aristotle (Ross, 1913). He suggested that points located further from the centre of mass of a pebble rotate more rapidly and are therefore subject to greater attrition. Although intriguing, this explanation, now termed distance-driven flow, is not consistent with observations. A different explanation, more recently developed, shows stronger agreement with empirical evidence. According to this theory, the rate at which a pebble's surface shrinks inward is proportional to its local curvature (Domokos and Gibbons, 2018; Pál et al., 2021). Thus, sharp edges and corners wear down

more quickly than flatter faces or areas of lower curvature. This alternative explanation is known as curvature-driven flow.

To apply such a theory to explain the rounding of river sediments, a metric for quantifying shape is required. Over the years, many shape parameters have been suggested in the scientific literature (Wadell, 1932; Barrett, 1980; Domokos et al., 2014). Their adoption in field studies depends, in part, on the ease with which they can be measured under real field conditions. A commonly used parameter in recent studies is the isoperimetric ratio, $IR = \frac{4\pi A}{P^2}$, (Pokhrel et al., 2024; Takahashi et al., 2025b), which can be calculated from a pebble's outline as a function of its area, A, and perimeter, P. This parameter measures how close a shape is to a perfect circle and can be estimated simply from images. Under curvature-driven flow, the isoperimetric ratio is expected to increase monotonically with the mass lost through attrition (Novák-Szabó et al., 2018). In other words, as a particle continues to lose mass, its isoperimetric ratio should steadily increase. To use the isoperimetric ratio as a proxy for travel distance, the latter must therefore be linked to the amount of mass lost through attrition. Theoretical arguments and results from discrete element models suggest that particle mass decreases exponentially with distance travelled along a river (Litwin Miller et al., 2014; Pál et al., 2021).

Nonetheless, as previously mentioned, sediment transport is a complex phenomenon due to the presence of thresholds, nonlinearities, and feedback mechanisms, which can affect the accuracy of estimates based on mean-field approaches. Establishing a mechanistic link between mass loss and travel distance requires a level of detail in the description of sediment transport that is currently unavailable. In particular, the threshold for motion of bedload particles has historically been considered dependent on sediment size, with higher shear stresses needed to entrain larger particles (Shields, 1936; Einstein, 1950; Ancey et al., 2008; Lamb et al., 2008; Houssais et al., 2015). Nonetheless, recent studies have started to recognise the importance of particle shape and density on the threshold for motion (Lane and Carlson, 1954; Schmidt and Ergenzinger, 1992; Cassel et al., 2021). This implies that the threshold for motion of a particle can vary, as it undergoes attrition.

The amount of mass lost by a particle to cover a certain length depends, in the most general case, on its impacts on the riverbed ("in motion" state) and on the impacts it receives from moving particles, while resting ("in place" state). The amount of mass lost in each impact depends on the kinetic energy of the moving particle and on the mechanical properties of the moving and the impacted particle (Sipos et al., 2020; Bodek and Jerolmack, 2021; Litwin Miller and Jerolmack, 2021; Bray et al., 2024). For a given river reach, the frequency of "in motion" states of particles depends on their size, shape, and density, but the former two vary over time and space due to attrition. This means that the estimation of the amount of mass lost by a particle to cover a certain distance can, in the general case, depend on the properties (size, shape, density) of the bulk of particles, which can all vary in time and space.

Modelling all these interactions for a real stream is not feasible due to epistemic and computational limits. For this reason, this work adopts a different approach: it investigates whether it is possible to establish a relationship between the shape of an ensemble of particles and their travel distance, instead of establishing a mechanistic relationship between mass lost by a particle and its travel distance.

As previously mentioned, recent findings raise the possibility of using the isoperimetric ratio as an indicator of sediment travel distance. However, several open questions and practical challenges remain, and this thesis aims to contribute towards addressing them.

1.3 Research Gaps and Novelty

While considerable progress has been made in understanding sediment transport, major gaps remain in tracing the origin and transport history of coarse sediments in mountainous rivers. A variety of techniques have been tested in the literature (Williamson et al., 2014) and multiple sediment properties can be used in conjunction to estimate their age and source type (e.g., surface vs. subsurface, forested vs. agricultural). Such properties can include colour, size, texture, mineralogical and geochemical properties, etc (Collins et al., 2017). Nonetheless, existing fingerprinting techniques are largely restricted to fine sediments (Chapkanski et al., 2020), and source areas are commonly distinguished by erosion type rather than their spatial configuration. As a result, there is currently no established property of sediment particles that allows reliable inference of their transport distance or history.

This gap is particularly critical in mountain and piedmont rivers, where the complex geological and geomorphological setting produces a highly heterogeneous spatial distribution of sediment sources. In such environments, conventional fingerprinting methods struggle to provide meaningful constraints, and sediment connectivity models remain difficult to calibrate and validate due to equifinality. The absence of a transport-related fingerprinting property, therefore, limits both scientific understanding and the practical application of sediment connectivity models in river basin management.

The novelty of this thesis lies in addressing this gap by investigating whether sediment shape can serve as such a property. Specifically, this work introduces:

- A new image segmentation method that enables the reproducible measurement of pebble shape under field conditions, without controlled lighting.
- The use of lithology-specific outcrops as natural tracers, allowing the distinction between inherent lithological variability and the effects of downstream attrition.
- Application and inversion of a mechanistic model for sediment circularity, providing, for the first time, estimates of sediment travel distance from shape data.

- A Bayesian framework to update prior estimates of sediment travel distance distributions using field-based shape measurements.

Together, these contributions provide both methodological advances and conceptual insights. They demonstrate the feasibility of using sediment shape as a proxy for transport distance, and open new avenues for calibrating and validating sediment connectivity models at the catchment scale.

1.4 Research Questions

The overarching objective of this work is to improve our understanding of sediment attrition in mountain catchments. Within this general objective, three specific objectives were defined:

1. Develop a method to collect reliable sediment shape data in the field.
2. Develop a model to estimate sediment shape as a function of their travel distance.
3. Propose a methodology to estimate sediment travel distance based on their shape and assess the accuracy of such estimates.

The work, therefore, comprises three contributions, reflecting the three specific objectives. Each contribution addresses a specific set of research questions.

With respect to the measurement of pebble shape in the field:

4. How can repeatable measurements of pebble shape be obtained from field images when lighting conditions cannot be controlled?
5. What is the relative importance of the segmentation method and the shape characterisation algorithm in the accuracy of estimates of sediment shape from field-collected images?

With respect to the estimation of sediment shape as a function of travel distance:

1. How can the spatial evolution of sediment shape in mountainous streams be modelled, starting from a localised point source?
2. What is the relative importance of the parameters associated with rounding rates and the spatial scaling of mass loss in controlling the rate of shape evolution?
3. How can the contributions of multiple sediment sources be incorporated when modelling shape evolution in mountainous streams?
4. Do outcrops exhibit lithology-specific shape properties?

With respect to the estimation of sediment travel distance based on shape:

1. What is the accuracy and precision of travel distance estimates derived from sediment shape?
2. How can sediment shape be used to update prior estimates of the probability distribution of sediment travel distances?

Each chapter addresses the corresponding research questions, while a comprehensive discussion of all findings is presented in the concluding chapter.

1.5 METHODOLOGY

The main objective of this work is to assess the extent to which sediment shape can be used to infer travel distance, the expected accuracy and precision of such estimates, and the factors that influence them. As mentioned in section 1.2, the achievement of such an objective requires overcoming a series of practical and theoretical challenges, which were detailed in the research questions. This section describes the methodological approach used to answer them. The overall methodology is summarised in Figure 1.2.

This work uses a field data-based approach: a catchment was selected where specific lithologies could be employed as tracers. The shapes of sediments from the tracer lithologies were obtained through image analysis.

The first practical challenge concerns the measurement of sediment shape in the field. While sediment size can be accurately measured from unmanned aerial vehicle (UAVs) imagery (Carbonneau et al., 2004; Woodget and Austrums, 2017; Cattapan et al., 2018; Chen et al., 2022), shape measurements require higher resolution and are strongly affected by imbrication, overlap, and partial exposure due to vegetation (Steer et al., 2022). A more controlled setting is therefore usually needed to obtain accurate estimates of sediment shape. Optical and laser scanning techniques can achieve high accuracy (Hodge et al., 2009; Tunwal and Lim, 2023), but they are typically expensive, time-consuming, and logistically demanding, particularly when applied to large sample sizes in a laboratory. Field measurements, in contrast, allow relatively quick analysis of larger numbers of samples, but uncontrolled conditions, such as variable lighting and shadows, may affect shape estimates. The first contribution of this work is therefore the development of a method for segmenting pebble images collected in the field, enabling reproducible shape measurements even under light shadow conditions.

This segmentation method was applied to collect sediment shape data in a 25 km² Alpine catchment, the Sarzana Stream, in Italy (Figure 1.1). The two lithologies used as tracers are arenites and metabasalts, as their outcrops occupy a limited part of the catchment area.

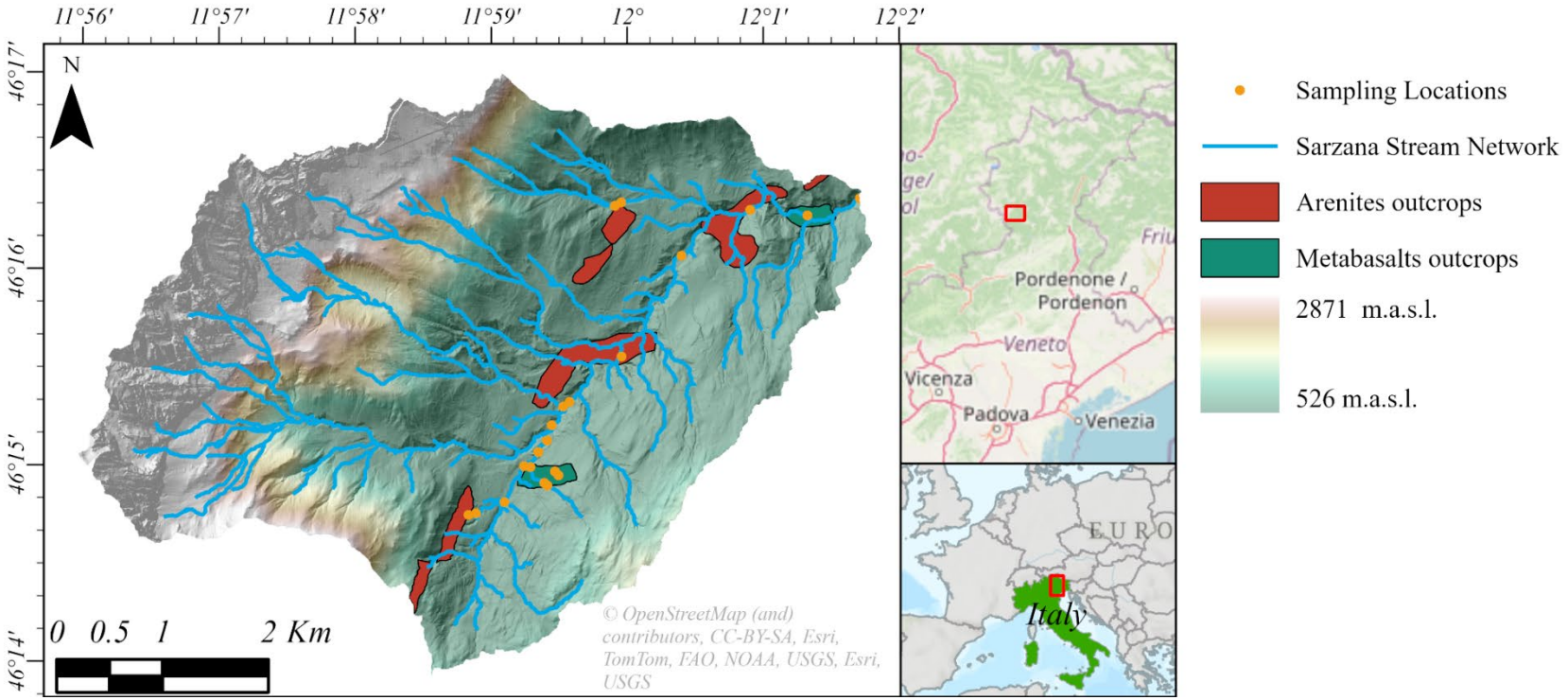

Figure 1.1. Map of the Sarzana Stream, extent of arenites and metabasalts outcrops, and sampling locations.

This data made it possible to test a new physically based model linking sediment shape to travel distance, in agreement with the theoretical frameworks described in section 1.2. In addition, the dataset provided insights into the shape properties of fragments produced directly at outcrops.

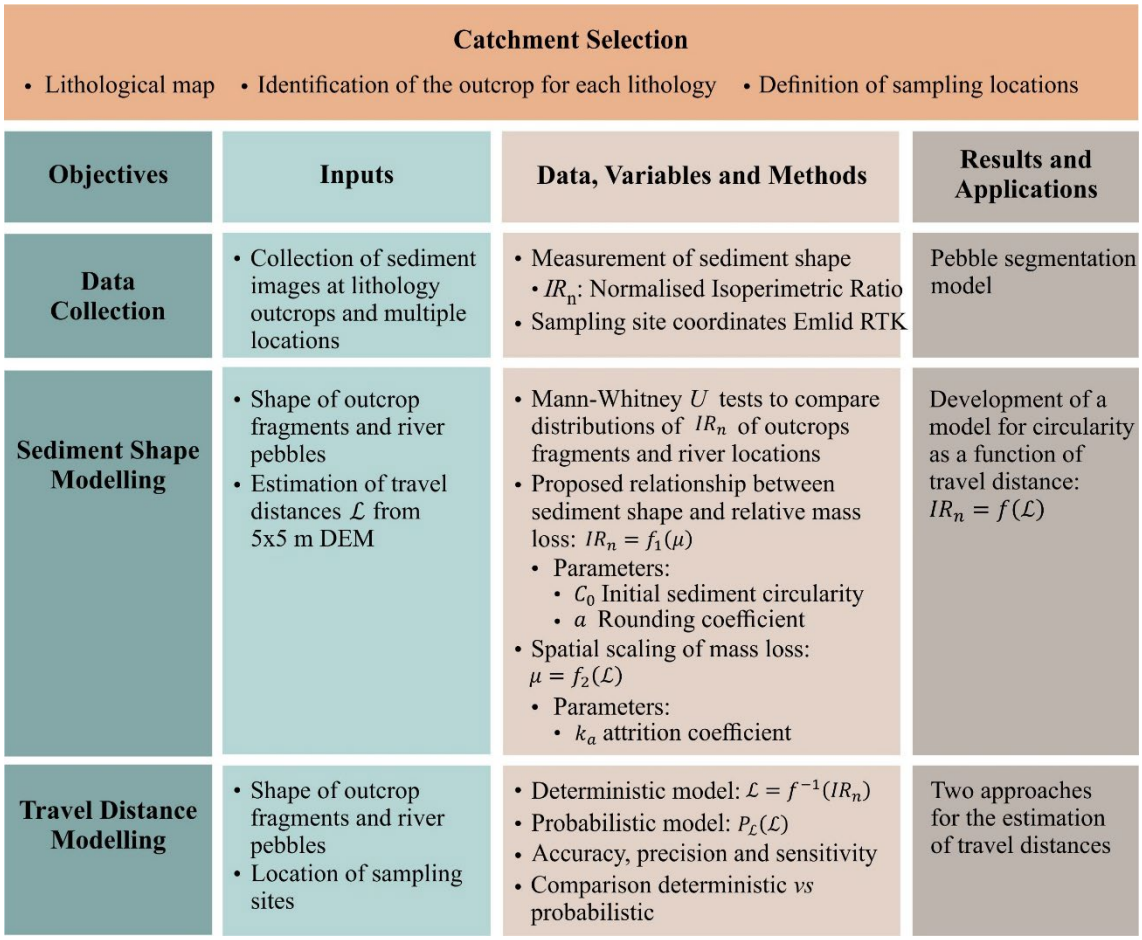

Figure 1.2. Research framework.

Sampling locations were chosen based on accessibility and to capture the evolution of sediment shape from its point of entry into the river network. Their positions were measured using a differential GPS (RTK), while travel distances were determined along the steepest descent paths using a 5x5 m resolution digital elevation model (DEM). While other studies have used sediments of known lithologies as tracers, this research is the first to identify the precise locations of outcrops and to measure the shape of the fragments they produce. This monitoring approach has, for the first time, enabled assessment of the relative importance of inherent heterogeneity versus attrition in shaping particle circularity measured in the field.

As such, it challenges earlier models (Pokhrel et al., 2024; Takahashi et al., 2025a) that attributed all variability in sediment shape solely to differences in transport distance. Furthermore, this approach has allowed for the evaluation of similarities and differences in the shape properties of fragments from different lithologies.

Finally, the previously developed model for sediment circularity was inverted to estimate travel distance from sediment shape. This direct inversion method was evaluated in terms of its accuracy and precision, and its applicability for estimating travel distances of particles from multiple sources was explored. Furthermore, a Bayesian approach was proposed to update prior probability distributions of sediment travel distance using observed shape distributions. Although this Bayesian method has not yet been applied, its expected advantages and limitations relative to direct inversion are discussed.

The methodology does not allow for tracking individual particles and, therefore, cannot directly estimate mass loss due to attrition or the time taken for particles to travel specific distances. Attrition experienced by particles while stationary on the riverbed is consequently neglected. This is a limitation of the study, and its contribution to overall attrition remains unclear in the literature, although this possible attrition mechanism is seldom addressed in similar work. To the best of the author's knowledge, the dependence of this process on sediment properties, such as density, size, and mechanical strength, has not yet been investigated.

1.6 Outline of the Thesis

This thesis is organised as follows.

Chapter 2 presents the image segmentation model developed to obtain reproducible measurements of pebble shape and its application to images collected during the field campaign.

Chapter 3 presents the outcomes from the field campaign, including the analysis of sediment shape, the assessment of fragments produced by outcrops, and the development of a model to estimate the circularity of sediments originating from single and multiple sources.

Chapter 4 discusses two methods for estimating sediment travel distances from shape. The first method involves the direct inversion of the circularity model introduced in Chapter 3, while the second proposes a Bayesian approach for estimating the probability distribution of sediment travel distance.

Finally, Chapter 5 summarises the main findings, answers the research questions, discusses methodological limitations, and outlines areas of further research.

2

A METHOD FOR SEGMENTATION OF PEBBLE IMAGES IN THE PRESENCE OF SHADOWS

The quantification of pebble shape from image analysis involves two steps: the segmentation of pebble contours and the application of a computational geometry algorithm to estimate shape parameters. When images are taken in the field, unavoidable shadows might hinder the possibility of using automatic segmentation methods. This chapter introduces a new method for automatic segmentation of pebbles that improves segmentation accuracy in the presence of shadows.

The algorithm was calibrated on a sample of five pebbles and then validated on a sample of 1696 pebbles. Its accuracy has been estimated by comparing the resulting shape parameters with those obtained using reference software, which was used as ground truth.

The proposed segmentation method was capable of accurately segmenting around 91% of the sample. The relative importance of the segmentation method and of the computational geometry algorithm used on the overall accuracy of pebble shape was also assessed, using for the latter, the models proposed by Zheng and Roussillon, respectively.

This chapter is mostly based on: Cattapan, A., Gurini, A., Paron, P., Ballio, F., Franca, M. J. (2024). A method for segmentation of pebble images in the presence of shadows. *Earth Surface Processes and Landforms*, *49*(15), 5202–5212. https://doi.org/10.1002/esp.6027

2.1 INTRODUCTION

The detailed description of sediment transport processes in rivers is still hindered by technological measurement limitations (Schneider et al., 2016; Wyss et al., 2016; Cassel et al., 2017a, b; Rickenmann, 2017). Historically, sediment transport rates have been considered to depend on pebbles' mass, almost invariably expressed by a linear measure representative of their size and by their density (Engelund and Hansen, 1967; Meyer-Peter and Müller, 1948; van Rijn Leo C., 1984). Recently, the impact of pebble shape on transport rates was also acknowledged (Cassel et al., 2021; Deal et al., 2023). Changes in sediment size and shape as a function of their transport history within a river basin have been observed in the field and studied empirically, analytically, and numerically for decades. These changes have been attributed to the combination of a series of processes: attrition (Wentworth, 1919; Krumbein, 1941; Kodama, 1994; Lewin and Brewer, 2002; Attal and Lavé, 2009), selective transport (Bradley et al., 1972; Dawson, 1988; Seal and Paola, 1995; Ferguson et al., 1996) and physical and chemical weathering (Bradley, 1970; Jones and Humphrey, 1997). Some authors also suggested the possibility of "in-place abrasion" (Schumm and Stevens, 1973; Brewer et al., 1992), which is the process of sediment deterioration due to vibrations that pebbles are subject to because of fluctuations in lift and drag forces.

Two of the most widespread technologies providing quantitative data on sediment size and shape are laser scanning and image-based techniques. Both techniques have been applied to untouched samples in the field (Adams, 1979a; Butler et al., 2001; Warrick et al., 2009; Hodge et al., 2009; Chang and Chung, 2012; Wang et al., 2013; Huang et al., 2018), and on pebbles collected and later analysed under controlled conditions, and by applying several methods (Hayakawa and Oguchi, 2005; Cassel et al., 2018). In general, image-based methods represent a cheaper solution, especially if the analysis is limited to pebble size, whose accurate estimation can be achieved even with lower-resolution images (Roussillon et al., 2009; Detert and Weitbrecht, 2012; Zheng and Hryciw, 2015). In this case, the grain size distribution of the surficial material can also be estimated using images collected by Unmanned Aerial Vehicles (UAV) (Carbonneau et al., 2004; Langhammer et al., 2017; Woodget and Austrums, 2017; Carbonneau et al., 2018). This method allows the acquisition of a large number of pebbles in a relatively short time, however, pebbles' imbrication and coverage by vegetation and soil material limit its applicability to shape estimation. Furthermore, while mean grain size can be inferred from the spectral decomposition of images of exposed sediment deposits (Buscombe et al., 2010), a similar approach has not yet proven applicable for shape estimation. Several algorithms were proposed to allow the segmentation of contacting and overlapping objects, both in 2D and 3D settings (Koh et al., 2007; Zheng and Hryciw, 2016; Sun et al., 2019), but their effect on the accuracy of shape estimates is still unclear.

For these reasons, accurate estimates of sediment shape still mostly rely on the analysis of samples collected in the field and analysed under controlled conditions.

During field surveys, sediment images are often taken by placing the sampled pebbles against a flat surface capable of providing a uniform colour background (Roussillon et al., 2009; Vangla et al., 2017; Cassel et al., 2018; Tunwal et al., 2020). Field conditions do not always allow shadow elimination, which affects image segmentation (Figure 2.1 a). Shadow elimination is a classic problem in image analysis and computer vision, which has therefore produced a vast literature (McCallister and Hung, 2003; Al-Najdawi et al., 2012; Ecins et al., 2014; Le and Samaras, 2020). These methods are not applicable to sediment pebble analysis, mainly due to the high variability in hue and texture, and the lack of controlled lighting conditions that can be achieved in the field. Under more controlled conditions, the geometric projection of pebbles' shadows has been used to infer their third dimension (Montenegro Ríos et al., 2013). This method requires a background capable of producing a strong hue difference to the target pebbles. Unfortunately, although many silicate and carbonate rocks present a higher intensity in the red and blue spectrum, some rocks also show relevant intensity in the green hue (e.g., rocks rich in olivine, serpentine, or chlorite minerals). This makes the data acquisition process complex in the field since one should use different backgrounds for pebbles of different hues.

This manuscript proposes a new method to segment the 2D contour of pebbles from sediment images in the presence of shadows. The method is based on a probabilistic application of the Canny edge detection algorithm (Canny, 1986) and uses grayscale images; therefore, it does not require the selection of a specific background colour. Its application shows that this new method allows an accurate assessment of sediment shape properties from images collected in the field using relatively inexpensive equipment. The model is written in MATLAB ™, The MathWorks, Inc., and is available at https://github.com/ACattapan/Probabilistic-Canny-Segmentation.

2.2 METHODS

2.2.1 Segmentation Method

Sediment images collected in the field are generally characterised by irregular shadowing and by intra-granular variations in texture and colour (Figure 2.1 b). Since shadows reduce the local contrast near the edge of a pebble, common methods for edge detection, loosely based on intensity gradients, might not provide an accurate segmentation, e.g., Canny edge detector (Canny, 1986), Sobel operator (Sobel, 2014), and Watershed algorithm (Zheng and Hryciw, 2016).

The proposed method comprises two phases. Phase 1 consists of a pre-processing of the input image where the model identifies the background board on which target pebbles are placed to exclude undesired objects and roughly identifies each pebble, which will then be analysed individually. Phase 2 consists of the application of the proposed method to each pebble. The proposed method is based on the iterative application of the Canny edge detection algorithm with variable thresholding values. For each set of these values, an image of the edges of variable strength is produced. These images are then averaged to calculate the relative frequency with which each pixel has been identified as an edge, hence the probabilistic nature of the method. This probabilistic approach improves the performance of the classical Canny algorithm by considering additional criteria for the definition of the outline of a pebble, on top of the local contrast. The detailed method will be explained in Chapter 2.2.3.

2.2.2 Phase 1: Image pre-processing

The first phase of the model aims at removing from the initial image areas of non-interest (Figure 2.1 b). For this purpose, the true-colour image is first transformed into grayscale. Given the sharp change in colour and texture between the outer material and the background board, the board's edge represents a discontinuity in the light intensity, i.e., these points are characterised by a significant gradient in greyscale. The image is therefore initially enhanced, increasing the contrast between the background board and the material present on the background. The contrast enhancement increases the probability that the maximum absolute value of the intensity gradient will be placed on the edges of the background board. The intensity gradient is computed by the convolution of the Sobel operator (Sobel, 2014) and the contrast-enhanced image. The background board segmentation method searches for the edges in the vertical and horizontal directions separately and proceeds sequentially by column and row, respectively. As an example, the process for the identification of the top horizontal edge is explained below; the identification of the other edges will follow an analogous process.

Assume the enhanced image to be a N by M pixels matrix. Each pixel is identified by its row and column indices, i and j respectively. The search for the pixels composing the top horizontal edge of the background board starts from the top left of the image (row $i = 1$ and column $j = 1$) and proceeds by column. The code searches for the pixel with the highest positive gradient in the vertical direction along the column j and evaluates the following conditions:

When the image includes external material that encircles the background board, then the horizontal edge might not lay on the column j. In this case, none of the pixels in column j have a positive gradient, so the code moves to the first row of column $j + 1$.

If the highest positive gradient is found on pixel (i^*, j), which is located in the upper half of the image $(i^* \leq N/2)$ and no previous pixel had been identified as an edge, then (i^*, j) becomes the first pixel of the horizontal edge. If other pixels had already been identified as part of the edge, the code computes the distance from the pixel identified as an edge in column $j-1$. If this distance is smaller than 10 pixels, then the pixel (i^*, j) will also be classified as part of the horizontal edge. Hence, all pixels of column j located on rows $(i < i^*)$ will be assigned a value of 0 and all pixels on rows $(i \geq i^*)$ will be assigned a value of 1. The code will then move to the first row of column $j+1$.

If the highest positive gradient is found on pixel (i^*, j) and this is located in the lower half of the image $(i^* > N/2)$ or at a distance higher than 10 pixels from the pixel identified as an edge in column $j-1$, this means that the top edge along column j is not characterised by the maximum gradient. This can be due to the presence of pebbles inside the board that produce a stronger contrast with the board itself. The upper edge along column j is therefore approximated by the pixel located on the same row as the edge pixel of column $j-1$ and the analysis will move to column $j+1$. This implies that the board edge is assumed to be parallel to the edge of the image.

The result is a binary mask splitting the image into two: all pixels above the top horizontal edge will have a value of 0, while all pixels on the edge and below will have a value of 1. A similar process is repeated to identify the three remaining edges. The final four binary masks are then overlapped, resulting in a binary mask where all pixels belonging to the background whiteboard have a value of 1 (Figure 2.1 c).

This mask is then applied to the original RGB image so that the output is a true-colour representation of the whiteboard and the pebbles positioned on top of it. The outer material in the area of non-interest is replaced by a uniformly coloured region. To reduce the contrast, the colour of the outer region can be selected to be as similar as possible to the colour of the background board (Figure 2.1 c).

Since the next phase of the model involves the analysis of each pebble individually, the image obtained at this point is converted to black and white and enhanced. Since the contrast between the whiteboard and the pebbles is generally high, their outline can be roughly identified and labelled as a separate 8-connected component. The (8-) connection is defined according to this criterion: a pixel a is 8-connected to a pixel b if b is located in a $3x3$ square window surrounding pixel a, which is therefore composed of 8 pixels plus pixel a itself. Each component represents the set of pixels that have been assigned a value of 1 in the black-and-white image. Comparing Figure 2.1 c and d, it is possible to notice that, due to the presence of shadows and colour and texture changes on the surface of some pebbles, this rough segmentation can be quite inaccurate, often leading to the overestimation of the pebbles' outline. The model builds a bounding box around each connected component, which will be the area of focus for the second phase.

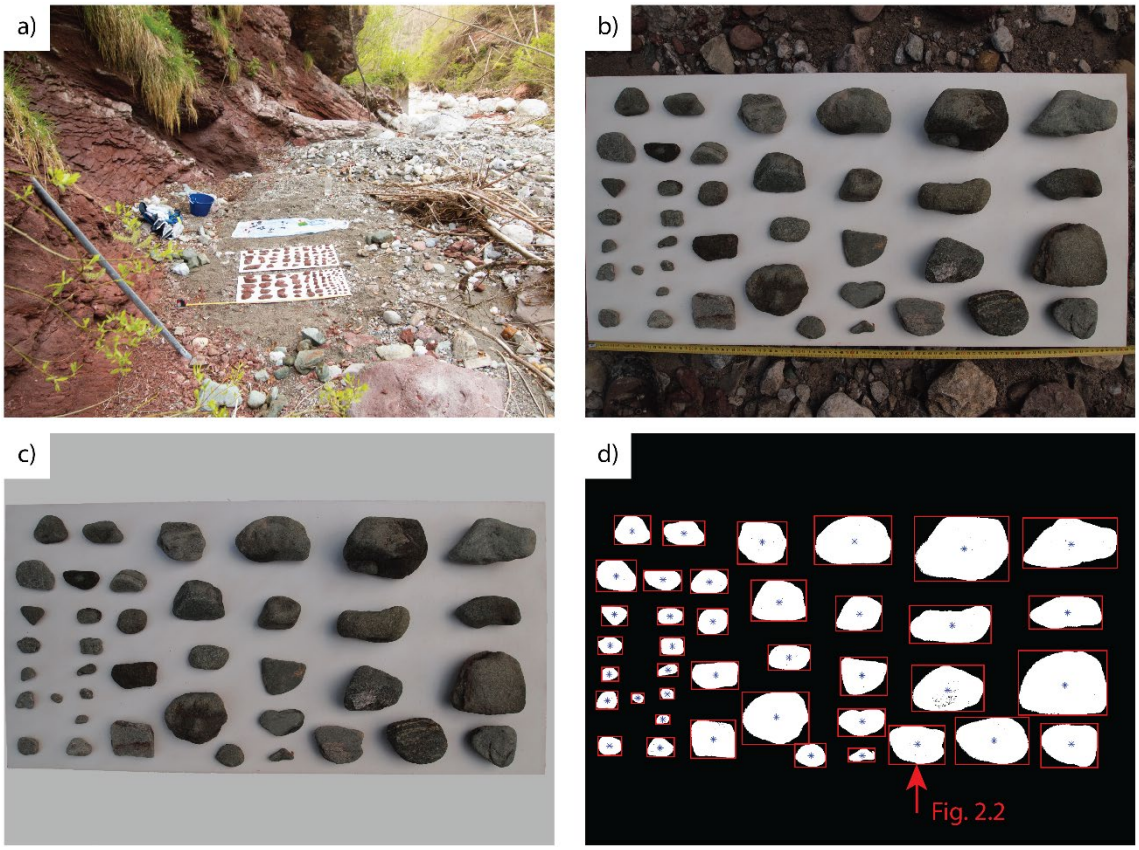

Figure 2.1. a) Example of the field survey process. b) JPG Image of a sample of pebbles of mixed lithology collected on the Sarzana Stream, Italy in 2019. This image is 4032x3024 pixels, with a resolution of 300 dpi and a spatial resolution of around 0.26 mm/px. c) Image resulting after the elimination of the material outside of the whiteboard. d) Example of rough segmentation with the indication of centroids and bounding boxes for each pebble.

2.2.3 Phase 2: Probabilistic Canny segmentation method

In order to assure the quality of the segmentation and immediately remove poorly segmented pebbles, the model considers one pebble at a time, which can be thought of as a two-step process.

The first step is based on the Canny edge detection algorithm (Canny, 1986; Gonzalez et al., 2009), which is widely used in image segmentation and incorporated in MATLAB ™. A general overview of the method is given here, while a detailed explanation can be found in the literature (Canny, 1986; Gonzalez et al., 2009). The method is usually applied to a grayscale image, which is initially smoothed by a convolution with a Gaussian function with a given standard deviation (σ_C) and a 16×16 pixel support. The magnitude and direction of the local gradient of the smoothed image are then computed for each pixel.

The underlying hypothesis is that pixels belonging to an edge should be characterised by a local maximum of the gradient in the direction of the gradient. Nonetheless, the gradient magnitude image is generally characterised by the presence of wide ridges instead of sharp edges. The algorithm, therefore, proceeds with a non-maximum suppression step: if the value of the gradient in a certain pixel is the maximum among the ones located along the gradient direction, its value is maintained, otherwise, it is suppressed, i.e., replaced by zero. This step produces a non-maximum suppressed gradient image, which may contain false-positive and false-negative edges. The selection of the important ones for the segmentation of the objects is performed by a hysteresis thresholding process. Edges can be classified according to the "strength", i.e., the magnitude of the gradient. The algorithm defines two thresholds for the gradient magnitude: a higher threshold (C_h) and a lower one (C_l). All pixels with a gradient magnitude higher than C_h are defined as "strong" and are automatically kept as edges. All pixels with a gradient magnitude lower than C_l are automatically discarded, while pixels with a gradient magnitude between C_h and C_l are defined as "weak" and are kept only if they are connected to a "strong" edge. Overall, the Canny edge detection algorithm requires the definition of three parameters: the standard deviation of the Gaussian filter (σ_C) and two thresholds C_h and C_l for edges' strength. The model first applies the algorithm using the default values for all the parameters: $\sigma_C = \sqrt{2}$, while C_h and C_l are defined in terms of percentage of the gradient magnitude values, $C_l = 0.28$ and $C_h = 0.70$.

When applied to images of sediment collected in the field, e.g., Figure 2.1 a, this method might categorise as edges not only a pebble's contour but also internal discontinuities due to variations in colour or texture (Figure 2.2 a). The presence of significant shadows might also worsen the quality of the segmentation because the maximum gradient might happen along the shadow, resulting in artificial edges not associated with the shape of the physical object (Figure 2.2 a). To assess whether the default application of the Canny algorithm successfully segmented the whole outline of a pebble, the edges resulting from its application are first classified as 8-connected components, and the longest connected component is identified.

In the absence of shadows and internal colour or texture changes, the outer border is characterised by a strong contrast with the background, and therefore, the longest connected component properly approximates the pebble's outline. In this case, the longest connected component will be a closed path; the segmentation process will stop, and the model will print an image of the original pebble superimposed by the longest connected component to allow the operator to assess the quality of the segmentation and decide whether to keep the outline for further shape analysis or discard it due to insufficient accuracy. On the other hand, in case of strong shadows or colour variations, the longest connected component properly identifies only the part of a pebble's outline facing the light source, where the image contrast is higher, e.g., the red outline in Figure 2.2 a.

In this case, the longest connected component will be an open path, characterised by two endpoints. The process will therefore continue with the Probabilistic Canny segmentation method, which represents the second step of Phase 2.

The second step of Phase 2 is based on the hypothesis that the composite statistics of multiple applications of the Canny algorithm with different parameterisations will reveal the most significant edges, i.e., the ones which are identified more frequently. The parameters that the model varies to assess the relative frequency with which edges are detected are the standard deviation of the Gaussian filter and the lower and upper thresholds on edges' strength. Parameters are selected from independent uniform distributions (see also Chapter 2.4). Each combination of these three parameters produces a binary image of edges. The relative frequency f with which each pixel is identified as an edge can therefore be computed. The output representation is a grayscale image, where pixels with a higher probability of being edges appear in a lighter colour (Figure 2.2 b). The model then starts from one endpoint of the previously computed longest connected component and uses the edge frequency map to select new pixels to attach to, eventually closing the pebble's outline. The algorithm uses a square search window of size l pixels placed around each endpoint of the longest connected component (Figure 2.2 b). The selection of which pixels to attach to the actual longest connected component is based on two assumptions. The first assumption is that pixels that have been more frequently identified as edges have a higher likelihood of being true edges. The second assumption is that pebbles tend to be overall convex, therefore, true edges should contribute to closing the pebble outline.

To implement these assumptions, the pixels' relative position must be defined. The model uses a polar coordinate system cantered on the centroid of the actual longest component. The position of each pixel within the search window is therefore defined by its distance from the centre d_{C-P} and by its angle α (Figure 2.2 b). δ is the angle formed between a pixel in the search window and the opposite endpoint. d_{E-P} is the distance between a pixel in the search window and the endpoint at the centre of the window. ∇f is the gradient of the frequency map computed between each pixel in the search window and the actual endpoint. Δ is the angular distance between the current endpoints. Pixels within the search window are initially filtered according to three conditions:

$$f > 0 \qquad 2.1$$

$$d_{E-P} > 0 \qquad 2.2$$

$$\delta < \Delta \qquad 2.3$$

The first condition (equation *2.1*) filters out all pixels that were never identified as edges since their frequency f is lower or equal to zero. The second condition (equation *2.2*) filters out the current endpoint by imposing that the distance of the selected pixel from the centre of the search window should be positive ($d_{E-P} > 0$). The third condition (equation *2.3*) states that the selected pixel should contribute to the decrease of the angular distance between the endpoints ($\delta < \Delta$), in agreement with the second assumption. The first and second conditions must always be met, while, if any pixel within the search window satisfies the third condition, the model selects the pixel with the minimum value of δ (even if $\delta > \Delta$). This allows the identification of locally non-convex edges. Multiple pixels may fulfil all three conditions. In this case, the model will select the new endpoint according to a list of conditions, where each further condition is assessed only if multiple pixels meet the previous one. The list of conditions is:

$$\max(\nabla f) \qquad 2.4$$

$$\min(d_{E-P}) \qquad 2.5$$

$$\min(\delta) \qquad 2.6$$

The meaning of these criteria is: the new endpoint is selected based on the maximum gradient of the probability of it being an edge (equation *2.4*); its distance from the current endpoint should be the minimum to guarantee the continuity of the object's outline (equation *2.5*); and its position should be such that the angle between current endpoints will decrease (equation *2.6*). The pixel resulting from such selection will become the new endpoint and, should it not be adjacent to the actual centre of the search window, it will be connected to the current endpoint with a linear interpolation.

At this point, the model moves to the opposite endpoint, and the process is repeated. The angular distance between endpoints iteratively decreases, bringing them closer together alternatively from both sides. This process stops either if it is not possible to identify additional edges, or if the position of the endpoints is such that one of the two following conditions is met:

$$\Delta < \Delta_{thr} \qquad 2.7$$

$$d_{E-E} < \frac{l}{2}\sqrt{2} \qquad 2.8$$

The first condition (equation *2.7*) states that the angular distance between the endpoints is smaller than a certain threshold Δ_{thr} (6° in this application). The second condition (equation *2.8*) states that the linear distance between endpoints is smaller than half of the diagonal of the search window. At this moment, the two endpoints are connected by a straight line that closes the pebble's outline.

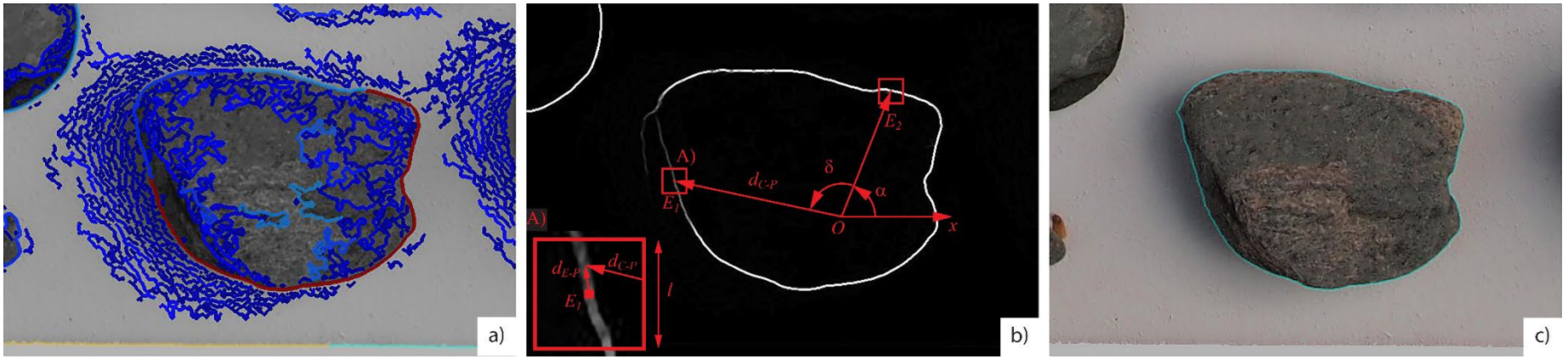

Figure 2.2. a. Connected components resulting from the application of the classical Canny segmentation algorithm. The red contour represents the longest connected component. Notice that, in the area where a shadow is present, on the left of the pebble, the algorithm identifies a series of possible edges, each with a different "strength" and length. b. Scheme representing the variables used by the pebble segmentation model. O is the centroid of the connected component and x is the horizontal axis. E_1 and E_2 are the two endpoints of the longest connected component, α is the angle of the first endpoint with respect to the horizontal axis, while δ is the angle between the endpoints. d_{C-P} is the distance between the centroid and a generic pixel within the search window (see particular A), which has a size l. Finally, d_{E-P} is the distance between an endpoint and a generic pixel within the search window. c. Outline of a pebble obtained from the application of the proposed method, after calibration.

At the end of the segmentation process, the identified contour is plotted on top of the true colour image to allow a visual assessment of the quality of the result (Figure 2.2 c). The method was capable of properly segmenting the pebble (Figure 2.2 c), despite the presence of a shadow; the application of the classical Canny algorithm would have produced a set of possible edges in the area on the left of the pebble (Figure 2.2 c).

2.3 Application Area and Data Collection

The data used for calibrating and validating the proposed method were collected in the Sarzana Catchment: a 25 km^2 alpine basin in North-East Italy (Figure 2.3). The Sarzana Stream is a tributary of the Cordevole River, which joins the Piave River around 31 km downstream of the Sarzana Confluence. The Sarzana Catchment is characterised by an alpine climate, with cold winters and temperate summers. The average annual precipitation, measured at the nearby ARPAV station of Col di Prà (https://www.arpa.veneto.it/dati-ambientali/open-data/clima) over the period 2000-2021 is about 1620 mm (Brenna and Surian, 2023). The Sarzana Stream drains the Southeast face of the Agner Mountain group, while its right-hand side is bounded by the Armarolo Mount. The elevation varies between about 2872 and 563 m above sea level.

Sediment samples ranging between fine gravel and cobbles have been collected from 11 locations, from outcrops, first-order tributaries, and along the main river. Individual sediment particles have been collected, washed to remove loose soil and vegetation, dried with a cloth to avoid sparkles, and placed on a 0.5 m by 1.0 m rectangular white wood board that was used as a background. Sediments were placed on the background board following two criteria: their orientation was such that the projected area on the board was maximum, and their relative distance was large enough to avoid overlaps of their edges when seen from the point of view of the camera. In the current manuscript, the first criterion was applied to ensure that the maximum projected area was captured, providing reliable measures of both maximum and intermediate axes (a and b, respectively).

Images were taken using an Olympus® E-PL1 digital camera, whose lens was placed as parallel as possible to the background board to limit tangential distortion, and with the board and the sampled particles well within the edges of the image to limit radial distortion. For these reasons, images were not corrected for distortion before the analysis. A metal ruler was placed along the longest side of the board and was used to scale each image. The resolution of the images depends on the size and resolution of the camera sensor, the focal length, and the distance between the lens and the object. The data presented here were taken standing at a distance of about 1.0 m from the board, the camera used has a 12.3 MP sensor, and the resulting images have an average resolution of 0.26 mm/px. The total number of pebbles present in the sample is 1696.

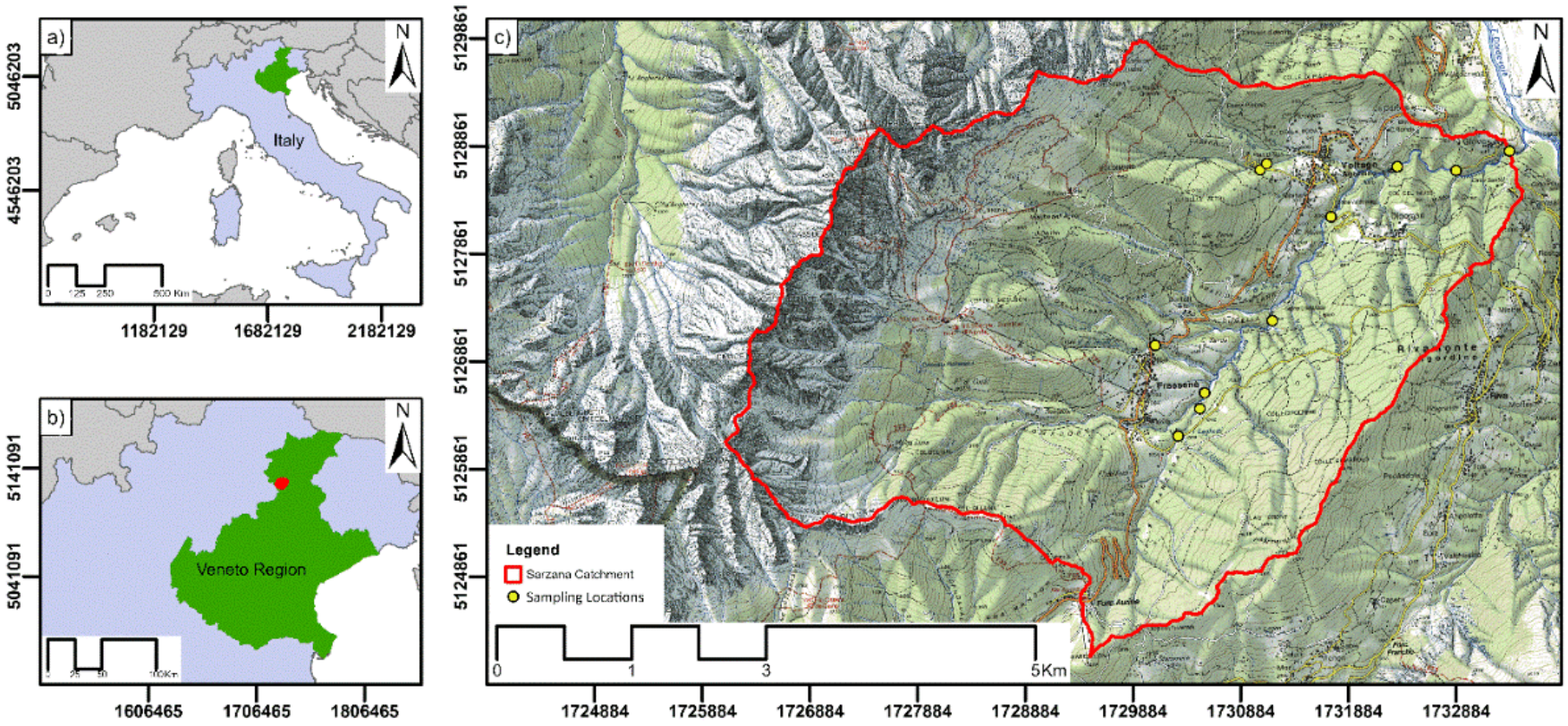

Figure 2.3. Location of the Sarzana River basin and of the locations where the sediment images used in this study have been collected.

The minimum size of the particles collected was chosen following the criteria recommended by Roussillon et al. (2009): in order to achieve accurate shape values, for a given image resolution, each particle perimeter should be composed of at least 150 pixels. The minimum dimensions considered were therefore about 20 mm and 12 mm for the maximum and intermediate size, respectively.

In order to assess the relative importance of the toolbox used for shape parameters estimation, we created a set of eight black and white images using Adobe Illustrator CC, for which we could compute shape descriptors analytically. These will be further referred to as "analytical shapes". Examples and details regarding the analytical shapes can be found in the supplementary material. Table 2.1 summarises the ranges of values used for shape descriptors of analytical shapes (Equations *2.9*, *2.10* and *2.11*).

Table 2.1. Overview of shape descriptor values for analytical shapes

Parameter	Lower limit	Upper Limit
e	0.18	0.74
C	0.44	0.97
R_W	0.29	1.00

2.4 MODEL CALIBRATION

The probabilistic nature of the model implies the definition of boundaries for the random selection of the parameters used. The quality of the model's result depends on these boundaries. The model was calibrated to identify the optimal ranges of C_l, C_h and σ_C. The space of possible values considered during the calibration is reported in Table 2.2.

Table 2.2. Range tested for calibration parameters.

Parameter	Lower limit	Upper Limit
C_l	0.0	1.0
C_h	0.0	1.0
σ_C	0.2	5.0

In order to calibrate the values of the model's parameter and to assess its accuracy, the outline of each pebble manually obtained using the "Quick Selection tool" available in Adobe Photoshop CC was chosen as the ground truth (GT). The use of this tool requires, especially in the case of shadows, the manual refinement of the segmentation by the operator and might therefore be time-consuming and subject to operator bias.

The model's parameters have been calibrated using five pebbles that have been selected because they differ in shape, colour, texture and intensity of the shadow. The outlines resulting from the application of our model with each combination of the calibration parameters have been processed using the toolboxes developed by (Roussillon et al., 2009) and (Zheng and Hryciw, 2015) for the estimation of shape parameters. Both toolboxes have been used to process the outlines obtained from the segmentation with Adobe Photoshop CC. We used as an accuracy metric the mean absolute relative error (ε) of three common shape descriptors: elongation, circularity and roundness. The definitions of these three shape descriptors are as follows:

$$e = \frac{I}{L} \tag{2.9}$$

$$C = \frac{4\pi A}{P^2} \tag{2.10}$$

$$R_W = \frac{\frac{1}{N_c}\sum_{i=1}^{N_c} r_i}{R} \tag{2.11}$$

Where elongation e is the ratio of the intermediate to the longest dimension of the 2D contour (I and L respectively), A and P are the area and the perimeter of the 2D contour, respectively and R_W is the roundness according to (Wadell, 1932). This is defined as the ratio between the average radius of curvature (r_i) of the N_c corners of the 2D contour and the radius of the biggest inscribed circle (R). The relative error (ε) for each descriptor is defined as follows (equation *2.12*):

$$\varepsilon = \frac{1}{N_p}\sum_{i=1}^{N_p} \frac{|\beta_{GTi} - \beta_{PCi}|}{\beta_{GTi}} \tag{2.12}$$

Where N_p is the number of pebbles in the sample ($N_p = 5$ for the calibration phase), β_{GTi} is the value of a generic shape descriptor obtained using the ground truth outline for the i[th] pebble, while β_{PCi} is the value of the same shape descriptor obtained using the outline produced by the Probabilistic Canny segmentation method for the same pebble. This metric was chosen since it does not allow compensation for positive and negative relative errors. We also assessed the general performance of the model using an overall error metric defined by equation *2.13*.

$$E = \sqrt{\varepsilon_e^2 + \varepsilon_C^2 + \varepsilon_{R_W}^2} \tag{2.13}$$

Where ε_e is the relative error for pebbles' elongation, ε_C is the relative error for pebbles' circularity and ε_{R_W} is the relative error for pebbles' roundness, as defined above.

The combination of parameters selected for the calibration was the one that produced the minimum of the objective function (Ω) defined as the square root of the sum, over all five pebbles, of the squares of the overall error metric (equation *2.14*).

$$\Omega = \sqrt{\sum_{i=1}^{5} E_i^2} \qquad 2.14$$

The combination of values corresponding to the minimum of the objective function is provided in Table 2.3. The parameters were tested between the lower and upper limits in Table 2.2 with an equidistance of 0.01. The size of the search window around each endpoint was kept constant and equal to 17 pixels. The calibrated model was then applied to the full dataset of images taken in the Sarzana River basin, Italy, as described in Chapter 2.3.

Table 2.3. Values of model parameters after calibration.

Parameter	Lower limit	Upper Limit
C_l	0.1	0.2
C_h	0.0	0.3
σ_C	0.2	5.0

The relative importance of the segmentation method and of the computational geometry tool for the overall accuracy of the shape values estimation was also assessed. For a given shape descriptor β, the bias of the toolbox by Zheng and Hryciw, (2015) was assessed with respect to the one by Roussillon et al., (2009); the average absolute relative difference between the values produced was used $\varepsilon_{Z-R\,\beta}$ (equation 2.15). We used three datasets: the ground truth outlines, the outlines produced by the Probabilistic Canny segmentation model, and the analytical shapes.

$$\varepsilon_{Z-R\,\beta} = \frac{1}{N_p}\sum_{i=1}^{N_p}\frac{|\beta_{R\,i} - \beta_{Z\,i}|}{\beta_{R\,i}} \qquad 2.15$$

Where, N_p is the number of pebbles in the dataset, $\beta_{R\,i}$ is the value of the shape descriptor estimated using the toolbox by Roussillon et al., (2009) for the ith pebble and $\beta_{Z\,i}$ is the associated value estimated using the toolbox by Zheng and Hryciw, (2015).

2.5 RESULTS AND DISCUSSION

Out of the 1696 pebbles present in the sample, 1541 passed the visual inspection, meaning that the outline produced by the model appeared to be perfectly matching the actual pebble outline. In terms of visual inspection, therefore, the model allowed the accurate segmentation of around 91% of the sample. To quantitatively assess its performance, the outline of all pebbles that passed the visual inspection was also processed using the toolboxes developed by Roussillon et al., (2009) and Zheng and Hryciw, (2015). The same toolboxes were also used to analyse the outline of ground truth pebbles. Table 4 summarises the performances of the proposed segmentation model compared to ground truth for each shape descriptor and for both toolboxes.

Table 2.4. Model results in terms of mean absolute error (E), standard deviation of the absolute error (σ) and mean absolute relative error (ε) for elongation (e), circularity (C) and roundness according to Wadell (Rw).

Model	E_e	σ_{E_e}	ε_e	E_C	σ_{E_C}	ε_C	E_{Rw}	$\sigma_{E_{Rw}}$	ε_{Rw}
Zheng	0.006	0.021	0.9%	0.013	0.025	1.5%	0.044	0.038	7.5%
Roussillon	0.010	0.025	1.0%	0.007	0.015	0.7%	0.028	0.029	4.3%

Roundness is the parameter that showed the highest relative error, irrespective of the toolbox used for the estimation of shape parameters. Results for elongation and circularity showed instead good agreement with ground truth values. Table 2.5 provides the values of the bias of the toolbox by Zheng and Hryciw (2015) with respect to the one by Roussillon et al. (2009) for elongation, circularity, and roundness.

Table 2.5. Bias of the toolbox by Zheng and Hryciw (2015) with respect to the one by Roussillon et al. (2009) for elongation, circularity and roundness, respectively.

Bias	Ground truth	Prob. Canny	Analytical shapes
$\varepsilon_{Z-R\,e}$	3.5%	3.7%	52.2%
$\varepsilon_{Z-R\,C}$	7.2%	7.4%	6.0%
$\varepsilon_{Z-R\,Rw}$	14.1%	12.9%	2.6%

Although the size of the sample is limited to eight shapes, the comparison of the outputs of each toolbox with analytically computed shape descriptors suggests that the toolbox developed by Zheng and Hryciw (2015) is more accurate than the one by Roussillon et al. (2009) (see Table 2.6).

Table 2.6. Error of the toolbox by Zheng and Hryciw (2015) and Roussillon et al. (2009) with respect to analytical shapes for elongation, circularity, and roundness.

Error	Zheng et. al.	Roussillon et. al.
ε_e	3.7%	38.2%
ε_C	3.9%	18.4%
ε_{Rw}	8.9%	15.8%

Figure 2.4 provides a visual summary of these results: subplots a), c), and e) compare the two toolboxes for shape descriptors estimation considered in this study, while subplots b), d), and f) compare our Probabilistic Canny segmentation method with ground truth: the "Quick selection tool" of Adobe Photoshop CC. In these plots, it is possible once more to observe that, within the limits of our experiment, the choice of a certain toolbox for shape descriptors estimation had a much higher impact on the overall accuracy than the segmentation method used. These plots are also coherent with the comparison of results reported in Table 2.4 and Table 2.5.

The time required to process an image with several pebbles depends on the number of pebbles and the available computing power. As a reference, in the experiments presented in this manuscript, using 16 GB RAM and 4 cores, 1.8 GHz CPU, an image with 39 pebbles was processed in around 12 minutes, including the time needed to visually assess the quality of the segmentation of each pebble.

The accuracy of the Probabilistic Canny segmentation method presented varies depending on the specific shape parameter used to assess it. In particular, the accuracy in terms of elongation results to be the highest, with lower values for circularity and even lower for roundness. This result provides quantitative evidence for the intuitive argument that the impact of the segmentation method on the shape estimation accuracy increases with increasing detail required to compute the shape descriptor itself.

The comparison of the results reported in Table 2.4 and Table 2.5 suggests that the bias associated with the selection of one of the two computational geometry toolboxes is larger than the error introduced by the use of the proposed Probabilistic Canny segmentation method instead of the "Quick selection tool".

In practical terms, these results can be relevant for studies aiming at correlating sediment morphometry with attrition rates and/or transport, entrainment, and deposition conditions.

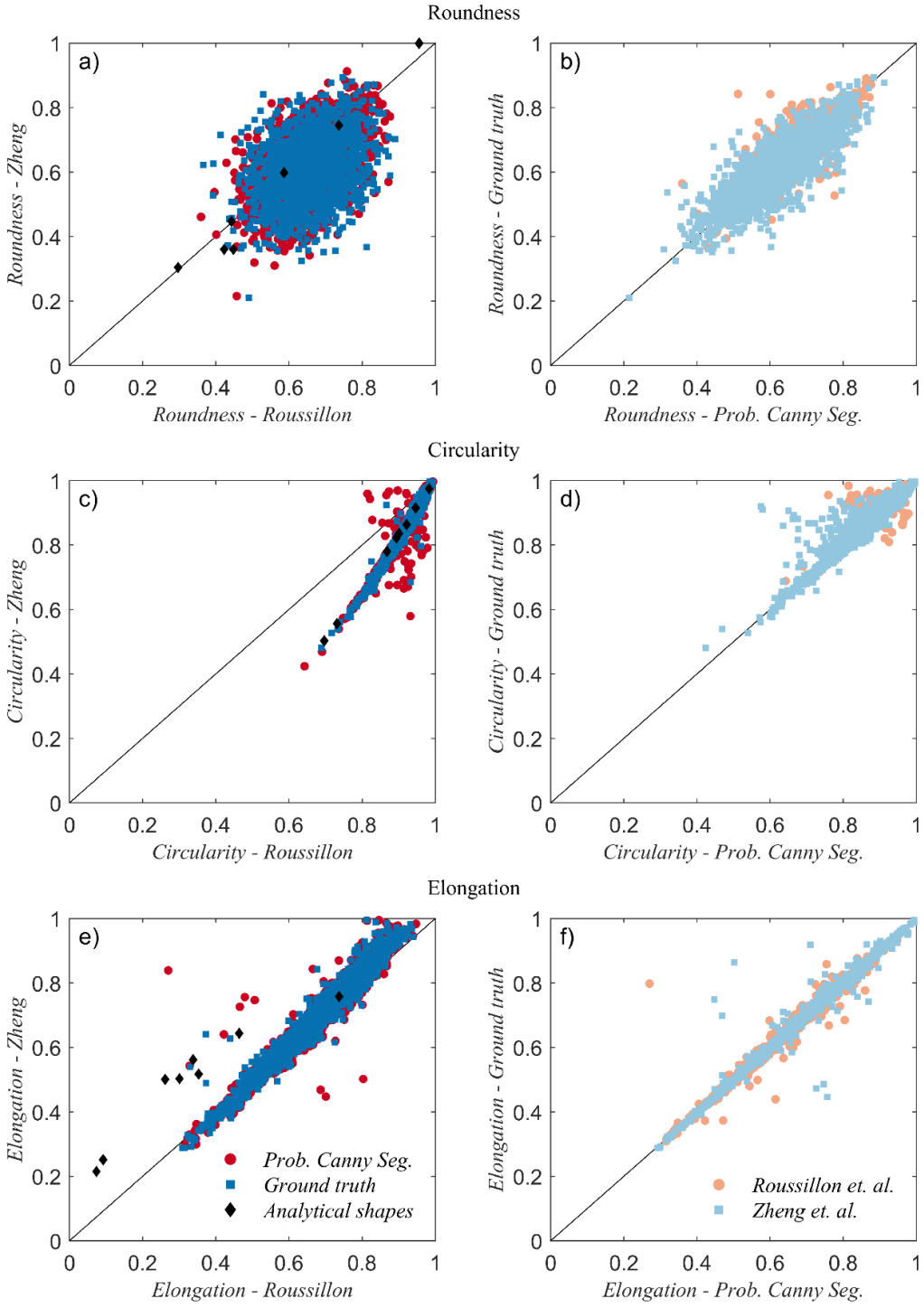

Figure 2.4. a), c), e) Scatterplots representing the bias of the toolbox by Zheng and Hryciw (2015) with respect to the one by Roussillon et al., (2009) for elongation, circularity, and roundness, respectively. The legend is consistent for all plots. Scatterplots b), d), and f) provide a visual assessment of the error between our segmentation model and ground truth outlines, obtained with manual segmentation (see Chapter 2.5). The legend is consistent for all plots.

They suggest that, when choosing which parameters to measure, the assessment of the measurement error should account for both the segmentation method and computational geometry tool used because their impact might be of comparable importance. In particular, both factors seem to become increasingly important with the increase in the detail required to compute a given shape property.

The proposed method is completely implemented in MATLAB ™, and it can be coupled with the computational geometry toolbox developed by Zheng and Hryciw, 2015. Given its complete automation, the method, therefore, allows results to be reproducible. At the same time, the method allows the user to visually check the quality of the segmentation and to discard pebbles that cannot be correctly segmented. This setup provides a time-efficient workflow since it removes the need to double-check the correctness of pebbles segmentation at the end of the process.

2.6 CONCLUSIONS AND RECOMMENDATIONS

This paper presents a new method for the automatic segmentation of pebble outlines from images collected during field surveys. The proposed model is applicable in a range of shadows and contrast conditions and, although the background board used had a similar hue to some of the pebbles, the model accurately segmented their outline. In terms of accuracy, the outlines produced were, in 91% of the examined cases, indistinguishable from true pebble outlines. Moreover, when compared against the herein-defined ground truth, the method showed a comparable accuracy. There is, however, a bias between different computational geometry toolboxes, which in certain cases can be higher than the error between the proposed segmentation method and the ground truth. As a result, when comparing sediment shape properties across environments or through time, the effects of both the segmentation method and the geometry description toolbox need to be taken into consideration, possibly through calibration and validation.

In terms of limitations, strong shadows or intergranular colour or texture changes might limit the ability of the model to accurately segment pebble outlines. In this case, the highest probability edge often occurs along the spurious interface between the background board and the shadow or within the pebble, decreasing the accuracy of automatic segmentation methods. For this dataset, only 9% of the samples presented the aforementioned limitation.

Future research might consider investigating whether the object shape properties fall within acceptable ranges and possible ways to decrease the probability of the edges responsible for such out-of-range values. This approach needs to be tested and verified against visual assessment. Moreover, the current work was based on images with a similar resolution, following the guidelines of existing literature. Future investigations could focus on the effect of different resolutions on segmentation accuracy.

3

MODELLING SEDIMENT CIRCULARITY IN MOUNTAINOUS CATCHMENTS

A physically-based approach considering the heterogeneity of the input sediments shape

Due to attrition, sediment particles become progressively rounder and lose mass as they are transported downstream a valley. Modelling pebble shape evolution in natural environments is challenging, and to date, no commonly recognised modelling framework exists. This chapter presents a new conceptual, physically-based model to represent the evolution of the shape of pebbles moving in mountainous rivers, represented by the normalised isoperimetric ratio (IR_n). It is built by combining a geometrical relationship between relative mass loss and IR_n with the empirical Sternberg Law, which defines an exponential decay of particle mass with the travelled distance. The model was validated using pebble shape data acquired by image analysis in the Sarzana Stream, Italy, where two lithologies, arenites and metabasalts, with well-located outcrops, were used as tracers. The results show that the proposed model is capable of successfully reproducing the observed shape evolution of both lithologies for point and diffuse sediment sources.

This chapter is mostly based on: Cattapan, A., Katsanou, K., Piégay, H., McClain, M., Franca, M. J. Tracing Pebble Shape Evolution in Mountain Streams: A Physically Based Model Incorporating Lithologic Heterogeneity. (Submitted), and will be referred to as Cattapan et al., 2026, in the rest of the thesis.

3.1 INTRODUCTION

Attrition is the process by which sediment particles lose mass due to impacts, and, in river systems, it contributes to the production of fine particles (Kuenen, 1956; Attal and Lavé, 2009; Manga et al., 2011). Mass loss is also generally associated with changes in sediment shape (Domokos et al., 2014). A wide range of shape parameters has been developed to characterise sediment particles (Wadell, 1932; Barrett, 1980; Cassel et al., 2018). However, the complexity of the underlying processes, combined with the heterogeneity of environmental conditions and material resistance, continues to limit our ability to model the evolution of sediment shape along a river network.

The attrition process in natural environments is complex because sediments move within a turbulent flow. The flow conditions, which are variable, and the sediment characteristics, such as the size, density, or shape, control the types of sediment motion, which can be in suspension in the water column or sliding, rolling, and jumping near the bed (Pähtz et al., 2020). Particles moving only in suspension have sizes of the order of 10^{-2} mm or smaller; therefore, their kinetic energy is small, and they are subject to little attrition. On the contrary, coarse particles can move by sliding, rolling, and jumping. These types of motion lead to more exposure of these sediments to different types of attrition, which, according to Novák-Szabó et al. (2018) can be classified, in order of increasing exchanged energy, as: friction, chipping, and fragmentation. The transition from friction to chipping is estimated to happen when the kinetic energy of the impacts E_i equals the energy thresholds for saltation, E_s, which is of the order of $E_s \sim 10^{-3}\ J$. The transition from chipping to fragmentation happens when the kinetic energy of the impact E_i equals a threshold value that, for quartzite particles with diameters $10^{-3}\ m < D < 10^{-1}\ m$, is of the order of $E_f \sim 10^{0}\ J$ (Yashima et al., 1987). The range of energy conditions within which chipping applies spans, therefore, around three orders of magnitude. Field data from Turowski et al. (2013) and flume data from Larimer et al. (2021), suggest that the probability of impact energies being outside the chipping range is extremely small, supporting the argument that such an attrition process is the most common in fluvial settings. Nonetheless, friction might have a non-negligible contribution in very low energy environments, such as low-gradient river reaches (Szabó et al., 2013), while fragmentation might become important in high-energy environments, like headwater streams with slopes higher than around 10^{-1} (Adams, 1979b; Attal and Lavé, 2009).

Aristotle provided the first known theory on the change of shape of natural sediments (Ross, 1913). He conjectured that the velocity of inward motion of a pebble's surface is proportional to its distance from the centre. This model translates into an integro-differential equation known as distance-driven flow (Domokos and Lángi, 2018). More recently, extensive literature has been published on modelling chipping as a geometric problem (Domokos and Gibbons, 2012; Domokos et al., 2014), where the velocity of shrinking of a pebble surface is proportional to its curvature.

This model is also an integro-differential equation called curvature-driven flow. Still, this shape evolution can also be cast in a simpler framework, where the shape of the particle's outline is simplified by considering only its three major axes (box equations). According to the curvature-driven flow model, the effects of attrition on sediment size and shape can be split into two phases (Litwin Miller et al., 2014): during Phase I, sharp corners and edges are eroded, while the overall dimension of the particle remains unchanged; only afterwards, during Phase II, a particle's dimensions start to decrease, while its shape changes at a slower rate. This theoretical framework has been successfully applied to natural settings to describe the shape of fluvial sediment. Szabó et al. (2013) applied the box equations to model the evolution of the size and shape of pebbles along the Williams River, Australia, and obtained excellent agreement with field data. Although excellent results were produced, the model has a significant limitation: its calibration and validation require the measurement of the three axes of pebbles, which is very time-consuming, since it is usually done manually. Litwin Miller et al. (2014) used the box equations, calibrated through direct measurements, and shape parameters derived by image analysis (e.g., convexity, circularity, and entropy of the curvature), to estimate the relative importance of attrition and selective transport in the Rio Mameyes, Puerto Rico. Their results showed that the shape parameters obtained by both direct measurements and 2D images agreed with the trends predicted by the curvature-driven flow. In particular, the curvature-driven flow predicts the isoperimetric ratio and the entropy of the curvature to be monotonically increasing. This suggests the possibility of establishing a mechanistic relationship between these shape parameters and the distance travelled by a particle along a river (Szabó et al., 2015; Pokhrel et al., 2024).

As previously discussed, chipping is the most common attrition process in rivers, but fragmentation might be significant in headwaters with slopes higher than around 10^{-1}. On the other hand, curvature-driven flow models predict that the majority of the shape changes take place during Phase I. The first objective of this work is to assess the accuracy of a model for the evolution of circularity based on the assumptions of curvature-driven flow in reproducing shape changes in steep headwater streams.

All existing evidence suggests that lithology has a significant impact on attrition rates and shape changes (Litty and Schlunegger, 2017; Litwin Miller and Jerolmack, 2021; Pfeiffer et al., 2022; Bray et al., 2024). In order to account for this effect, several studies have tracked the shape evolution of specific rock types, but their monitoring never considered sediment outcrops as initial points. The variability of the shape of newly produced fragments was therefore not accounted for. The initial shape of pebbles as they enter the river network can be considered as a boundary condition for their shape evolution along a river.

Knowledge of this aspect becomes critical when trying to model the integrated effect of sediment inputs from spatially distributed sources because it allows for assessing whether outcrops of a given lithology can be assumed to produce fragments with a similar shape distribution. To cover this gap by monitoring outcrops of the lithologies used as tracers, and to provide insights into the distributions of shapes of their fragments, is the second objective of this work.

Finally, since the pebble shape changes very rapidly in the initial stages of the attrition process, small variations in travel distance, close to the outcrops, translate into significant changes in their shape. The effect of multiple sediment sources, having different distances, would therefore translate into a very noisy shape signal. In order to capture a mean behaviour, most studies that used different rock types as tracers have considered subcatchments with almost homogenous spatial distribution for their outcrops. In this way, the strong shape variations that happen during the first kilometre of travel distance tend to be smoothed out. A third research objective, therefore, involves the integration of spatially distributed outcrops in a general model for the evolution of sediment shape along a river.

A conceptual, physics-based model to represent the changes of pebble shape in mountainous streams, which agrees with the theoretical constraints deriving from the curvature-driven flow and with the empirical evidence of exponential decrease in particle mass along a river (Sternberg's law), is herein proposed. The model uses the normalised isoperimetric ratio as a shape descriptor: a property that can be easily measured through image analysis. Moreover, it depends on only three parameters, which can be either measured in the field through image analysis techniques (Cattapan et al., 2024) or estimated by fitting field data. When applied to multiple source areas, the introduction of a weight function, accounting for valley source dispersion, is used to estimate the relative contribution of different sources to downstream locations.

A proof of concept of its application has been performed using field data from the Sarzana Stream, Italy, where two lithologies, arenites and metabasalts, have clear, discrete landscape sources. Sediments belonging to arenites and metabasalts were sampled starting from their respective outcrops, which have limited spatial extent. This sampling methodology allowed the establishment of a causal relationship between changes in shape and distance travelled by the particles. This also allowed the assessment of the variability of shape indices of freshly produced fragments, whose effect was accounted for by applying the model to different percentiles of the shape distribution. Moreover, these lithologies are expected to have very different mechanical properties, therefore allowing the qualitative comparison of the effect of material "resistance" on the evolution of sediment shape.

3.2 THEORETICAL FRAMEWORK

3.2.1 Background

Sediment particles in a river are subject to a range of forces due to their interactions with the fluid and other sediments. These forces vary in magnitude and frequency, depending on particle-specific properties, such as their size and mechanical resistance, as well as properties related to the transport environment, such as the hydrodynamics (Lamb et al., 2017; Yager et al., 2018; Maniatis et al., 2020; Pierce et al., 2022). The stresses imposed on sediment particles, therefore, may also vary in terms of their magnitude and frequency, and may lead to their partial or complete breakage (Bodek and Jerolmack, 2021; Larimer et al., 2022; Turowski et al., 2023). To upscale small-scale interactions at the grain level to the scale of a river reach, simplifications are required to capture essential dynamics while avoiding excessive parameterisation.

The study of sediment attrition in fluvial systems has a long-standing history (Wentworth, 1919; Wadell, 1932; Krumbein, 1941; Kuenen, 1956; Firey, 1974; Bloore, 1977; Kodama, 1994). A key empirical observation by Sternberg (1875) is the exponential reduction in median particle size along the length of a river, expressed by equation 3.1.

$$D_{50}(x) = D_{50}(x = 0)e^{-k \cdot x} \qquad 3.1$$

Where D_{50} is the median size of the sediment population at a distance x, from a chosen reference point along the river, and k is the Sternberg coefficient, which controls its spatial scaling, with units inverse to distance. Such observation has been repeated in different settings (Surian, 2002; Frings, 2008; Szabó et al., 2013) and, albeit being empirical in nature, this relation is often referred to as Sternberg's law. Although in most cases, the longitudinal decay of the median size of sediment could be explained using a constant Sternberg coefficient, a spatially variable value has also been proposed (Adams, 1979b). The decay of sediment size along a river depends, though, also on the nature of the sediment transport process itself. The transport of sediment by a moving fluid is a process characterised by thresholds and strong nonlinearity. Thresholds refer to the fact that a flow with a certain "strength" is only capable of entraining particles smaller than a certain size. Nonlinearities refer to the fact that, once particles are in motion, the relationship between the sediment transport rate and the fluid velocity can be approximated by a power law with an exponent much larger than 2. The combination of these two facts leads to smaller particles moving, on average, more frequently and covering longer distances in the same amount of time, compared to bigger ones.

This phenomenon is referred to as "selective transport" and contributes to the empirical observations that, further downstream, it is possible to find a higher proportion of smaller particles. The empirical observation of Sternberg has therefore been attributed to a combination of attrition and selective transport (Surian, 2002; Frings, 2008; Litwin Miller et al., 2014), with these two processes having different relative importance in different cases.

Since the exponential decay of sediment sizes can be attributed to the combination of attrition and selective transport, it is relevant to assess which spatial trend should be expected as a consequence of attrition alone. Litwin Miller et al. (2014) provided a theoretical explanation assuming the variation of the mass of a particle, M, due to attrition, to be proportional to its kinetic energy: $\frac{dM}{dt} \propto -M{u_s}^2$. The velocity of a particle, u_s, can be considered proportional to the fluid velocity, u_f, (Lajeunesse et al., 2010) which in turn varies very slowly with discharge (Parker, 1991). A particle's velocity can therefore be considered constant, in first approximation, which means that the distance it covered is proportional to time: $dx \propto u_s dt$. Consequently, $\frac{dM}{M} \propto -u_s dx$, which leads to an exponential decay of the particle's mass due to attrition alone:

$$M(x) \propto M(x = 0)e^{-k_a x} \qquad 3.2$$

Where k_a is the coefficient of Sternberg's law accounting for the effects of attrition. Additional evidence of an exponential decay of particles' mass due to attrition (equation 3.2) comes from the results of discrete element models. In the experiments by Pál et al. (2021), the mass M of a particle subject to impacts was found to decay exponentially with the number of impacts, N_j, multiplied by a certain threshold velocity v_0 required to produce chipping, raised to an exponent $\alpha \approx 2$ (equation 3.3):

$$M \propto e^{-N_j \cdot v_0^{\alpha}} \qquad 3.3$$

In channelised sediment transport, this may be interpreted as the cumulative kinetic energy received from repeated N_j impacts with velocity v_0, against the boundaries and other particles.

Finally, since both selective transport and attrition, independently, lead to an exponential decay of particles' masses, Sternberg's coefficient, k, can be conceptualised as the sum of two components: one due to selective transport, k_s, and another due to attrition, k_a (equation 3.4) (Szabó et al., 2015).

$$k = k_s + k_a \qquad 3.4$$

To summarise, particles' attrition leads to their mass loss, which scales exponentially with the distance they have travelled along a river course. In this respect, mass loss is usually considered in relative terms: the relative mass loss of a particle that had an initial mass M_0, and reached a mass M after a distance $\mathcal{L}$, is defined as: $\mu(\mathcal{L}) = \frac{M_0 - M}{M_0}$.

On the other hand, attrition also leads to particles changing their size and shape. Relationships between the relative mass loss of a particle and its shape are called geometric models of attrition. They suggest the possibility of linking the particle's shape to its relative mass loss, which can then be scaled spatially using an exponential function as previously discussed. As mentioned in the Chapter 3.1, several geometric models have been proposed (Domokos and Gibbons, 2018; Domokos and Lángi, 2018) but curvature-driven flow has proven capable of reproducing the evolution of a series of shape parameters due to chipping in different fluvial contexts. According to this model, the surface of a pebble will "shrink" (flow) under the effect of chipping, in such a way that the velocity of shrinking v (locally normal to the surface) is proportional to the curvature of the surface:

$$v = -c_v(1 + c_H H + c_G G) \qquad 3.5$$

Where $H = \frac{1}{2}(k_1 + k_2)$, is the mean of the two principal curvatures of the surface, $G = k_1 k_2$, is the Gaussian curvature, and c_v, c_H and c_G are scaling parameters. The application of equation 3.5 to model the shape evolution of sediments collected in the field requires the acquisition of the 3D shape of each particle. This is because the principal curvatures, k_1 and k_2, are orthogonal to each other and, therefore, they cannot be estimated using 2D images. Since the acquisition of the 3D shape of a large number of particles requires expensive instruments, most studies use shape parameters that can be measured using 2D images (Szabó et al., 2013; Pokhrel et al., 2024; Cattapan et al., 2024; Takahashi et al., 2025b). In particular, the isoperimetric ratio IR, defined as:

$$IR = \frac{4\pi A}{P^2} \qquad 3.6$$

where A is the particle's projected area and P is its perimeter, measures how a 2D shape differs overall from a perfect circle. This parameter is often also called circularity, and its values are bounded between 0 and 1, only reached by a circle. Circularity is widely used because a series of theoretical constraints are known on its relationship with the relative mass loss μ of a particle, under the assumption of curvature-driven attrition, equation 3.5 (Novák-Szabó et al., 2018). Specifically, the function $IR = f(\mu)$, should exhibit a vertical tangent for $\mu = 0$, a horizontal tangent for $\mu = 1$, be monotonically increasing, and possess a negative second derivative, indicating convexity (Figure 3.1 b).

Out of these properties, the most important is the monotonic increase of circularity with relative mass loss, because it implies a univocal relationship with travel distance. The isoperimetric ratio has been used to estimate pebbles' travel distances on Mars (Szabó et al., 2015) and is increasingly applied to terrestrial river systems (Pokhrel et al., 2024). However, shape descriptors like the isoperimetric ratio may be influenced by particle elongation and roundness (Roussillon et al., 2009;Quick et al. 2019). Elongation (e) is defined as the ratio of the intermediate (l_2) to the longest (l_1) axis, while roundness relates to the sharpness of its vertices. A smooth, but elongated particle may exhibit the same isoperimetric ratio as a more angular one with elongation equal to 1. To remove the effect of elongation, the normalised isoperimetric ratio is used:

$$IR_n = \frac{IR}{IR_t} \tag{3.7}$$

Where IR_t is the theoretical maximum isoperimetric ratio for an ellipse with the same elongation.

$$IR_t = \pi(l_1 + l_2)\left(1 + \left(3h/\left(10 + (4 - 3h)^{1/2}\right)\right)\right) \tag{3.8}$$

where

$$h = (l_1 - l_2)^2/(l_1 + l_2)^2 \tag{3.9}$$

The normalised isoperimetric ratio has already been used by Quick et al. (2019) and Pokhrel et al. (2024) to describe the rounding of conglomerates in the Himalayan rivers and estimate their travel distance. However, in their monitoring, they consider entire sub-catchments as contributing areas for the lithologies that were used as tracers. Without tracking particles from their outcrops, it is not possible to estimate what their initial circularity was for $\mu = 0$. This is important because it allows one to impose the theoretical constraint of the vertical tangent of the function $IR = f(\mu)$. For this reason, in the current study, tracer lithologies were sampled starting from their respective outcrops, along headwater streams. Monitoring headwater streams, with slopes close to 10^{-1} also allows us to assess the degree to which curvature-driven flow might be able to describe sediment shape evolution in reaches where fragmentation might be significant.

The vertical tangent of $f(\mu)$ implies that the circularity of particles changes extremely rapidly for small values of mass loss. This means that the initial part of the path of a particle is where it is subject to the sharpest change in shape. For this reason, two opposite approaches are possible for data collection campaigns, depending on the objective of a study. The first is the approach adopted by most field studies to date, and it involves using tracer lithologies whose source areas are quite wide, extending over entire sub-catchments.

These will be called diffuse sources. Doing this allows one to average the travel distance of particles, coming from different parts of the sub-catchment, and smooth the initial sharp changes of circularity due to particles having $\mu \approx 0$. One drawback of this approach is that, without knowing the initial distribution of circularity of fragments produced by the outcrops, the observed variability in sediment shape is fully attributed to different mass loss values, and therefore to different travel distances, without considering the inherent heterogeneity of IR at the sources.

An alternative approach is the one proposed in this study, which uses small outcrops of lithologies that are relatively rare within a catchment and are monitored starting from their outcrops. This allows the estimation of their initial circularity and the monitoring of their sharp transition to a more circular shape. These will be called point sources.

3.2.2 Proposed model and research hypotheses

We propose a model for the spatial evolution of normalised isoperimetric ratio of pebbles based on the following premises: the relationship between normalised isoperimetric ratio and relative mass loss is assumed to agree with the constraints of curvature flow attrition; and the mass of a particle is assumed to decrease exponentially with the distance it has travelled, in agreement with Sternberg's law. This exponential decrease represents one possible spatial scaling for the attrition process, although alternative assumptions can be easily implemented and tested. In the following, the term circularity, C, will be used, for simplicity, as a synonym for the normalised isoperimetric ratio, IR_n. The model is based on the following assumptions:

- A Lagrangian coordinate system is adopted, with the spatial coordinate, x, starting from each source for the lithology of interest and following the direction of steepest descent.
- Particles' attrition is a consequence of their impacts during motion, while passive attrition due to them being impacted by moving particles while remaining stationary on the riverbed is neglected. Consequently, changes in particles' circularity are assumed to depend only on their travel distance, irrespective of the passing of time, t.
- Chipping attrition is the process responsible for the majority of mass loss of particles, so that curvature-driven flow can be applied.
- The probability distribution of the normalised isoperimetric ratio of the fragment at the sources is assumed to be independent of time and space. This means that all outcrops of a given lithology are assumed to produce fragments whose IR_n has the same probability distribution everywhere at any moment. This independence can be summarised by the following relationship: $P_0(IR_n|x,t) = P_0(IR_n)$, where P_0 represents the probability of IR_n, at the source for the lithology of interest.

- Particles have homogeneous mechanical properties, as can be the case when considering a single lithology. If the variability in resistance among different particles is negligible, their trajectories in the IR_n, μ space can be assumed to converge to a meaningful average behaviour.

The model aims to describe the evolution of pebble shape starting from their individual point source. If the drainage area, at a certain position x, is characterised by the presence of multiple sources; their relative contribution must be estimated.

This estimation should account for the fact that different outcrops might produce fragments at different rates, as could be the case for streams with different stream power, cutting through different outcrops. Moreover, bedload particles are known to diffuse as they move downstream. Consequently, the relative contribution of sources located at greater distances from the position x, should be smaller than that of closer sources, for the same relative production. In the current application of the model, all outcrops are assumed to produce fragments at the same rate, while the contribution of different sources is assumed to decrease exponentially with their distance from the sampling location.

The probability distribution of particles' normalised isoperimetric ratio is independent of their mass. This assumption implies the possibility to disentangle the effects of attrition and selective transport because particles' selection as a function of the flow "strength" happens primarily based on their mass, and shape has a second-order effect (Cassel et al., 2021; Deal et al., 2023).

The proposed model is based on a superelliptical relationship for the function between circularity and relative mass loss ($IR = f(\mu)$). This functional relationship was chosen to satisfy the theoretical constraints outlined in Chapter 2.1, meaning a vertical tangent for $\mu = 0$, a horizontal tangent for $\mu = 1$, monotonic increase for increasing μ, and convexity; and to ensure dependency on the smallest number of measurable parameters:

$$\left(\frac{C - C_0}{C_{max} - C_0}\right)^a + \left(\frac{\mu_{max} - \mu}{\mu_{max}}\right)^a = 1 \qquad 3.10$$

Where C_{max} refers to the theoretical maximum value that C can attain: 1 in the case of a perfect circle, μ_{max} is the maximum value that the relative mass loss can potentially achieve, which is 1 when a particle is completely dissolved due to attrition, C_0 is the initial circularity of particles produced by an outcrop, and finally, the exponent a controls the rate at which particles' circularity increases as a function of relative mass loss. This parameter will hereafter be referred to as the rounding coefficient (Figure 3.1 b).

As discussed in Chapter 3.2.1, mass loss scales with the cumulative energy imparted by collisions. In the fluvial context, the spatial scaling of mass loss due to chipping is assumed to follow an exponential decay with travel distance, $\mathcal{L}$:

$$\mu(\mathcal{L}) = 1 - e^{-k_a \cdot \mathcal{L}} \qquad 3.11$$

Where k_a is the attrition coefficient, representing the balance between the energy delivered to the particles and the lithological unit's resistance to abrasion (Figure 3.1 a). This parameter reflects both the environmental energy (e.g., impact velocity and frequency) and the lithological properties of the sediment, potentially parametrised through quantities such as the brittle attrition number (Litwin Miller and Jerolmack, 2021). At present, k_a can only be determined through the fitting of field measurements. While decoupling the dependency on material and environmental factors is feasible, it lies beyond the scope of this work. Once such a decoupling is achieved, the proposed framework could allow for predictions of particle shape evolution based solely on measurable properties.

By combining equations 3.10 and 3.11, the resulting model provides a physically grounded formulation for estimating the circularity of coarse sediment particles (Figure 3.1 c):

$$C(\mathcal{L}) = C_0 + (C_{max} - C_0)\left[1 - \left(1 - \frac{1 - e^{-k_a \mathcal{L}}}{\mu_{max}}\right)^a\right]^{\frac{1}{a}} \qquad 3.12$$

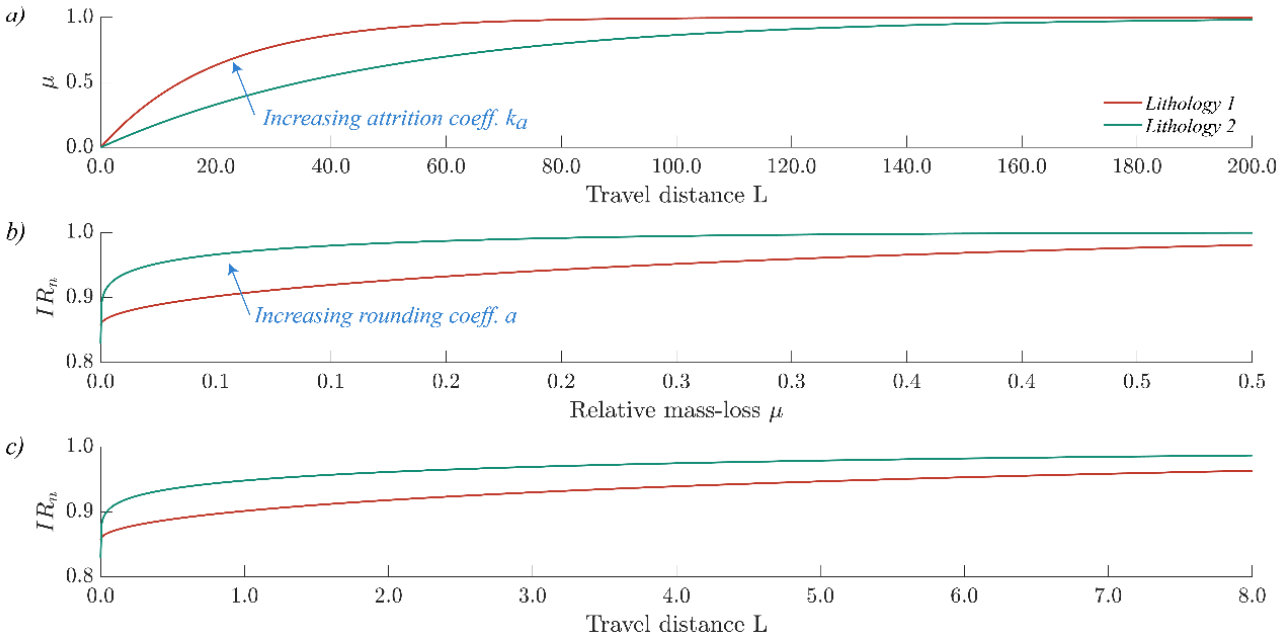

Figure 3.1. Graphical representation of the proposed model. a) Increase of relative mass loss with distance according to the Sternberg Law. b) Proposed superelliptical relationship between normalised isoperimetric ratio and relative mass loss. c) Combination of a) and b).

3.3 METHODS

3.3.1 Study area

The Sarzana Stream, a small alpine tributary in the middle reach of the Piave River basin (north-eastern Italy), was selected to test the performance of the proposed model. This alpine stream is 8.7 km in length and drains a catchment of approximately 25.2 km^2. Elevations range from 2872 m a.s.l. at the summit of Mount Agner to around 563 m a.s.l. at the confluence with the Cordevole Torrent, with a mean elevation of approximately 1413 m a.s.l. The catchment has a SW-NE orientation and is bounded by the dolomites of the Agner group on the northwest side (hydrographic left-hand side) and the gentler slopes of the Col Alt and Col Armarolo on the southeast side (hydrographic right-hand side), with elevations around 1527 m a.s.l. (Figure 3.2).

The morphology of the catchment is highly asymmetric, with the northern side accounting for 18.6 km^2 and an average slope of 72%, compared to 6.6 km^2 and 44% on the southern side. Forests cover approximately 68% of the catchment, with coniferous and broadleaf species representing 38.4% and 23.1% of the area, respectively (European Union, Copernicus Land Monitoring Service, 2018). The climate is classified as Cfc under the Köpen classification, with mean annual temperatures between 3.3°C and 13.1°C, annual precipitation of about 1391 mm, and maximum annual evapotranspiration of 564 mm (Barbi et al., 2013).

The Sarzana Catchment is geologically shaped by the Alpine Orogeny, with bedrock comprising predominantly Mesozoic sedimentary and volcanic formations. Arenites (sandstones), formed in marine environments during the Jurassic–Cretaceous, are widespread, while metabasaltic outcrops, interpreted as ophiolitic remnants of the Tethys Ocean, are locally present alongside interbedded marls and limestones. According to the Veneto Region lithological map (2016), sandstone, siltstone, and conglomerate units cover ~3.1% of the catchment, and metabasalts and metavolcaniclastic rocks ~0.7%, with just two localised outcrops (Figure 3.2). The limited extent of these types of rocks and their different mechanical properties make this catchment an ideal setting to evaluate the proposed model for coarse sediment shape evolution in mountainous river systems.

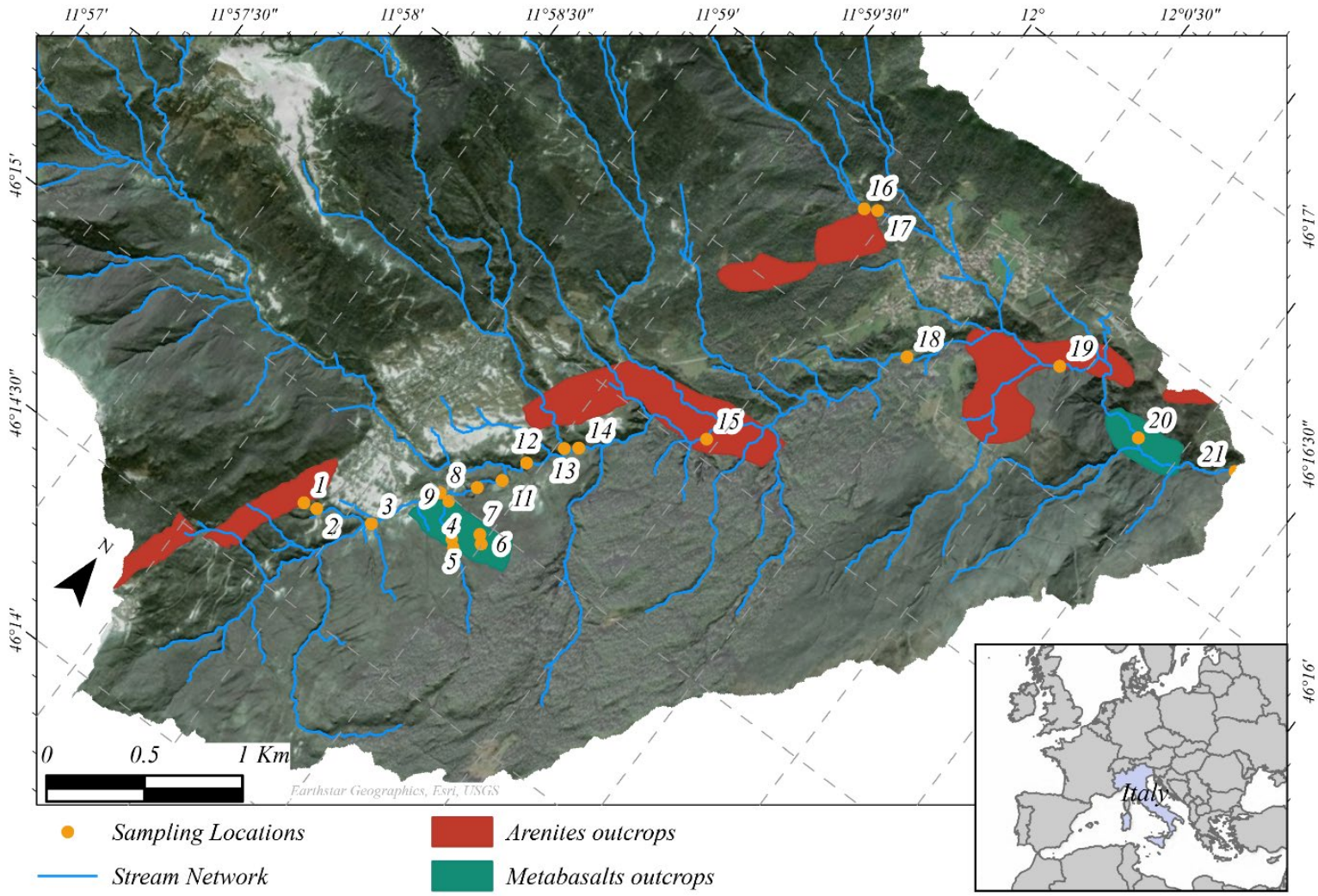

Figure 3.2. Map of the Sarzana Stream catchment with indication of arenites and metabasalts outcrops and sampling locations.

3.3.2 Data collection

Outcrops of different lithologies were identified using the official digital map "Database of the different lithologies that make up the territory of the Veneto Region scale 1:250,000" (2016), and verified in the field. This database consists of a polygon shapefile, providing the position and extent of the different lithologies within the Veneto Region, of which the Sarzana Catchment is part. This map illustrates seven arenites outcrops and two metabasalts outcrops within the Sarzana Catchment. Field observations confirmed that sediment sources of these lithologies are limited to the banks of minor creeks, eroding through the outcrops, with negligible diffuse inputs, which were not observed during this study (Figure 3.4 a-d).

For the metabasalts, one outcrop is located on the upper side of the catchment and is intersected by two small creeks on the hydrological right-hand side, which act as point sources. The first, location 4 (Figure 3.2), is situated at a distance of approximately 6140 m from the outlet, along a creek identified as Val. d'Uglioni, the second (location 6 in Figure 3.2) is at a distance of around 6010 m from the outlet. The second outcrop is located along the Sarzana Stream, at a distance of approximately 667 m from the outlet. There, it was not possible to clearly separate newly produced fragments from the metabasalts transported from upstream. Therefore, only the most upstream outcrop and all locations upstream of the second outcrop were considered for the calibration of the proposed model. These sampling locations define the calibration path for metabasalts, which includes locations 4, 5, 9, 10, 11, 12, 14, 15, 18, and 19.

For the arenites, seven outcrops are located both on the left-hand side of the catchment and along the Sarzana Stream itself. The most upstream point source sampled was chosen due to accessibility constraints, and is part of the second most upstream outcrop (location 1 in Figure 3.2). The set of locations composing the calibration path for arenites was locations 1, 2, 3, and 12. Moreover, two additional arenite sources were sampled: one along the Sarzana Stream, location 15, and one on a tributary, location 16. Given the presence of seven arenite outcrops, additional locations were sampled to assess the model's performance in the presence of multiple point sources (locations 13, 14, 15, 16, 17, 18, and 19).

In six locations along the Sarzana Stream (locations 11, 12, 15, 18, 19, and 20), sediments representing a mixture of all available lithologies were collected using the Wolman pebble count method (Figure 3.3).

Sediment shape data were obtained from digital image analysis. Pebbles were collected during surveys between April 2019 and April 2024. Within the channel, particles were sampled from bars and in riverbeds during low-flow conditions.

Each particle was washed to remove dust or vegetation, dried with a cloth to avoid reflection, and placed on a white background with its maximum projected area facing upwards. A scale was included in each image for accurate scaling. Image processing followed the methodology of Cattapan et al. (2024) (Figure 3.4 e-h). Shape analysis was conducted using the model developed by Zheng and Hryciw (2015).

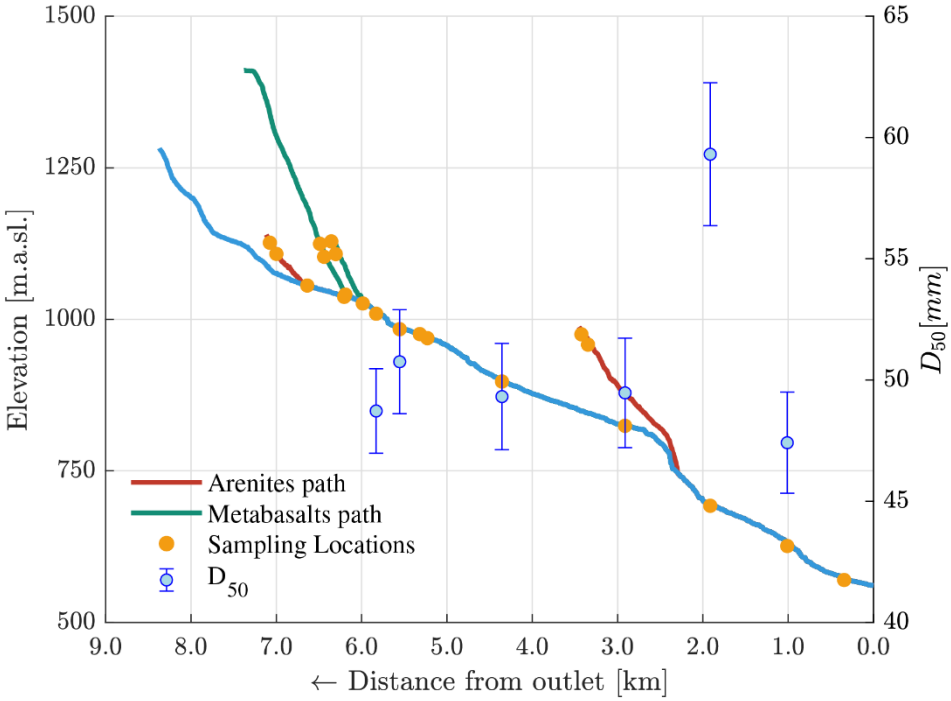

Figure 3.3. Elevation profile and sampling locations. Median and standard error of grain size of the bed material.

Arenite and metabasalt outcrops cover a very small portion of the catchment area; therefore, their relative contribution to the overall sediment flux is limited. As a consequence, their relative presence in the riverbed material is also limited, and, in most sampling locations, it was difficult to find a high number of tracer particles. The analysis presented here is based on a total of 449 arenite particles from source locations, 797 arenite particles from non-source locations, 105 metabasalt particles from metabasalt sources, and 659 metabasalt particles from non-source locations. The average number of particles sampled per location is 96, 51, and 125 for Arenites, Metabasalts, and mixed lithology samples, respectively. A detailed summary of the dataset is provided in Table A1a-A1d.

Sampling coordinates were acquired using an RTK GNSS receiver (Emlid RS3). Distances between sites were computed along the steepest descent, using a 5x5 m digital elevation model (DEM) from the Veneto Region (derived from Lidar; https://idt2.regione.veneto.it/).

The spatial extent of both lithological units was determined using the previously mentioned polygon shapefile "Database of the different lithologies that make up the territory of the Veneto Region scale 1:250,000," (2016). For each sampling point, intersections between local drainage catchments and mapped lithological outcrops were computed to identify which point sources contributed to each sampling location.

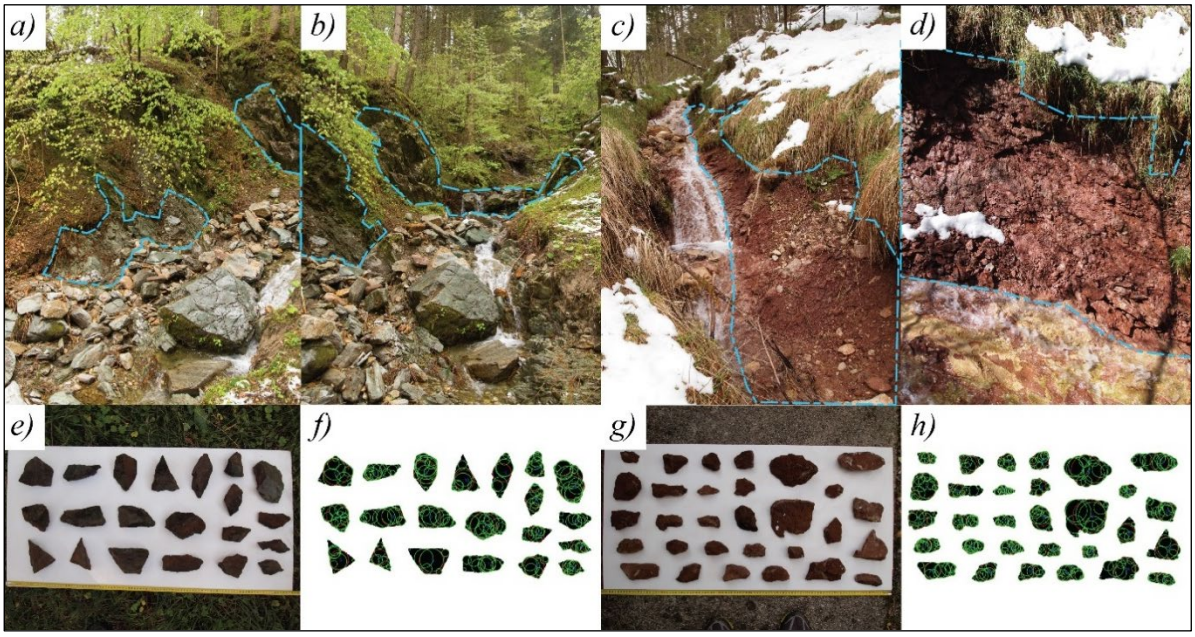

Figure 3.4. a–b: Outcrop of metabasalts, with boundaries highlighted by dashed blue lines. c–d: Outcrop of arenites, also delineated by dashed blue lines. e,g: Photographs of metabasalts (e) and arenites (g) taken at their respective source sites. f,h: Corresponding processed images.

3.3.3 Selection of the Shape Parameter

Several parameters have historically been proposed to characterise sediment shape, and the image analysis method used in the field campaign provides a wide selection of them (Cattapan et al., 2024). Since the objective of this work is to propose and test a mechanistic relationship between sediment shape and their travel distance, the chosen parameter needs to be a monotonic function of the mass lost by the sediment. The selection of which shape parameter presented a closer evolution to that of a monotonic function was done by plotting their longitudinal evolution for one point source of metabasalts and visually comparing their behaviour (Figure 3.5).

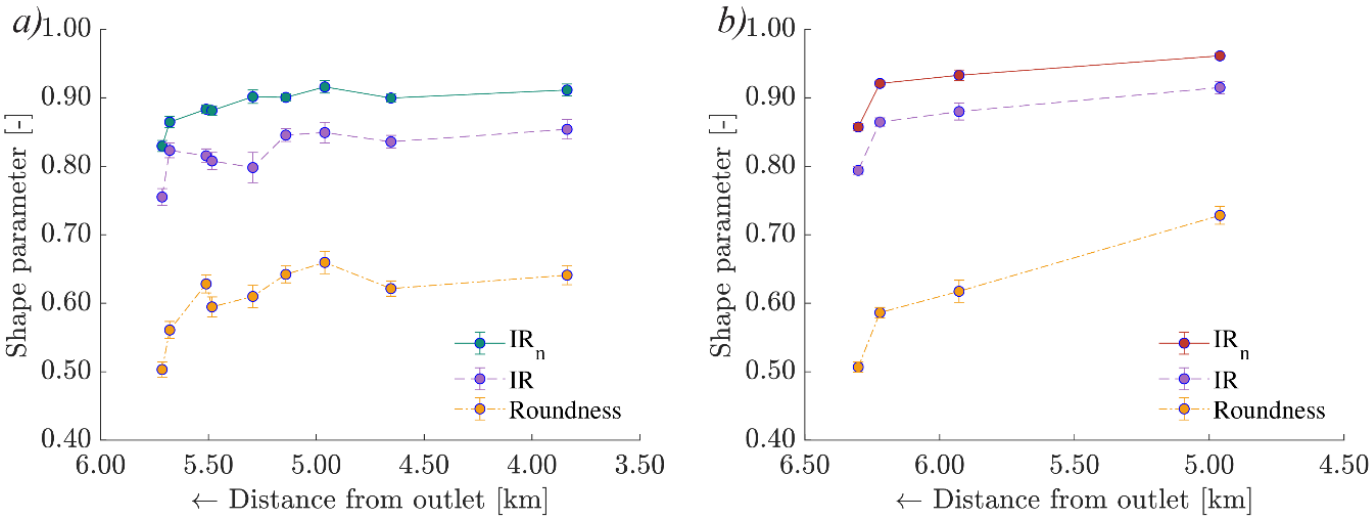

Figure 3.5. Longitudinal evolution of grain shape indices for: a) metabasalts, and b) arenites.

No statistical test was needed, since the normalised isoperimetric ratio (IR_n) clearly showed the most continuously increasing trend. The selection was based on the metabasalts data because the spatial extent of their outcrop is very limited, which translates into very similar travel distances. Therefore, the evolution of shape parameters reflects primarily the relationship between shape and mass loss, being less affected by the variability of travel distances.

3.3.4 Modelling approaches

The image analysis does not allow tracking the shape evolution of individual particles. The proposed model 3.12 is therefore applied to reproduce different statistics of the distribution of the shape parameter. Three modelling approaches are then used to answer three research questions.

Model for mean cross-section shape parameter for single-sourced lithologies (approach M1)

Initially, the model is applied to estimate the average of IR_n from single point sources. For each lithology (arenites and metabasalts), one point source is considered (locations 1 and 4 in Figure 3.2, respectively), while the set of locations composing the calibration path for each lithology can be found in the Chapter 3.3.2. In this case, the rounding coefficient a is assumed to depend solely on lithology, while the attrition coefficient k_a is considered constant across the river network, consistent with Sternberg's Law. This modelling approach allows for assessing how well the proposed model can reproduce the evolution of mean particles' circularity and will be referred to as M1.

Model for cross-section shape parameter percentiles for single-sourced lithologies (approach M2)

Since the curvature-driven flow model predicts an asymptotic convergence of particles' shape, the proposed model (equation 3.12) is also applied to different percentiles of the distribution of IR_n, for the same locations used in M1. In this case, the rounding coefficient a can vary across different percentiles, while the attrition coefficient k_a is considered constant across the river network. In this way, it is possible to assess whether the initial distribution of IR_n tends to converge or disperse, and which is the relationship between the initial circularity of pebbles at their source and their rounding coefficients. The percentiles used are 5%, 10%, 20%, 30%, 40%, 50%, 60%, 70%, 80%, 90% and 95%. This modelling approach will be referred to as M2.

Model for mean cross-section shape parameter for spatially distributed lithology sources (approach M3)

Finally, since there are multiple arenite outcrops within the catchment, the proposed model (equation 3.12) is then applied to represent the evolution of the average IR_n along the Sarzana Stream, considering multiple point source locations. These point sources are used to simplify the spatial distribution of arenites outcrops. This modelling approach will be referred to as M3.

3.3.5 Model parametrisation

Calibration of the model parameters is carried out in the modelling approaches M1 and M2 but since the model is applied to different statistics of the distribution of IR_n, namely, the mean of IR_n in M1 and different percentiles of IR_n in M2, the calibration procedure will be described using the generic term "shape parameter".

The error function is defined as the difference between the measured value of the shape parameter at each sampling location i, denoted $IR_{n,i}^{mes}$, and its modelled counterpart $IR_{n,i}^{mod}$, which is a function of the calibration parameters a and k_a: $Error = IR_{n,i}^{mes} - IR_{n,i}^{mod}(a, k_a)$.

The optimisation consisted of the minimisation of the Root Mean Squared Error ($RMSE$), which is chosen as the objective function. This is defined as (equation 3.13):

$$RMSE(a, k_a) = \sqrt{\frac{1}{N}\sum_{i=1}^{N}\left(IR_{n,i}^{mes} - IR_{n,i}^{mod}(a, k_a)\right)^2} \qquad 3.13$$

Where the sum is performed over the N sampling locations composing the calibration path for a given lithology, as described in the Chapter 3.3.2.

The optimisation procedure followed a trial-and-error approach: parameters a and k_a are sampled from a uniform and exponential distribution, respectively (Table 3.1 and Figure A2 in the Annexes), and the $RMSE$ for each parameter combination was computed. The set of parameters a and k_a that minimised the $RMSE$ is then selected as the optimal configuration.

Table 3.1. Model parameter ranges used for calibration.

Parameter	Unit	Min	Max	Spacing	Distribution
a	[-]	0.1	10	0.01	uniform
$k_{a,exponent}$	[-]	0.0	10	0.01	uniform
$k_a = 10^{-k_{a,exponent}}$	[km^{-1}]	1.0	10^{-10}	variable	exponential

3.4 RESULTS

3.4.1 General sedimentological characterisation

Samples having mixed lithology, collected using the Wolman pebble count method, show that the riverbed is composed mostly of pebbles and coarse gravel. The median grain size has an almost constant value of 49.6 mm in a range of distances between 5.7 and 2.6 km from the outlet. At a distance of approximately 1.6 km from the outlet (location 19 in Figure 3.3), the median grain size increases to 59.3 mm, but it soon decreases to 47.4 mm, after around 900 m.

The relatively small size of the samples did not allow splitting the datasets by size to analyse the IR_n of homogeneous size classes. Nonetheless, the correlation between dimensional metrics (longer and intermediate sizes, surface area, and perimeter), and the normalised isoperimetric ratio was computed using Pearson's r coefficient and its significance was tested with a t-test, using a significance level $\alpha = 0.05$.

Results show that, for both lithologies, IR_n is weakly correlated with any dimensional metric (see Table 3.2). This supports the hypothesis that, for this case study, the distributions of sediment shape and size are independent, so that selective transport has a negligible effect on the sampled distributions of sediment shape.

One aspect of novelty of this study involves the analysis of the shape of fragments produced by outcrops, which are used as sediment sources.

Table 3.2. Pearson's correlation coefficients (r) *and* p *values for correlations with normalised isoperimetric ratio and sediment size metrics.*

Lithology	Parameter	Area [mm^2]	Perimeter [mm]	l_1 [mm]	l_2 [mm]
Arenites	r	-0.109	-0.250	-0.214	-0.184
	p	0.00012	3.7E-19	2.4E-14	6.4E-11
Metabasalts	r	-0.091	-0.167	-0.110	-0.154
	p	0.01066	2.5E-06	0.00210	1.5E-05

For each lithology, IR_n values in point source locations are compared to those in non-source locations. First, IR_n distributions are tested for normality using an Anderson-Darling test, with a significance level $\alpha = 0.05$. Results lead to rejecting the null hypothesis of normality of all distributions. To compare the median of IR_n for source locations versus non-source locations, a Mann-Whitney U-test is then performed, with the same significance level. Results lead to rejecting the null hypothesis of same median values for the two distributions.

This suggests that the median IR_n in source locations are significantly different from non-source locations (Figure 3.6 a and b). Moreover, the same statistical analysis is performed to compare IR_n values for source locations of arenites against metabasalts. Results suggest that the median IR_n in source locations is specific to each lithology (Figure 3.6 c). A similar test leads to the same conclusion for non-source locations: the median IR_n in non-source locations are different for arenites and metabasalts (Figure 3.6 d).

After this initial analysis, where data are grouped based on their origin in source and non-source, irrespective of their sampling location, data are analysed in more detail. For each lithology, distributions of IR_n are compared for all possible pairs of sampling locations, using an Anderson-Darling test. This test assumes, as the null hypothesis, that the distribution of IR_n in two sampling locations is the same, and this is rejected if the $p < \alpha = 0.01$. Results indicate that, in almost all cases, the distribution of normalised isoperimetric ratios in source locations is significantly different from that in non-source locations. The only exception to this is represented by the comparison of the distributions of IR_n in location 4, which is a source of metabasalts, against location 7, which produced a $p \approx 0.26$. The distance between these two locations is only around 180 m, therefore, although the attrition process produces very fast initial changes in sediment shape, this distance is too small to lead to a significant change in the IR_n distributions (see Figure A1 and Table A2 and Table A3 for the results of these tests).

This shows that the distribution of IR_n in locations where particles have already been subject to a certain degree of mass loss is significantly different from the distribution in source locations. This result holds for both lithologies.

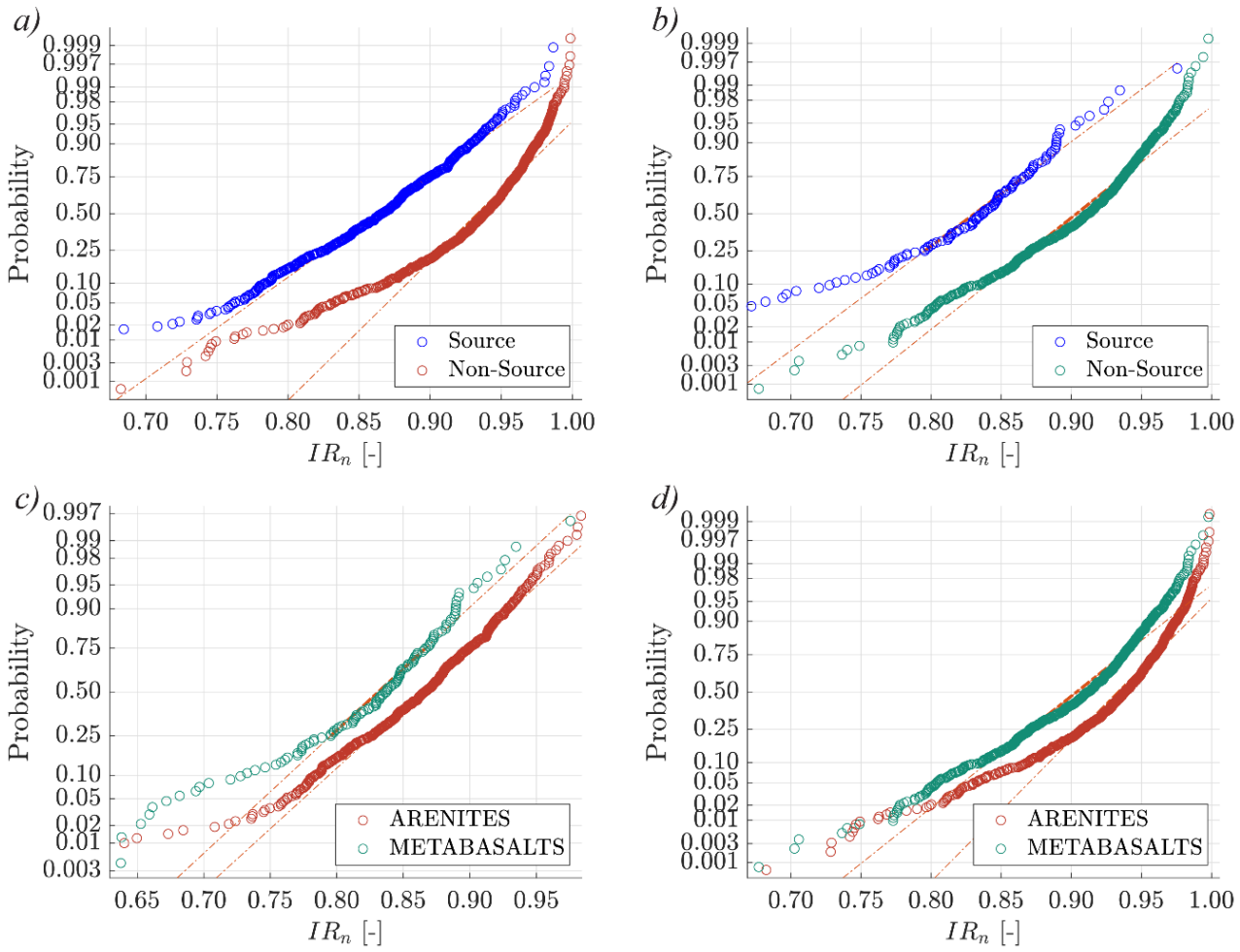

Figure 3.6. Cumulative distribution plots to test for normality. Dot-dashed lines represent values for normal distributions. a) Comparison of arenites source and non-source locations; b) Comparison of metabasalts source and non-source locations; c) Comparison of source locations; d) Comparison of non-source locations.

Overall, field data suggest that each lithology possesses a distinct signature in terms of the normalised isoperimetric ratios of the sediment fragments produced at the source. As a result, when modelling the evolution of particle shape using the normalised isoperimetric ratio, the initial distribution of this parameter should be specified according to the local lithology.

3.4.2 Model for mean cross-section shape parameter for single-sourced lithologies (approach M1)

In the modelling approach M1, one single point, location 4, is considered as a source for metabasalts. The minimisation of the RMSE for the average normalised isoperimetric ratio yields a rounding coefficient, a . of 5.94. This indicates a highly nonlinear relationship between metabasalts' shape and their relative mass loss. In contrast, the optimal attrition coefficient, k_a , is approximately $1x10^{-3}$ km-1, suggesting that metabasalts, due to their resistance, lose mass very slowly relative to the distance travelled along the river network (Table 3.3). As a reference, this means that in order to experience a relative mass loss of 10%, metabasalt particles would have to cover around 105 km.

The Mean Absolute Percentage Error ($MAPE$) of 0.64% indicates a good agreement between the model predictions and the observed values of normalised isoperimetric ratio (Figure 3.7).

Table 3.3. Optimised model parameters for averages of metabasalts.

C_0	a	k_a	$RMSE$	$MAPE$
0.83	5.94	0.00100	0.007	0.640%

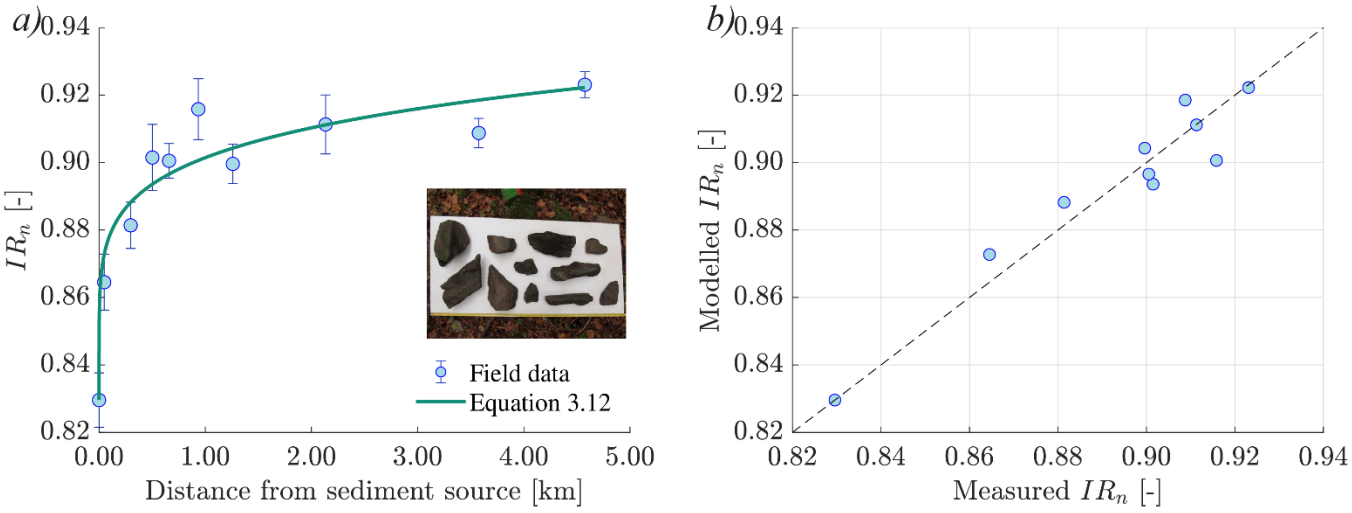

Figure 3.7. Model calibration results for metabasalts. a. Longitudinal evolution of the average normalised isoperimetric ratio along the calibration path; b. Scatter plot of modelled versus measured normalised isoperimetric ratios.

For arenites, one single point, location 1, is considered as a source for the calibration of model parameters in M1. The minimisation of the RMSE for the average normalised isoperimetric ratio results in a rounding coefficient, a, of 5.71, indicating that the shape

of these particles evolves just a bit slower with respect to relative mass loss compared to metabasalts. In contrast, the optimum attrition coefficient is approximately 0.017 km-1, suggesting that arenites, due to their lower mechanical strength, lose mass over a very short travel distance, an observation consistent with field evidence (Table 3.4). As a reference, this means that, in order to experience a relative mass loss of 10%, arenite particles would have to cover around 6.2 km, which is the same order of magnitude as the length of the Sarzana Stream.

The Mean Absolute Percentage Error of 0.34% confirms the model's strong ability to reproduce the observed values of the normalised isoperimetric ratio (Figure 3.8).

Table 3.4. Optimised model parameters for averages of arenites.

C_0	a	k_a	RMSE	MAPE
0.86	5.71	0.01698	0.004	0.336%

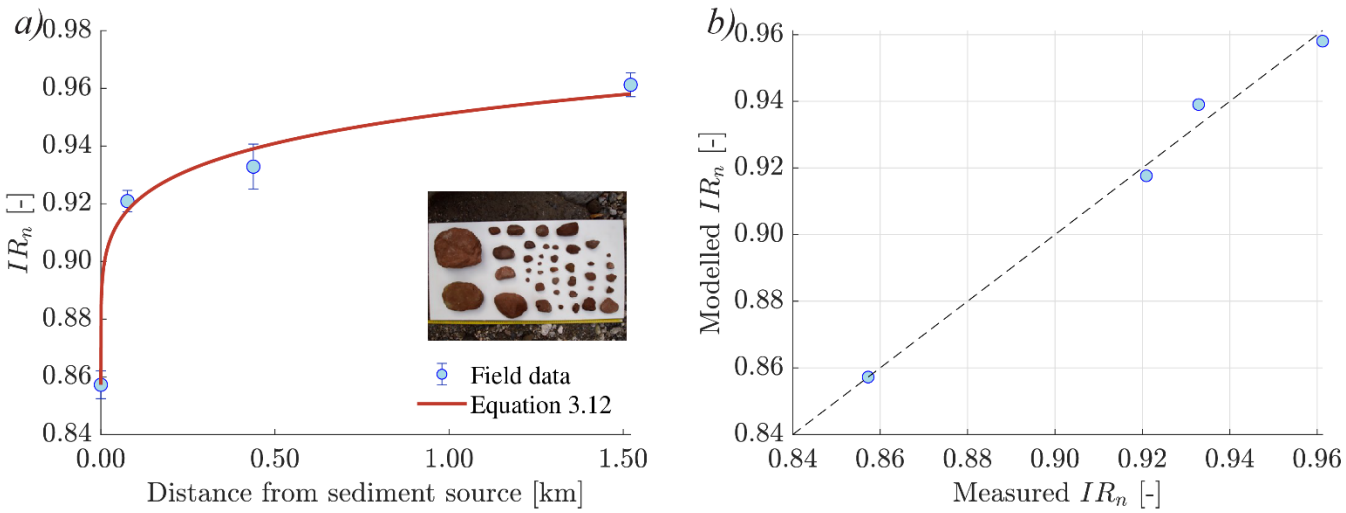

Figure 3.8. Model calibration results for arenites. a. Longitudinal evolution of the average normalised isoperimetric ratio along the calibration path; b. Scatter plot of modelled versus measured normalised isoperimetric ratios.

The comparison of the parameters' optimisation for arenites and metabasalts indicates that the relationship between normalised isoperimetric ratio and relative mass loss seems to be characterised by a similar rounding coefficient, a. On the contrary, the spatial scaling of mass losses is very different for the two lithologies, with the attrition coefficients, k_a, that differ by around one order of magnitude. This difference agrees with the intuitive expectation of higher resistance to attrition of metabasalts with respect to arenites. Plots of the objective function and of its minimum are provided in the Annexes.

3.4.3 Model for cross-section shape parameter percentiles for single-sourced lithologies (approach M2)

In this modelling approach, the sampling locations used to calibrate the model parameters are the same as in M1. The minimisation of the RMSE of the percentiles of the normalised isoperimetric ratio requires further explanation. In this case, the attrition coefficient, k_a, is assumed to be uniform for the whole river network, while different percentiles of IR_n were allowed to have different rounding coefficients. The algorithm is set up in this way: first, a value for the attrition coefficient, k_a, is sampled from the exponential distribution (Table 3.1). While keeping k_a constant, the model is applied to all percentiles, sampling the attrition coefficient, a, from a uniform distribution (Table 3.1). For each value of a, the RMSE is calculated for that percentile. The value of the rounding coefficient, a, that minimised the RMSE of a given percentile and for the current value of the attrition coefficient, k_a, is identified. This process is repeated for all percentiles and, summing their respective minimum RMSE, it is possible to find an overall RMSE, associated with the current value of the attrition coefficient, k_a, and with a set of rounding coefficients, a, one for each percentile. After cycling over all k_a values, it is possible to find the global minimum, therefore, the attrition coefficient, k_a, and the set of associated rounding coefficient values, a, that, overall, minimises the RMSE.

Application of the model to the percentiles of metabasalts normalised isoperimetric ratio results in slightly higher RMSE for small and large percentiles, while for percentiles close to 50%, results are coherent with those obtained in M1, where the model is applied to reproduce the averages of IR_n (Figure 3.9 a,b). This observation leads to a reflection on the relationship between IR_n and travel distance. Particles with low initial values of the normalised isoperimetric ratio are expected to provide the most information about the relationship between shape evolution and the travel distance because they are the ones with more potential for shape change. At the same time, though, they exhibit ample shape fluctuations compared to those with an average initial circular (Figure 3.9 a,b).

Interestingly, the optimal parameter values obtained in M2 differ from those obtained in M1, even when comparing the parameters for the average with those for the median (Table 3.5). This discrepancy arises because the optimisation algorithm aims to minimise the overall error across all quantiles, resulting in a compromise solution rather than the optimal parameter set for any single percentile.

Table 3.5. Optimised model parameters for metabasalts quantiles.

$\boldsymbol{Percentile}$	$\boldsymbol{C_0}$	$\boldsymbol{a}$	$\boldsymbol{k_a}$ $[\boldsymbol{km^{-1}}]$	$\boldsymbol{RMSE}$	$\boldsymbol{MAPE}$
5%	0.73	4.73	0.00065	0.015	1.285%
10%	0.76	5.07	0.00065	0.009	0.776%
20%	0.80	5.27	0.00065	0.012	1.130%
30%	0.81	5.75	0.00065	0.011	0.865%
40%	0.83	6.23	0.00065	0.011	0.915%
50%	0.83	6.94	0.00065	0.009	0.829%
60%	0.84	7.50	0.00065	0.007	0.577%
70%	0.86	7.84	0.00065	0.006	0.473%
80%	0.88	7.70	0.00065	0.009	0.710%
90%	0.89	8.88	0.00065	0.011	0.808%
95%	0.91	10.00	0.00065	0.010	0.662%

Application of the model to the percentiles of arenites normalised isoperimetric ratio results in an even lower RMSE. The introduction of an additional degree of freedom to the model, in the form of a variable rounding coefficient, enabled a more accurate representation of the shape parameter distribution (Figure 3.9 c,d). Moreover, as observed for metabasalts, the optimal parameters' values for the median differ from those obtained when modelling the average (Table 3.6).

Table 3.6. Optimised model parameter for arenites quantiles.

$\boldsymbol{Percentile}$	$\boldsymbol{C_0}$	$\boldsymbol{a}$	$\boldsymbol{k_a\ [km^{-1}]}$	$\boldsymbol{RMSE}$	$\boldsymbol{MAPE}$
5%	0.77	4.25	0.02512	0.006	0.475%
10%	0.79	4.45	0.02512	0.008	0.629%
20%	0.82	4.52	0.02512	0.008	0.605%
30%	0.84	4.46	0.02512	0.010	0.654%
40%	0.86	4.91	0.02512	0.003	0.197%
50%	0.86	5.41	0.02512	0.006	0.434%
60%	0.88	5.50	0.02512	0.006	0.460%
70%	0.88	6.49	0.02512	0.004	0.263%
80%	0.89	7.54	0.02512	0.001	0.045%
90%	0.91	7.67	0.02512	0.001	0.085%
95%	0.93	8.32	0.02512	0.001	0.102%

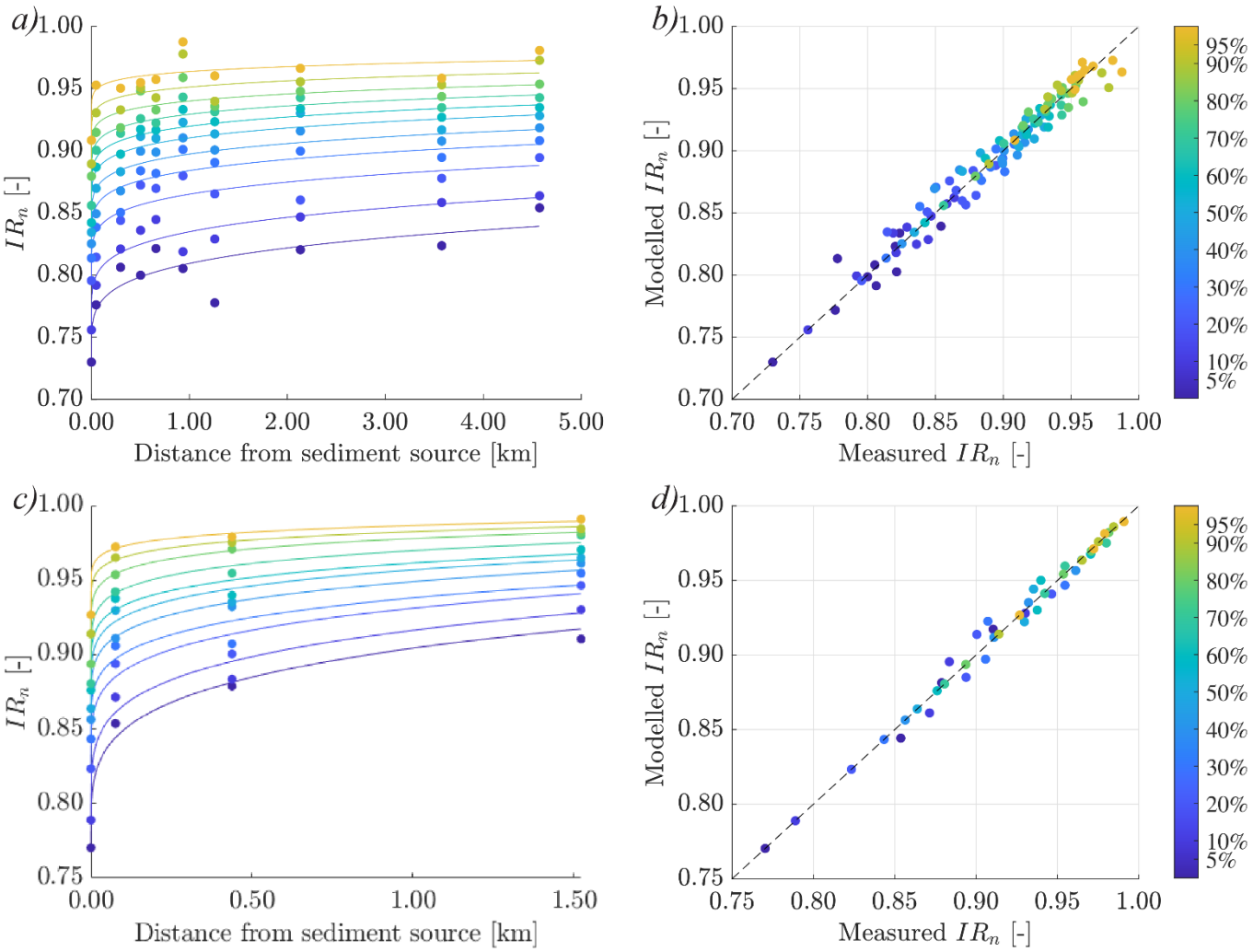

Figure 3.9 Model results for quantiles of normalised isoperimetric ratio of metabasalts (a, b) and arenites (c, d). Left: Longitudinal evolution of selected quantiles. Right: Scatter plot comparing modelled versus measured normalised isoperimetric ratios. The dashed 1:1 line serves as a reference.

3.4.4 Model for mean cross-section shape parameter for spatially distributed lithology sources (approach M3)

The "Database of the different lithologies that make up the territory of the Veneto Region scale 1:250,000" (2016) shows seven arenites outcrops within the Sarzana Stream catchment. This spatial configuration allowed the application of the proposed model to reproduce the shape evolution consequent to distributed inputs. In order to explicitly model the evolution of sediment shape deriving from spatially distributed inputs, one should compute, for each location x along a river course, the set of all travel distances between x and each outcrop pixel included in the local drainage area. This detailed description is quite complex and not justified, given the uncertainties related to the outcrops' extent present in the available lithological map. Different outcrops are therefore simplified according to two criteria: the areas most contributing with arenites particles to the Sarzana Stream are assumed to be the banks of streams cutting into the mapped outcrops. A buffer of 10 m around stream features is used to define the spatial extent of these contributing areas. This produces a set of areas, each of which is further simplified and treated as a point source. This simplification procedure produced sixteen point sources and is done to seek a balance between the realism of the representation of the spatial variability of the inputs and the treatability of the system.

The model is set up in this way: for each position located at a distance x from the outlet, the upstream contributing point sources are identified. Particles are assumed to enter the network with an initial normalised isoperimetric ratio equal to the average obtained by field measurements in source locations: $C_0 \approx 0.860$. For each of these sources, the equation 3.12 is used to estimate the shape that particles would have reached after having covered a distance $\mathcal{L}$ equal to the distance between the considered source area and the position x. Upstream sources are not equally contributing in terms of arenites sediments to a downstream location, but their relative importance decreases with increasing distance $\mathcal{L}$. In other words, the further away a source is from the position x, the less its contribution will be to the average shape of sediments found there. This is due to two main facts: the first is diffusion; bedload sediments are known to disperse while they move, and this dispersion implies that their relative presence in the riverbed decreases for longer distances. The second reason is that, since particles decrease in size due to attrition, some might become smaller than the smallest size sampled using the imaging method employed here. This truncation of the population of upstream contributing sources increases moving downstream, since a bigger proportion of particles can be expected to fall below the minimum size threshold. This process might be significant for less resistant rock types, like arenites, which can be estimated to lose around 10% of their mass in around 6 km of travel distance (see Chapter 3.4.2). Both processes, therefore, contribute to the decrease in the relative importance of further away sources. To account for these phenomena, a weighing function is introduced, estimating the relative contribution of source areas located at a distance $\mathcal{L}$ using an exponential probability density function:

$$P_{\mathcal{L}}(\mathcal{L}) = \frac{1}{\lambda} e^{-\frac{\mathcal{L}}{\lambda}} \quad 3.14$$

Where λ is the parameter of the distribution; it has the same unit of distance $\mathcal{L}$ and will be referred to as the weighing coefficient. The average normalised isoperimetric ratio, IR_n, of arenites at a distance x from the outlet is therefore computed as the weighted average of upstream sources' contributions (equation 3.12), using 3.14 as weights:

$$IR_n(x) = \frac{\sum_{i=1}^{N} IR_n(\mathcal{L}_i) P_{\mathcal{L}}(\mathcal{L}_i)}{\sum_{i=1}^{N} P_{\mathcal{L}}(\mathcal{L}_i)} \quad 3.15$$

Where the sum is performed over all N source areas located upstream of the position x along the network, and travel distances $\mathcal{L}_i$ are equal to the distance between the i^{th} source and the position x. The optimum value for the parameter λ is found by minimising the RMSE between the measured arenites' normalised isoperimetric ratio in the Sarzana Stream and model results. The minimisation is done through a trial-and-error algorithm, where λ is allowed to vary between 50 and 5000 m, with a spacing of 1 m. The minimum RMSE of 0.017 is obtained for a value of λ equal to 709 m (see Figure S5 in the Annexes). This means that the relative contribution of a source located at a distance higher than 2124 m is lower than 5%.

3.5 Discussion

3.5.1 Initial shape of fragments at sediment sources

While fragments produced by a series of brittle fracture processes have been shown to exhibit universal size and shape characteristics (Domokos et al., 2015), circularity was not among the parameters showing such behaviour. Some studies showed the dependence on lithology of the circularity of rock fragments produced by blasting in mine settings (Li et al., 2021). Other studies showed the difference in shape in natural gravel, compared to blasted rock fragments (Liu et al., 2025). The quantitative description of the shape of fragments produced in natural settings and their dependence on lithology has received less attention. The field data presented in the current study agree qualitatively with the previously mentioned results because the comparison of the shape distribution of fragments collected at their respective source locations suggests the existence of a distinct shape signature for each lithology. This observation merits further investigation, including a broader range of lithologies and an assessment of potential dependencies on mechanical properties and weathering conditions of the exposed outcrops. At the same time, this observation suggests the importance of using lithology-specific values of normalised isoperimetric ratio as boundary conditions when modelling the shape evolution of sediment in rivers.

3.5.2 Effect of lithology on spatial scaling of attrition

The results of the modelling approach M1 demonstrated that the model is capable of accurately reproducing the shape evolution of both lithologies, achieving MAPE values of 0.64% and 0.34% for arenites and metabasalts, respectively. Moreover, the values of attrition coefficients, k_a, estimated by model calibration against field data, show that arenites are expected to undergo a significantly higher mass loss than metabasalts for the same travel distance. Qualitative field observations might be misleading in this regard, because the initial size of arenites fragments is significantly smaller than that of metabasalts. As a consequence, one might be tempted to conclude that, since arenites particles are rarely found in sizes comparable to those of metabasalts, they undergo a faster mass loss, while they might be preferentially entrained and transported by the flow due to their smaller initial size, on average. These results are qualitatively in agreement with those of Takahashi et al. (2025), who tracked basalts and shale sediment along headwater streams. Nonetheless, they report a significant dependence of sediment shape on their size, which was not found in our data. In this respect, future research should solve a practical problem: the assessment of the combined effect of lithology and shape requires stratifying the sample into multiple subsets. This requires a large enough dataset, while, at the same time, in order to guarantee the source to be small enough to be considered as a point source, its relative contribution to the overall bed material would have to be small. The development of a sampling strategy that allows solving this dichotomy would represent a significant step forward.

3.5.3 Rounding rate and its dependence on the initial shape of fragments

The optimisation of model parameters performed in M1, concerning averages of IR_n, produced similar values for the rounding coefficient, a, of arenites and metabasalts, with slightly bigger values for the latter. This is in contrast with the values obtained in M2 and cannot be statistically verified. Moreover, the graph of the RMSE (see Figure A5.3 and Figure A5.4 in the Annexes) shows that this is more sensitive to changes in the attrition coefficient, k_a than in the rounding coefficient, a. This implies that possible uncertainties in the estimation of a are expected to produce smaller effects on the estimation of IR_n, compared to uncertainties in the attrition coefficient.

The results of M2 indicate that, for both lithologies, the values of the rounding coefficient, a, tend to increase for higher percentiles of IR_n. This means that fragments with an initial shape close to a circle tend to get round faster than originally less circular ones, for the same mass loss (Figure 3.10). This supports the intuitive interpretation that the nearer a particle is to a perfectly round form, the easier it is to increase its circularity by chipping off a small number of protruding edges. In this respect, recent results suggest a similar interpretation.

Figure 10 from Takahashi et al. (2025) shows a similar behaviour to Figure 3.10 and suggests that rounder particles at the sources tend to get rounder faster. In that case, authors could attribute the effect to particle size, which was not found to be significantly correlated with circularity, in the dataset of the current study.

Furthermore, for each quantile examined, metabasalts consistently display higher rounding coefficients than arenites. This implies that, for the same amount of relative mass loss, metabasalts tend to become rounder faster. A possible explanation is that, in the case of weaker materials such as arenites, the attrition process may fall outside the limits of applicability of the geometrical model, with fragmentation playing a greater role. This hypothesis deserves further investigation through controlled laboratory experiments. Nonetheless, the monotonic increase of the normalised isoperimetric ratio observed in the field data supports the model's applicability (Figure 3.10).

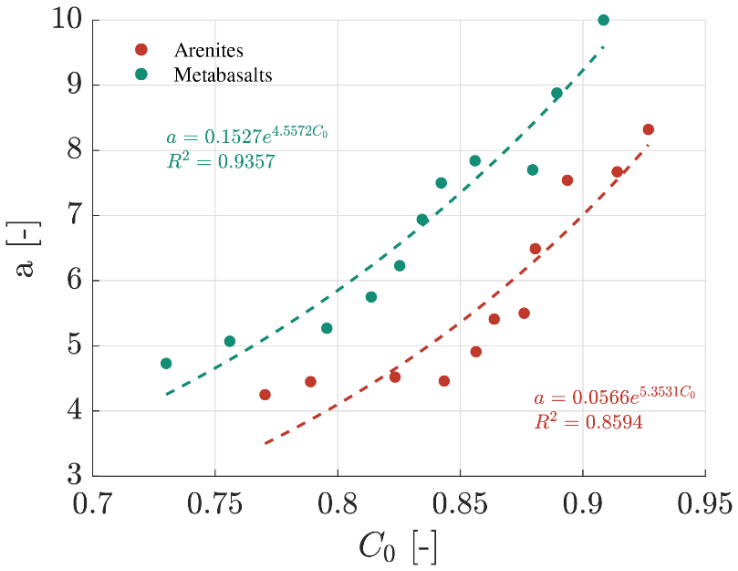

Figure 3.10. Relationship between the initial circularity of particles and the rounding coefficient.

3.5.4 Modelling sediment shape from point and distributed sources

As shown in Chapter 3.3.2, in the modelling approach M1, the model parameters are calibrated using four sampling locations 1, 2, 3, and 12, reported in Figure 3.11-a, without considering the outcrops located upstream of location 1. When assessing the combined effect of distributed sources, the model (equation 3.12) is applied to each point source location, using for a and k_a, the values obtained in M1.

The evolution of IR_n, for each point source is represented in Figure 3.11-a by a dashed blue line. Although the model is calibrated using only data relative to the point source 1, it is also able to capture the evolution of IR_n for the source 16, where field data are collected along a tributary to the Sarzana Stream. The superelliptical relationship has a vertical tangent for $\mu = 0$, which allows the IR_n to grow very rapidly from the values observed at arenites and metabasalts outcrops (0.86 and 0.83, respectively), to the higher values observed both along tributaries as well as along the Sarzana Stream. Unfortunately, no theoretical relationship between IR_n and μ is known to the authors for the case of fragmentation. Therefore, it is not possible to assess the relative contribution of fragmentation and chipping to the changes of shape that take place along steep headwater streams. Moreover, particles in locations 2 and 17, which are placed at a similar distance from their respective sources, have very similar IR_n, suggesting the consistency of the shape evolution for arenites close to their outcrops.

The model for multiple sources (3.15) is represented in Figure 3.11-a by a red line. It is possible to note that the model can reproduce quite well the spatial evolution of particles' shape from distributed sources. Nonetheless, in location 18, a significant drop in circularity is present, which is not captured by the model. This might be due to the presence of an arenite source that is not mapped in the lithological map with a scale of 1:250.000. The proposed model could be used, in this case, to estimate the maximum distance upstream of location 18 where such an unmapped source could be located, therefore turning the model into a diagnostic tool. Using the coefficients reported in Table 3.4 it is possible to estimate that the unmapped arenites source should be placed within 250 m upstream of the sampling location 18.

The integrated effect of spatially distributed sources produces a very noisy signal of normalised isoperimetric ratio (Figure 3.11). The small number of available sampling locations does not allow for the accurate estimation of the weighing coefficient and its dependencies on lithology and transport conditions. A spatially denser set of measures, possibly in different case studies, could provide more insights into these aspects.

Finally, the conclusions drawn here are subject to the hypothesis that the lithology database used covers all existing outcrops for the lithologies considered. Additional outcrops might impact the numerical values of model parameters estimated, but during the field campaign, no additional outcrop was found.

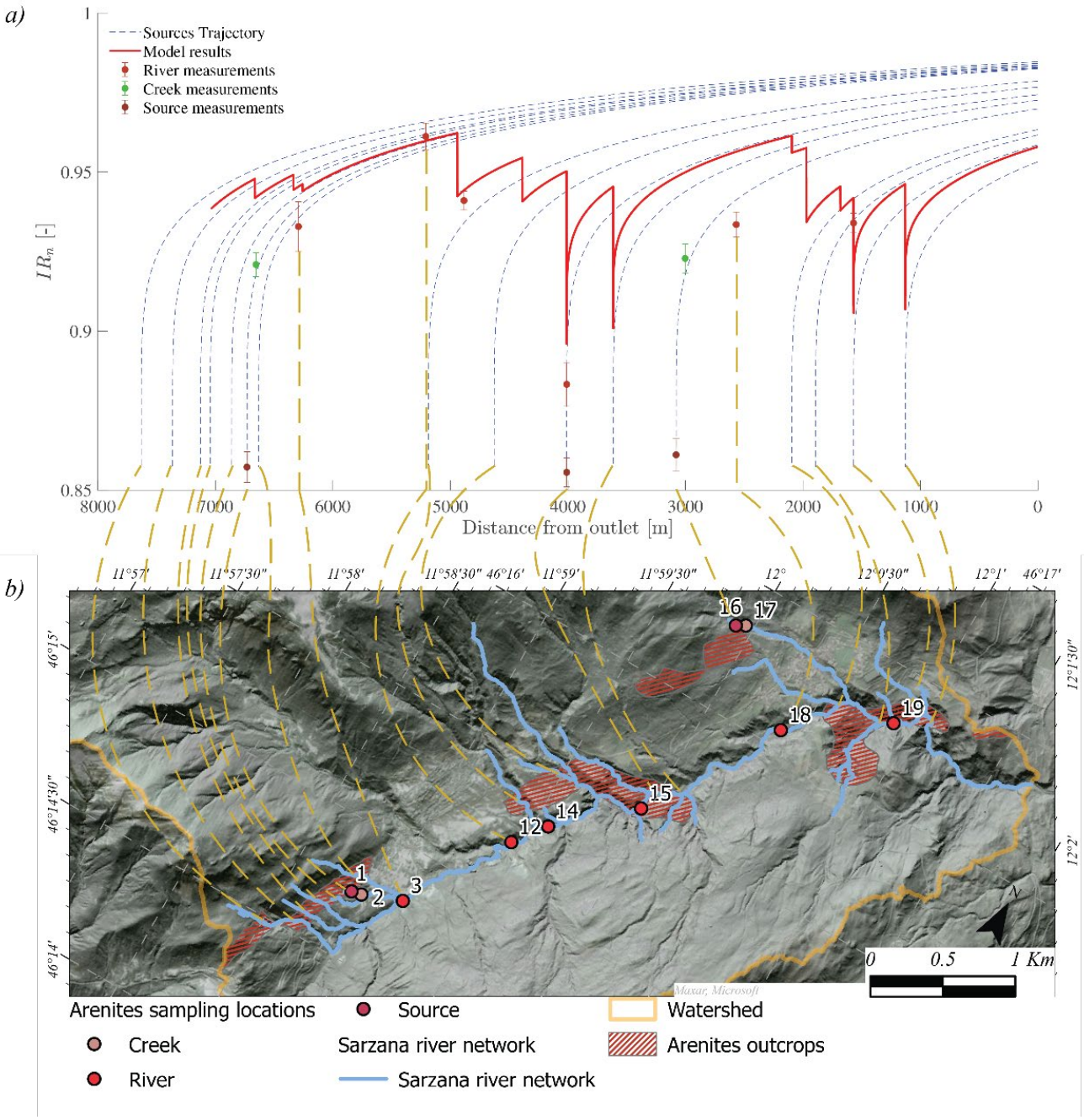

Figure 3.11. a) Longitudinal evolution of the normalised isoperimetric ratio of arenites from multiple sources. b) Map of sampling locations and arenites outcrops.

3.5.5 Test of an alternative geometric attrition pattern

The model presented in this study is developed to reproduce the average behaviour of particle shape evolution. When applied to different percentiles of the IR_n distribution, it is assumed that each subset of the population would evolve along its own trajectory in the μ, IR_n plane. This means that the slope of the curve $IR_n = f(\mu)$, for $\mu = 0$ may vary across percentiles (Figure 3.9-a and Figure 3.10-a) or, in other words, the initial rate of change of circularity is dependent on a particle's initial shape. More interestingly, this means that the rounding rate of a particle that is born more circular, is different from that of a particle that was born less circular, but has reached the same IR_n, after a certain mass loss μ. If confirmed, this modelling approach, which could explain well all percentiles of IR_n, would mean that the chipping attrition process is not only state-dependent, because the rate of change of IR_n depends on μ, but also dependent on initial conditions, because the rate of change of IR_n depends on $IR_n(\mu = 0)$. This deserves further investigation in controlled laboratory experiments.

An alternative approach is also tested, in which a single, universal attrition relationship is assumed. The parameters a and k_a are estimated by fitting only the lowest 10% percentile of the shape distribution. This curve is assumed to represent the shape-mass loss relationship for each percentile, so that a particle that is born with an initial value of circularity would get rounder at the same rate as another one that is born less circular, but that would have reached the same IR_n after attrition. Although this alternative functional relationship appears intuitively appealing, it failed to reproduce the field data.

3.6 CONCLUSIONS AND RECOMMENDATIONS

The objective of this chapter is to model the shape evolution of coarse particles subject to attrition in mountainous river systems. The model presented uses the normalised isoperimetric ratio as a shape descriptor, and it shows good agreement with field data when applied to two different rock types: arenites and metabasalts.

Field data indicate that the probability distribution of normalised isoperimetric ratio at the source is lithology dependent. Lithology also plays a critical role in determining the value of the attrition coefficient, which controls the spatial scaling of the attrition process. The rounding coefficient obtained by calibration assumes more similar values for the two lithologies, compared to the attrition rate, which varies by more than one order of magnitude.

When the model is applied to different percentiles of the shape distributions, the rounding rate is directly proportional to the normalised isoperimetric ratio of fragments at the sources.

These two last observations highlight the importance of accounting for the heterogeneity of sediment shape produced by outcrops when modelling the evolution of sediment shape.

The modelling approach that shows the best agreement with field data for different percentiles of the shape parameter considered implies that the rounding rate of a particle subject to attrition depends both on its initial shape and on how much mass it has lost up to that moment. The physical interpretation of this dependency is not yet fully understood and warrants further investigation, ideally through laboratory experiments.

The model was also able to reproduce the shape trends observed in the case of spatially distributed sources, provided the introduction of a weighing function whose objective is to account for the diffusion of bedload particles and the truncation of the sample population, which both lead to a smaller relative contribution of more distant sources.

Future applications of the proposed model to a wider range of lithologies and transport environments could enable a more complete assessment of how model parameters depend on the mechanical properties of sediments and the energy regime of the transport environment. Finally, the monotonicity of the proposed equation opens up the possibility of inverting the model to statistically estimate particle travel distances, with potential applications across different lithologies.

4

ON THE ESTIMATION OF SEDIMENT TRAVEL DISTANCE BASED ON THEIR SHAPE

This chapter presents two approaches for using shape to infer the distance pebbles have travelled since their entrance into the river network. First, a model for the estimation of the sediment normalised isoperimetric ratio is introduced. Subsequently, a deterministic method to infer travel distances is proposed, and its accuracy and precision are presented. The sensitivity of the proposed method to model parameters is also discussed. Finally, a probabilistic method, formulated within a Bayesian framework, is introduced. This approach incorporates a prior probability distribution of sediment travel distances, which is subsequently updated based on the available information on sediment shape. Advantages and limitations of both methods are discussed, and possible approaches to test them in field conditions are provided

4.1 INTRODUCTION

The identification of river sediment sources is essential for addressing and mitigating contamination problems (Domingo et al., 2023), directing conservation efforts (Xu et al., 2022), and making informed decisions on river basin planning and management (Schleiss et al., 2016; Ito et al., 2023). A variety of techniques, based on different sediment properties, have been developed to achieve this (Williamson et al., 2014). Examples include the physical properties of sediments, such as colour, size, texture; mineralogical and geochemical properties, for example, the presence of specific minerals; cosmogenic and fallout radionuclides, which can provide information on the sample age; and stable isotopes, which can be used to identify the land use of source areas. These properties are often used in combination to leverage their ability to provide different types of information on the source areas (Collins et al., 2017).

Sediment sources may also be classified according to their type (e.g., surface vs. subsurface; forested vs. agricultural, etc.) or their spatial position and extent (e.g., a specific sub-catchment or a geological formation). This distinction is important because the capacity of a chosen method to achieve the desired classification depends not only on the properties selected but also on the underlying spatial variability of the sources of interest and, potentially, on their temporal variability in sediment production (Juez et al., 2018; Collins et al., 2020). Moreover, the selection of sediment sources is usually made *a priori* (Collins et al., 2017), which implies that the classification is limited by the initial selection of sources, and the methods used do not allow for the identification of new sources that were not included in the original list.

Although these techniques provide valuable insights, most are only applicable to fine sediment (Chapkanski et al., 2020), and relatively little work has been undertaken on fingerprinting sediment in mountainous catchments with coarser particles (Carretier and Regard, 2011). An additional layer of complexity in such environments relates to the definition of source areas. In lowland rivers, sediment sources are typically distinguished by land use and land cover, or by surface versus buried material (e.g., stream bank material eroded without prolonged exposure to the atmosphere) (Xu et al., 2022). Their spatial configuration is therefore relatively simple, with each source clearly distinct and covering a significant area. By contrast, in mountain rivers, the heterogeneity of geology and land cover results in a far more complex spatial distribution of sediment sources. For these reasons, an effective set of properties for identifying sources in mountain and piedmont rivers is still lacking.

Recent technological developments now permit accurate measurements of sediment size and shape using field imagery (Roussillon et al., 2009; Hryciw Roman D. et al., 2016; Tunwal et al., 2020; Cattapan et al., 2024). These developments, combined with findings on sediment attrition, which link particle shape to the relative mass lost during transport (Domokos et al., 2014; Szabó et al., 2015; Pál et al., 2021), open up the possibility of using sediment images to estimate travel distance.

This chapter explores the potential use of sediment shape as a fingerprinting property, focusing on the coarser grain-size fraction of mountain and piedmont rivers. Here, the term fingerprinting carries a slightly different meaning from its conventional use: sediment shape enables inference of a particle's travel distance rather than its source. For example, a particle whose shape is measured at a given point in the river may yield an estimated travel distance, yet multiple tributaries might exist at that same distance from the sampling site (Ito et al., 2023). Sediment shape, therefore, provides information only on travel distance, while precise identification of the source area would require coupling this with other properties (Niu et al., 2019).

Beyond its scientific interest, this approach is motivated by the potential to use sediment travel distances for the calibration and validation of sediment connectivity models (Heckmann and Schwanghart, 2013; Khan et al., 2021; Tangi, 2023). Such models, which represent sediment transport through a river network in a simplified form, characterise the composition of both sediment fluxes and bed material in terms of relative contributions from upstream reaches. They thus establish the degree of connectivity from upstream to downstream reaches and vice versa. Because these models aim not only to simulate transport rates but also to quantify relative source contributions, calibration and validation cannot rely on transport rates alone. Multiple connectivity configurations may yield the same observed rates, a phenomenon known as equifinality (Beven and Binley, 1992; Schmitt et al., 2018b). In this respect, the probability distribution of travel distance derived from field-based shape measurements offers an additional constraint, allowing comparison with connectivity model outputs and supporting calibration and validation.

To evaluate the accuracy and usefulness of such travel distance estimates, a theoretical model linking sediment shape to travel distance is required. This study applies the model proposed in Chapter 3, which successfully reproduced the evolution of sediment shape, expressed by their normalised isoperimetric ratio, along the Sarzana Stream, an alpine catchment (25 km^2) in north-eastern Italy. Using data from this system, two approaches for estimating travel distance are compared. The first infers travel distance from the ensemble averages of sediment shape distributions across locations (Szabó et al., 2015; Pokhrel et al., 2024; Gehringer et al., 2025). The second employs a Bayesian framework, beginning with prior assumptions of possible travel distances for particles at a given site, and refines these estimates through sediment-shape data (Davies et al., 2018).

4.2 THEORETICAL BACKGROUND

The model proposed in Chapter 3 establishes a mechanistic relationship between sediment shape and travel distance, using the normalised isoperimetric ratio (IR_n), as a shape parameter. The isoperimetric ratio, IR, of a particle is defined as: $IR = \frac{4\pi A}{P^2}$, where A is its projected area and P its perimeter. This ratio measures how similar a planar shape is to a perfect circle, which has the maximum value $IR = 1$. The term isoperimetric ratio is also referred to as circularity (C) in the geophysical literature.

The elongation of a particle (e) is defined as the ratio between its intermediate (l_2) and longest (l_1) dimensions. Since the maximum value of the isoperimetric ratio that a particle can achieve depends on its elongation, the normalised isoperimetric ratio was introduced to allow comparisons between particles with different elongations. The normalised isoperimetric ratio of a particle (IR_n,), is defined as the ratio between its IR and its theoretical maximum value, IR_t, for an ellipse with the same elongation:

$$IR_n = \frac{IR}{IR_t} \tag{4.1}$$

where

$$IR_t = \pi(l_1 + l_2)\left(1 + \left(3h/\left(10 + (4 - 3h)^{1/2}\right)\right)\right) \tag{4.2}$$

and

$$h = (l_1 - l_2)^2/(l_1 + l_2)^2 \tag{4.3}$$

In the remainder of this document, the normalised isoperimetric ratio, IR_n, will also be referred to simply as circularity, C, for ease of reading.

The model proposed in Chapter 3 assumes that, due to attrition, particle circularity changes as a function of the amount of mass lost, consistent with the theoretical constraints of the curvature-flow model (Pál et al., 2021). To describe this relationship, a superelliptical function was chosen to link circularity to the relative mass loss, μ, defined as the ratio of mass lost during transport over distance $\mathcal{L}$ to the particle's initial mass, M_0:

$$\mu(\mathcal{L}) = \frac{M_0 - M}{M_0} \tag{4.4}$$

where M is the particle mass after traveling a distance $\mathcal{L}$. The relationship proposed in Chapter 3 is:

$$\left(\frac{C - C_0}{C_{max} - C_0}\right)^a + \left(\frac{\mu_{max} - \mu}{\mu_{max}}\right)^a = 1 \qquad 4.5$$

Where C_{max} is the theoretical maximum value that C (equal to 1 for a perfect circle), μ_{max} is the maximum relative mass loss (equal to 1 for complete dissolution by attrition), C_0 is its initial circularity, and a is the rounding coefficient, which controls the rate at which circularity increases with mass loss.

The spatial scaling of relative mass loss is assumed to follow Sternberg's law, which predicts an exponential decay of particle mass. Rewritten in terms of μ, this becomes:

$$\mu(\mathcal{L}) = 1 - e^{-k_a \cdot \mathcal{L}} \qquad 4.6$$

Where k_a is the attrition coefficient, with units inverse of those of $\mathcal{L}$. By combining equations 4.5 and 4.6 the following expression for circularity as a function of travel distance is obtained:

$$C(\mathcal{L}) = C_0 + (C_{max} - C_0)\left[1 - \left(1 - \frac{1 - e^{-k_a \mathcal{L}}}{\mu_{max}}\right)^a\right]^{\frac{1}{a}} \qquad 4.7$$

Overall, the model depends on three parameters: C_0 the ensemble-average normalised isoperimetric ratio of fragments at the sources (measurable in the field), a is the rounding coefficient and k_a the attrition coefficient. The latter two parameters can be obtained through calibration, which was done using shape data for arenites and metabasalts pebbles from the Sarzana Stream, Italy. One localised sediment source has been identified for each lithology, allowing the estimation of C_0, while a and k_a were chosen to minimise the root mean square error between model estimates and measured sediment shape at multiple locations downstream of their respective source.

This relationship successfully reproduced the ensemble average circularity of sediments from both lithologies. Moreover, it could also reproduce different percentiles of the circularity distributions through an appropriate selection of the rounding coefficient a, which appeared to be correlated with the pebbles' initial circularity, C_0.

The model parameters obtained after calibration, together with the associated values of Root Mean Square Error (RMSE) and Mean Absolute Percentage Error (MAPE), are reported in Table 4.1. Figure 4.1 illustrates the goodness of fit of equation 4.7 against field data and shows that the standard deviation of particle circularity, σ_C, tends to decrease, consistent with the curvature-driven attrition model. However, a Mann–Kendall test indicated that this trend is not statistically significant at the $\alpha = 0.05$ level ($p = 0.0736$ for metabasalts; $p = 0.0894$ for arenites). This slow decline in variability has implications for estimating travel distances, as will be explained later.

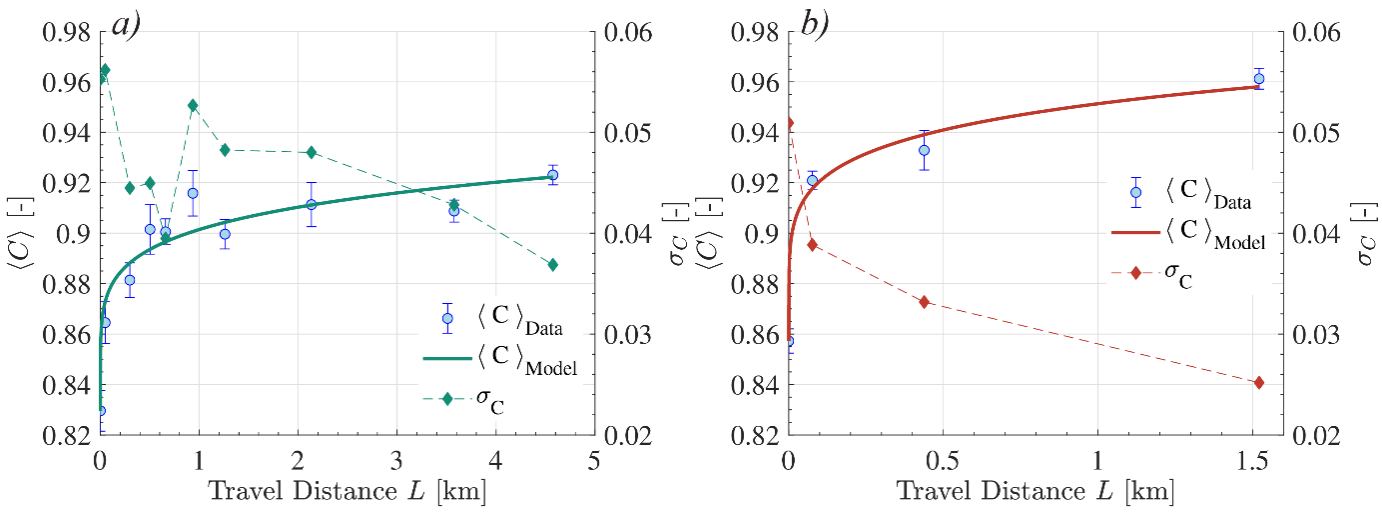

Figure 4.1. Comparison between field-measured and modelled circularity. Error bars indicate the standard error of the mean. The right-hand vertical axis shows the standard deviation of circularity. a) Metabasalts, b) Arenites.

Table 4.1. Optimum model parameters obtained by minimising the RMSE of the normalised isoperimetric ratio for each lithology.

Lithology	C_0	a	k_a	***RMSE***	***MAPE***
Metabasalts	0.83	5.94	0.00100	0.007	0.640%
Arenites	0.86	5.71	0.01698	0.004	0.336%

4.3 METHODS

4.3.1 Deterministic method for average travel distance

Equation 4.7 provides an estimate of the circularity, C, attained by a particle that entered the network with an initial circularity C_0, after traveling a distance, $\mathcal{L}$. At first glance, it might therefore appear possible to invert this function to estimate the travel distance of any particle sampled along a river, based on its observed circularity (Pokhrel et al., 2024; Gehringer et al., 2025). However, sediment fragments produced by outcrops do not share a unique initial circularity, C_0. Different particles may thus display different circularities after traveling the same distance $\mathcal{L}$, Conversely, a particle exhibiting a given circularity C may have traveled different distances depending on its initial value of circularity. As a result, knowledge of a particle's shape alone is insufficient for a deterministic estimate of its travel distance.

Field evidence presented in Chapter 3 indicates that fragments produced by outcrops of a given lithology tend to have an initial circularity whose distribution is characteristic of that lithology. This observation allows equation 4.7 to be applied not to individual particles, whose initial circularities remain unknown, but to the average shape of an ensemble of particles sampled at a distance $\mathcal{L}$ from their source. The ensemble average of circularity for fragments derived from outcrops of a given lithology can be considered constant and lithology-specific (Domokos et al., 2015). It can therefore be approximated by the average value of C_0 measured directly in the field.

Under this assumption, equation 4.7 can be inverted to estimate the average travel distance of an ensemble of particles sampled at a given point along a river, based on their average circularity:

$$\mathcal{L} = \frac{1}{k_a} ln \left(\frac{1}{\mu_{max} \left[1 - \left(\frac{\langle C \rangle - \langle C_0 \rangle}{C_{max} - \langle C_0 \rangle} \right)^a \right]^{\frac{1}{a}}} \right) \qquad 4.8$$

where the ensemble averages of particle shape are denoted by the symbol $\langle \quad \rangle$. In this equation, $\mathcal{L}$ represents the average travel distance of an ensemble of particles sampled at a given location along a river, with an average circularity $\langle C \rangle$. Figure 4.2 illustrates how the average travel distance, and its derivative with respect to the circularity, vary as functions of the ensemble average of particle circularity (equations 4.8 and 4.11).

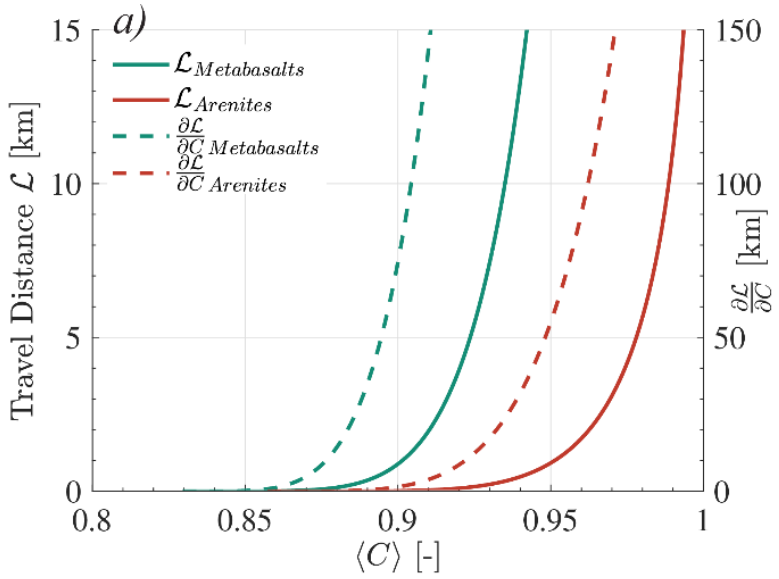

Figure 4.2. Travel distance and its derivative with respect to circularity, computed using Equations 4.8 and 4.11, respectively.

4.3.2 Probabilistic method for probability of travel distances

Although the equation expressing circularity as a function of travel distance (equation 4.7) appears to provide a deterministic relationship between circularity and travel distance, this is not the case because C_0 is not a deterministic quantity, but a random variable. Consider measuring the circularity of a pebble at a given location along a river and obtaining a value of C; equation 4.7 does not allow estimation of its initial circularity C_0 unless the travel distance $\mathcal{L}$, is known, and vice versa. Thus, equation 4.7 establishes a mapping between three random variables, C_0, C and $\mathcal{L}$, for an ensemble of particles. If one focuses on an individual particle and treats two of these variables as fixed (in a conditional sense), then equation 4.7 allows computation of the third.

This is the case, for example, when the distribution of initial circularity is known and assumed constant within the source areas, while the distribution of circularity C is known from field measurements. Under these conditions, the problem of estimating the travel distance of a particle sampled at a given location, with given circularity, can be formulated in a probabilistic framework.

Let us define a Lagrangian spatial coordinate, x, with origin at a sampling location along a river, where data on the normalised isoperimetric ratio of particles, IR_n, are available. The coordinate x extends upstream along the steepest descent and maps the position of each point, x_i in the contributing catchment (Figure 4.3).

The setup of a Bayesian framework requires defining the prior distribution of travel distances, which expresses the initial belief about the possible sources of the particles under consideration (Cooper and Krueger, 2017; Davies et al., 2018). Defining the prior involves two steps: selecting the domain of all possible sources and discretising this domain into individual elements. In the most general case, the domain of all possible sources is composed of the set of all points within the catchment, draining to the sampling location. If additional information regarding the sediment measured is available, such as geological or lithological maps showing the outcrop areas of the lithology of interest, the domain can be restricted to the intersection of these areas with the drainage area.

Once the domain of possible sources is defined, the prior probability distribution of travel distances can be estimated, as a first approximation, using a frequentist approach. The domain can be discretised into elements at an appropriate scale, with each element assigned a representative travel distance to the sampling location. The prior distribution of travel distances, $P_{\mathcal{L}}(\mathcal{L})$, can be approximated by the relative frequency of elements located at that distance from the sampling site:

$$P_{\mathcal{L}}(\mathcal{L}) = \frac{n_{se}(\mathcal{L})}{N_{se}} \qquad 4.9$$

Where $n_{se}(\mathcal{L})$ is the number of discrete source elements located at a distance $\mathcal{L}$ from the sampling site, and N_{se} is the total number of elements used to discretise the domain of all possible sources. The domain may be discretised either in terms of catchment areas, using two-dimensional (2D) source elements (pixels), or in terms of river network segments, using one-dimensional (1D) source elements of a specified unit length. The choice of discretisation depends on the characteristics of the case study and the research objective.

Figure 4.3 provides a schematic representation of source elements defined as 2D areas and illustrates their characterisation in terms of distance using the Lagrangian coordinate x.

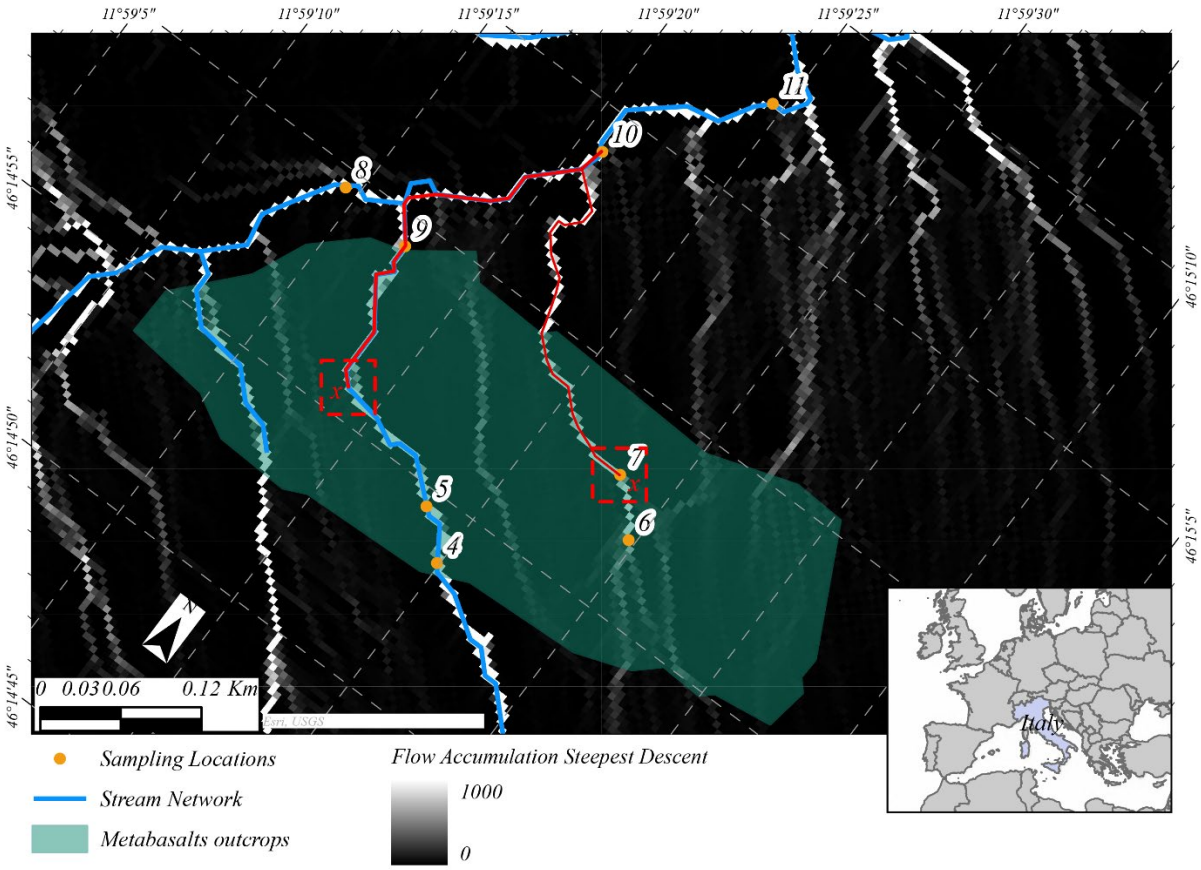

Figure 4.3. Schematic of the reference system used based on the Sarzana Stream case study presented in Chapter 3.3.1. The lithology considered is metabasalts, whose outcrop is shown in green. Dashed squares show a hypothetical discretisation of the source area. Lagrangian distances (x) from the sampling location 10 are shown as red lines. The left line indicates the distance to a possible source element, while the right line indicates the distance to sampling location 7.

The background map shows flow accumulation, with pixel colour proportional to drainage area, and is used to determine the flow paths of particles originating from each source element. In practical applications, 2D source elements may correspond to individual pixels in a raster map, while 1D source elements may be defined as consecutive one-meter segments along a vector representation of the river network. Once the prior distribution of travel distances has been defined, the distribution of sediment shape for each source element must be estimated. Field evidence suggests that the distribution of normalised isoperimetric ratios of fragments produced by outcrops can be considered lithology-specific and spatially invariant. Consequently, the same distribution of initial circularity of fragments, $P_0(C_0)$, can be assigned to each source element.

To summarise, the information available at this stage is:

- $P_C(C)$ which is the probability of sediments having circularity C, at the sampling location ($x = 0$), obtained from field measurement.
- $P_{\mathcal{L}}(\mathcal{L})$ which is the prior probability of travel distances $\mathcal{L}$ of particles with circularity C in $x = 0$, estimated as described previously.
- $P_0(C_0)$ which is the probability distribution of the circularity of fragments produced by each source element, measurable in the field.

The key idea in applying Bayes' theorem is to use information on sediment shape to update prior beliefs regarding the distances travelled. This relationship can be expressed as:

$$P_{\mathcal{L}}(\mathcal{L}|C) = \frac{P_C(C|\mathcal{L})P_{\mathcal{L}}(\mathcal{L})}{P_C(C)} \qquad 4.10$$

where $P_C(C|\mathcal{L})$ is the conditional probability of a particle's circularity C, given that it has travelled a distance $\mathcal{L}$. In Bayesian terminology, this term is called the likelihood, and it represents the probability of observing the sample data, given a particular value of the state variable $\mathcal{L}$. To update the prior distribution, the likelihood must be reformulated in terms of measurable quantities.

This can be achieved by introducing two functions. The first, $C = f(C_0, \mathcal{L})$ is the deterministic relationship describing the evolution of the shape C, of a particle that entered the river network with an initial circularity C_0 and subsequently travelled a distance $\mathcal{L}$. This corresponds to equation 4.7, but here the explicit dependence of a particle shape on its initial circularity is highlighted.

$$C(C_0, \mathcal{L}) = C_0 + (C_{max} - C_0)\left[1 - \left(1 - \frac{1 - e^{-k_a \mathcal{L}}}{\mu_{max}}\right)^a\right]^{\frac{1}{a}} = f(C_0, \mathcal{L}) \qquad 4.11$$

The second function, $C_0 = g(C, \mathcal{L})$ is the inverse of $f(C_0, \mathcal{L})$ and therefore it is also deterministic. It expresses the value of the initial circularity C_0 that a particle must have had in order to reach circularity C after travelling a distance $\mathcal{L}$.

$$C_0(C,\mathcal{L}) = \frac{C - C_{max}\left[1-\left(1-\frac{\mu_{max}-e^{-K_a\mathcal{L}}}{\mu_{max}}\right)^a\right]^{\frac{1}{a}}}{1-\left[1-\left(1-\frac{\mu_{max}-e^{-K_a\mathcal{L}}}{\mu_{max}}\right)^a\right]^{\frac{1}{a}}} = g(C,\mathcal{L}) \qquad 4.12$$

The probability distribution of the circularity of fragments produced by each source element, $P_0(C_0)$, can therefore be rewritten using equation *4.12* as $P_0\big(g(C,\mathcal{L})\big)$. Since the transformation functions, $f(C_0,\mathcal{L})$ and $g(C,\mathcal{L})$ are deterministic, this approach assumes that if a particle originated with a circularity C_0 and travelled a distance $\mathcal{L}$, its final circularity must be $f(C_0,\mathcal{L})$. Conversely, if a particle currently exhibits a circularity C after travelling a distance $\mathcal{L}$, then its initial circularity must have been $g(C,\mathcal{L})$. Consequently, the conditional probability of a particle's circularity, given that it travelled a distance $\mathcal{L}$, $P_C(C|\mathcal{L})$, is equal to the probability of it having had an initial circularity C_0, such that, after a distance $\mathcal{L}$, it would reach the observed value C. By definition, this is $P_0\big(g(C,\mathcal{L})\big)\left|\frac{\partial g(C,\mathcal{L})}{\partial C}\right|$, where $\frac{\partial g(C,\mathcal{L})}{\partial C}$ is the Jacobian of the transformation. This represents the likelihood of observing a circularity C given that the particle travelled a distance $\mathcal{L}$:

$$P_C(C|\mathcal{L}) = P_0\big(g(C,\mathcal{L})\big)\left|\frac{\partial g(C,\mathcal{L})}{\partial C}\right| \qquad 4.13$$

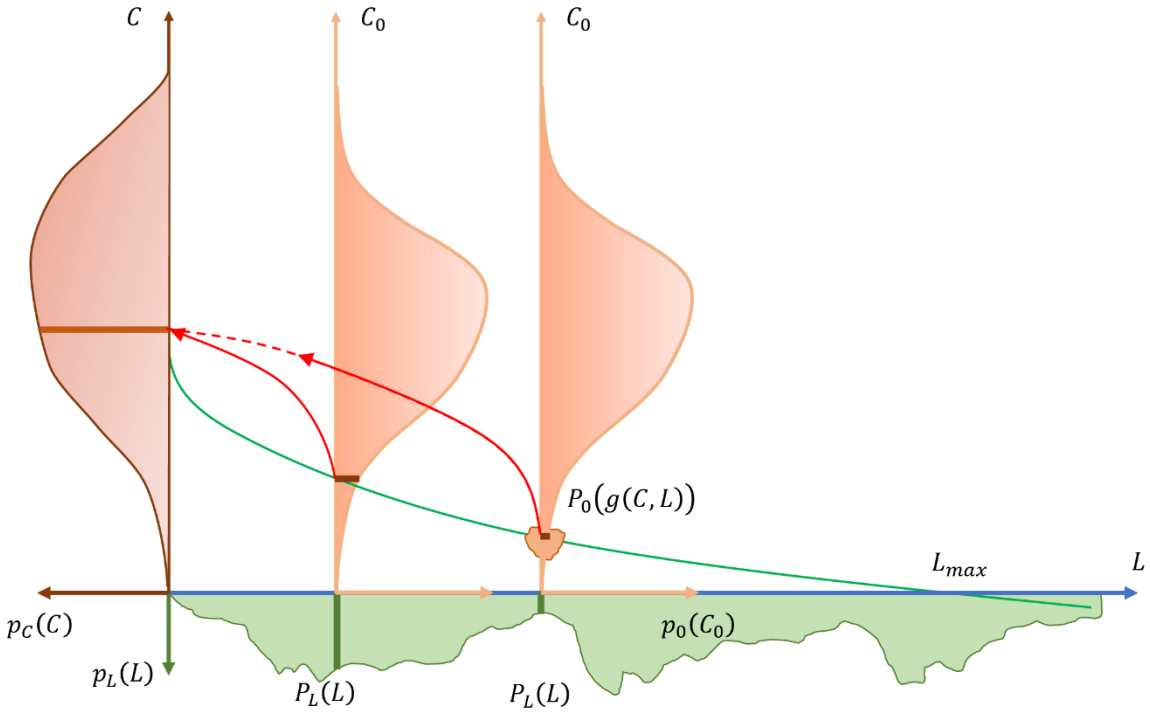

Figure 4.4. Schematic representation of the relationship between prior probability, likelihood and posterior probability.

Figure 4.4 provides a schematic representation of the Bayesian approach. The function $g(C, \mathcal{L})$ is represented by the green line, which indicates the initial circularity a particle must have had in order to reach a circularity C, depending on its entrance point. The term $P_0\big(g(C, \mathcal{L})\big)$ denotes the probability of observing such an initial circularity. The scheme also highlights that, although $P_0(C_0)$ does not vary spatially, the function $g(C, \mathcal{L})$ acts as a filter: for different distances from the sampling location, it selects the values of initial circularity that contribute to the observed final circularity C. Conversely, $f(C_0, \mathcal{L})$ is shown by the red lines, representing the trajectories of shape evolution of particles with different initial circularities that have travelled different distances $\mathcal{L}$.

The joint probability of C and $\mathcal{L}$ can therefore be expressed as:

$$P_{C,\mathcal{L}}(C, \mathcal{L}) = P_C(C|\mathcal{L})P_{\mathcal{L}}(\mathcal{L}) \qquad 4.14$$

Therefore, the marginal probability of a particle's circularity C can be computed by integrating over all possible values of travel distance $\mathcal{L}$:

$$P_C(C) = \int_0^{\mathcal{L}_{max}} P_{C,\mathcal{L}}(C, \mathcal{L})d\mathcal{L} \qquad 4.15$$

Where $\mathcal{L}_{max}$ represents the maximum distance from which a particle could have come, and it can be computed using equation 4.7 by setting $C_0 = 0$. By substituting equations *4.13* and *4.15* into Equation *4.10*, the update rule for the probability density of travel distances is obtained.

$$P_{\mathcal{L}}(\mathcal{L}|C) = \frac{P_C(C|\mathcal{L})P_{\mathcal{L}}(\mathcal{L})}{P_C(C)} = \frac{P_0\big(g(C, \mathcal{L})\big)\left|\frac{\partial g(C, \mathcal{L})}{\partial C}\right| P_{\mathcal{L}}(\mathcal{L})}{\int_0^{\mathcal{L}_{max}} P_0\big(g(C, \mathcal{L})\big)\left|\frac{\partial g(C, \mathcal{L})}{\partial C}\right| P_{\mathcal{L}}(\mathcal{L})d\mathcal{L}} \qquad 4.16$$

Finally, by integrating over the observed values of circularity, the updated marginal probability distribution of travel distances can be obtained.

$$P_{\mathcal{L}}(\mathcal{L}) = \int_0^1 P_{\mathcal{L}}(\mathcal{L}|C)P_C(C)dC \qquad 4.17$$

Equation *4.17* provides an estimate of the distribution of travel distances of particles by integrating the available information on their sources, through the choice of the prior, with the information on their shape, measured at each sampling location.

Its practical application in the field requires measurements of the normalised isoperimetric ratio of fragments produced by the outcrops of the lithology used as a tracer, as well as of sediment shapes at different sampling locations. Tracers equipped with tracking devices (e.g. RIFD or active UHF transponders) could also be used, provided

they share the same mechanical properties and their initial circularity is known (Liébault et al., 2023).

4.4 APPLICATION OF THE DETERMINISTIC MODEL

4.4.1 Accuracy

Measurement methods are usually characterised by their accuracy and precision (Menditto et al., 2007). The accuracy of equation 4.8 in reproducing the average travel distance of an ensemble of particles was evaluated using RMSE and MAPE. The results are presented in Table 4.2 and, visually, in Figure 4.5-a and Figure 4.5-c. They indicate that the accuracy of travel distance estimates is considerably lower than that achieved for estimates of sediment shape (Table 4.1).

Table 4.2.Errors in the estimated average travel distances for metabasalts and arenites.

Lithology	$\boldsymbol{RMSE}$ $[\boldsymbol{km}]$	$\boldsymbol{MAPE}$
Metabasalts	0.940	63.5%
Arenites	0.208	31.0%

This result is not unexpected, because the function $C(\mathcal{L})$ (equation 4.7) has a horizontal asymptote for $\mathcal{L} \to \infty$ (Figure 4.1) and consequently, its inverse (equation 4.8) has a vertical asymptote for $C \to 1$ (Figure 4.2). This implies that, as the ensemble average circularity increases, estimates of travel distance become increasingly sensitive to uncertainties in the measurement of particle shape.

These uncertainties may arise from two main sources. The first is measurement error, which is assumed to be independent of the value of circularity C and is therefore not discussed further. The second is the inherent variability of particle shape, represented by the standard deviation of C at different locations. This effect is particularly evident for metabasalts (Figure 4.1-a and Figure 4.5-a). In this case, because the measured normalised isoperimetric ratios were not monotonically increasing, the estimated average travel distance was also not monotonic, an unrealistic outcome, unless additional metabasalt sources exist that were not identified during the field campaign.

While RMSE provides an aggregated measure of error in the estimation of travel distances, assessing the practical usefulness of the method requires an evaluation of how accuracy changes with increasing distance from the outcrops. To this end, for each location i, the absolute $\Delta_{\mathcal{L}_i}$, and relative $\delta_{\mathcal{L}_i}$, errors were computed as follows:

$$\Delta_{\mathcal{L},i} = |\mathcal{L}_i^{mes} - \mathcal{L}_i| \tag{4.18}$$

$$\delta_{\mathcal{L},i} = \frac{\Delta_{\mathcal{L},i}}{\mathcal{L}_i^{mes}} \tag{4.19}$$

Where $\mathcal{L}_i^{mes}$ denotes the average travel distance measured along the steepest descent path from the source to each sampling location i; while $\mathcal{L}_i$ represents the average travel distance estimated using equation 4.8. Results are presented in Table 4.3 and Table 4.4 for metabasalts and arenites, respectively.

Table 4.3. Accuracy metrics of the method: absolute and relative errors in travel distance estimates for metabasalts.

Lithology	$\mathcal{L}oc.\,i$	$\mathcal{L}_i^{mes}$ $[km]$	$\mathcal{L}_i$ $[km]$	$\Delta_{\mathcal{L},i}$ $[km]$	$\delta_{\mathcal{L},i}$ [%]
Metabasalts	4	0.000	0.000		
Metabasalts	5	0.048	0.014	0.035	71.48%
Metabasalts	9	0.298	0.143	0.155	52.04%
Metabasalts	10	0.502	1.005	0.503	100.13%
Metabasalts	11	0.659	0.927	0.268	40.65%
Metabasalts	12	0.934	2.973	2.038	218.11%
Metabasalts	14	1.259	0.857	0.402	31.92%
Metabasalts	15	2.133	2.155	0.022	1.04%
Metabasalts	18	3.576	1.783	1.793	50.15%
Metabasalts	19	4.574	4.827	0.253	5.53%
Average				0.547	63.5%

Table 4.4. Accuracy metrics of the method: absolute and relative errors in travel distance estimates for arenites.

Lithology	$\mathcal{L}oc.i$	$\mathcal{L}_i^{mes}$	$\mathcal{L}_i$	$\Delta_{\mathcal{L},i}$	$\delta_{\mathcal{L},i}$
		$[km]$	$[km]$	$[km]$	[%]
Arenites	1	0.000	0.000		
Arenites	2	0.076	0.103	0.027	35.1%
Arenites	3	0.438	0.278	0.160	36.6%
Arenites	12	1.521	1.843	0.322	21.2%
Average				0.170	31.0%

The relative error of travel distance shows a mildly decreasing trend, although it fluctuates considerably between locations, particularly for metabasalts, reaching about 5.5% at a distance of about 4.5 km from the source, and about 21% at a distance of about 1.5 km from the arenite source (Figure 4.5-b and Figure 4.5-d, respectively). This decrease is not the result of reduced absolute error but rather reflects the increasing denominator in equation 4.19.

In summary, as the distance from the source increases, the method improves in terms of relative error, but not in terms of absolute error.

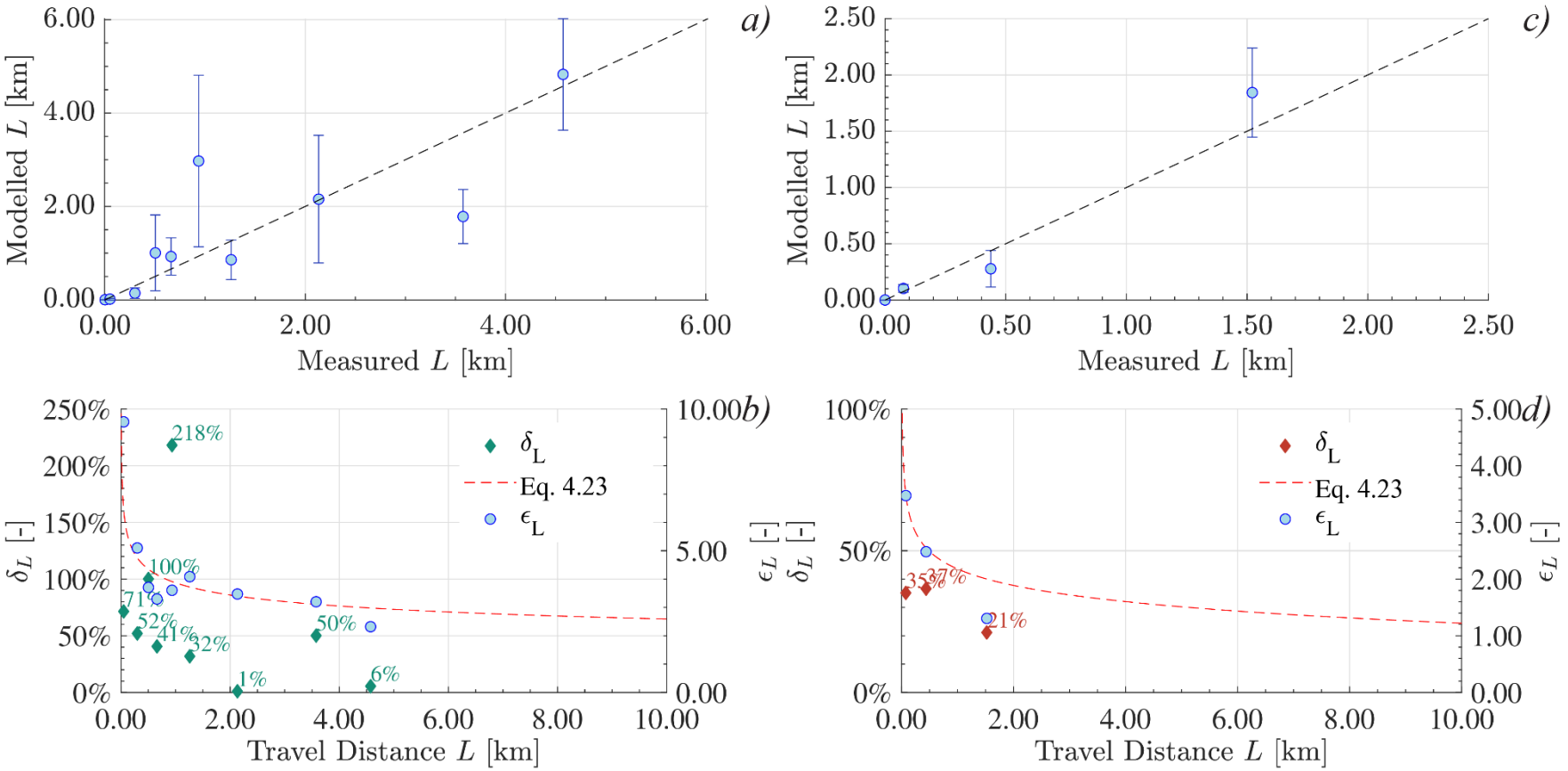

Figure 4.5. a, c) Comparison of modelled and DEM-derived travel distances for metabasalts (a) and arenites (c). Error bars indicate standard errors. b, d) Relative errors of travel distances (left) and relative standard deviation of travel distances (right): computed from measured circularity at each location (dots) and from estimates based on equation 4.23 (line) for metabasalts (b) and arenites (d). .

4.4.2 Precision and practical constraints

The shapes of sediment fragments produced by outcrops can vary considerably. Although the theory of curvature-driven attrition suggests that particle shapes should asymptotically converge (Pál et al., 2021; Havasi-Tóth and Fehér, 2025), the circularity distribution of particles sampled in the field still displays variability (Figure 4.1).

To assess the influence of this variability in particle shape C, on the estimation of the average travel distance $\mathcal{L}_i$, at each location i, the derivative of $\mathcal{L}$ with respect to circularity was computed for each sampling location using equation 4.11:

$$\frac{\partial \mathcal{L}_i}{\partial C} = \frac{\left(\frac{\langle C_i \rangle - \langle C_0 \rangle}{C_{max} - \langle C_0 \rangle}\right)^a}{k_a(\langle C_i \rangle - \langle C_0 \rangle)\left(1 - \left(\frac{\langle C_i \rangle - \langle C_0 \rangle}{C_{max} - \langle C_0 \rangle}\right)^a\right)^{\frac{1}{a}}} \qquad 4.20$$

where $\langle C_i \rangle$ denotes the ensemble average of normalised isoperimetric ratios of particles at location i, and $\langle C_0 \rangle$ the ensemble average at their source. Given the standard deviation of measured circularity at each location, $\sigma_{C,i}$, the associated standard deviation of travel distance, $\sigma_{\mathcal{L},i}$, was obtained using equation 4.21:

$$\sigma_{\mathcal{L},i} = \left|\frac{\partial \mathcal{L}}{\partial C}\right| \sigma_{C,i} \qquad 4.21$$

The relative standard deviation, $\epsilon_{\mathcal{L},i}$, was then used to quantify the uncertainty of travel distance estimates at each location i, modelled with equation 4.21, as a result of the inherent variability in sediment circularity:

$$\epsilon_{\mathcal{L},i} = \frac{\sigma_{\mathcal{L}i}}{\mathcal{L}_i} \qquad 4.22$$

However, $\epsilon_{\mathcal{L},i}$ only reflects variability at the specific sampling sites where circularity measurements were available. To evaluate how the uncertainty of travel distances evolves with increasing distance from outcrops, the relative standard deviation must be expressed as a continuous function of travel distance.

For this purpose, the mean standard deviation of circularity across all sampling locations was used as a representative metric of expected variability: $\overline{\sigma_C} = \frac{1}{N_{sl}} \sum_{i=1}^{N_{sl}} \sigma_{C,i}$, where N_{sl} is the number of sampling locations. The relative standard deviation of travel distance was then computed as a continuous function of $\mathcal{L}$, using equation *4.23* :

$$\epsilon_{\mathcal{L}} = \frac{\left|\frac{\partial \mathcal{L}}{\partial C}\right| \overline{\sigma_C}}{\mathcal{L}} \qquad 4.23$$

Figure 4.5-b and Figure 4.5-c show that the relative standard deviation of travel distance predicted by equation *4.23* decreases only very slowly. This is particularly evident for metabasalts, where the results of equation *4.23* are in close agreement with field data (Figure 4.5-b). This behaviour occurs because, as discussed previously, none of the terms in the numerator of Equation *4.23* decreases significantly with increasing travel distances.

In the case of arenites, $\frac{\partial \mathcal{L}}{\partial C}$ increases with C and, therefore, with travel distance. At the same time, $\sigma_{\mathcal{L}i}$ tends to decrease (Figure 4.1-b). These two competing effects lead to a slightly faster decline in the relative standard deviation observed in the field compared with the estimates obtained from equation *4.23* (Figure 4.5-d).

To summarise, the relative accuracy of the method, expressed as the relative error of estimates of travel distances, is initially relatively high owing to the small denominator of equation 4.10, but decreases with increasing distance from the source. At around 4.5 km from the source, the relative error is 5.5% for metabasalts and 21% and arenites. The absolute accuracy, expressed as the absolute error, showed no significant trend with distance.

The precision of the method, expressed as the expected relative standard deviation of travel distances, decreases only very slowly with increasing travel distances. This has practical implications for field monitoring campaigns, where it is standard practice to determine the minimum number of samples required to achieve a specified level of precision. Different statistics may be used as precision targets; in this case, a hypothetical standard error of travel distances equal to 20% was adopted to illustrate the limitations of the method. Detailed results are reported in Table 4.5 and Table 4.6. At certain locations, achieving this level of precision would require collecting ~3000 particles. With current technologies, the collection and analysis of such large sample sizes is extremely time-consuming and economically unjustifiable. Although drones allow the collection of a high number of images at relatively low costs and time (Mörtl et al., 2022), (to the best of the author's knowledge) existing algorithms do not allow the accurate calculation of shape parameters. needed to perform this type of analysis. This is due to the fact that particles in natural environments overlap and therefore their shape cannot be accurately measured. This outcome highlights the combined effects of the high sensitivity of $\mathcal{L}$ to variations in C (steep $\frac{\partial \mathcal{L}}{\partial C}$), and decreasing variability of sediment circularity ($\sigma_{\mathcal{L}}$ decreasing only slightly with increasing $\mathcal{L}$).

In conclusion, estimating the average travel distance of sediments from the ensemble average of their circularity yields a method whose absolute accuracy does not improve with increasing distances, and whose precision improves only slowly.

Finally, consider a catchment with two distinct sources of the same lithology, located at distances $\mathcal{L}_1$ and $\mathcal{L}_2$ from a sampling point. As the method provides only the average travel distance of particles based on circularity, the outcome will be an intermediate distance, representing a mixture of contributions from both sources. This example illustrates that the approach cannot resolve the relative contributions of multiple source areas to a downstream location.

Table 4.5. Precision metrics of the method: standard deviation ($\sigma_{\mathcal{L}}$) relative standard deviation, $\epsilon_{\mathcal{L}}$,and standard error ($\sigma_{\mathcal{L},ST}$), of travel distances derived from the circularity of metabasalts. $\sigma^*_{\mathcal{L},ST}$ denotes the target standard error for a hypothetical field campaign, and N_S is the minimum number of samples required to achieve it.

$\mathcal{L}oc.i$	N_{Sample}	C_i	σ_C	$\partial\mathcal{L}/\partial C$	$\sigma_{\mathcal{L}}$	$\epsilon_{\mathcal{L}}$	$\sigma_{\mathcal{L},ST}$	$\sigma^*_{\mathcal{L},ST}$	N_S
		$[-]$	$[-]$	$[km]$	$[km]$	$[-]$	[%]	[%]	
4	47	0.830	0.055	0.000	0.000		0%	20%	0
5	46	0.865	0.056	2.340	0.131	9.547	2%	20%	1
9	42	0.881	0.044	16.363	0.728	5.098	11%	20%	14
10	21	0.901	0.045	82.809	3.723	3.705	81%	20%	347
11	59	0.901	0.039	77.442	3.057	3.298	40%	20%	234
12	34	0.916	0.053	203.541	10.719	3.606	184%	20%	2873
14	68	0.900	0.048	72.591	3.502	4.085	42%	20%	307
15	30	0.911	0.048	155.966	7.487	3.474	137%	20%	1402
18	97	0.909	0.043	133.261	5.705	3.200	58%	20%	814
19	88	0.923	0.037	303.795	11.200	2.320	119%	20%	3136
Average	53	0.894	0.047	104.811	4.625	4.259	67%	20%	913

Table 4.6. Precision metrics of the method: standard deviation ($\sigma_{\mathcal{L}}$) relative standard deviation ($\epsilon_{\mathcal{L}}$),and standard error ($\sigma_{\mathcal{L},ST}$) of travel distances derived from circularity of metabasalts. $\sigma^*_{\mathcal{L},ST}$ denotes the target standard error for a hypothetical field campaign, and N_S is the minimum number of samples required to achieve it.

$\mathcal{L}oc.i$	N_{Sample}	C_i	σ_C	$\partial\mathcal{L}/\partial C$	$\sigma_{\mathcal{L}}$	$\epsilon_{\mathcal{L}}$	$\sigma_{\mathcal{L},ST}$	$\sigma^*_{\mathcal{L},ST}$	N_S
		[−]	[−]	[km]	[km]	[−]	[%]	[%]	
1	112	0.857	0.051	0.000	0.000		0%	20%	0
2	109	0.921	0.039	9.207	0.358	3.473	3%	20%	4
3	18	0.933	0.033	20.781	0.689	2.483	16%	20%	12
12	37	0.961	0.025	95.643	2.408	1.306	40%	20%	145
Average	69	0.918	0.037	31.408	0.864	2.421	15%	20%	40

4.4.3 Sensitivity analysis

Estimates of sediment travel distance are also influenced by uncertainties in the model parameters (Saltelli et al., 2002). Figure 4.6 illustrates how travel distance (equation 4.8) varies as a function of the rounding coefficient, a, and the attrition coefficient, k_a.

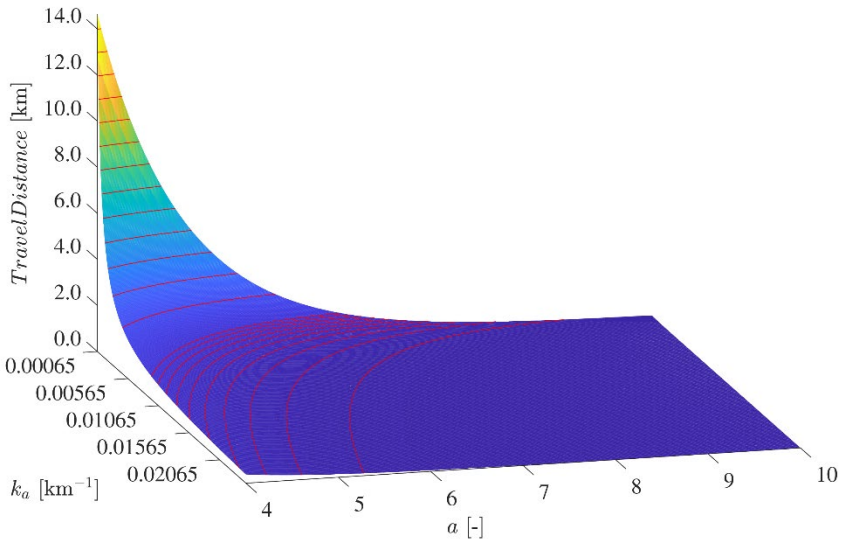

Figure 4.6. Dependence of travel distance on the rounding coefficient and the attrition coefficient, a, k_a. Parameters used: C_0=0.8572; C=0.92.

The values of C_0 and C chosen for this example refer to locations 3 and 4 for arenites, respectively, and are reported in the caption. Red horizontal reference lines are shown, spaced at 0.1 km intervals within the first kilometre and at 1 km intervals thereafter.

To provide a quantitative assessment of the relative importance of these parameters, the partial derivatives of $\mathcal{L}$ with respect to a and k_a were computed for all sampling locations and both lithologies using equations *4.24* and 4.25. Parameter uncertainties were assumed to be equal to 10% of their respective value obtained through calibration (Table 4.1).

$$\frac{\partial \mathcal{L}}{\partial a} = \frac{\frac{\left(\frac{C-C_0}{C_{max}-C_0}\right)^a ln\left(\frac{C-C_0}{C_{max}-C_0}\right)}{\left(1-\left(\frac{C-C_0}{C_{max}-C_0}\right)^a\right)a} + \frac{ln\left(1-\left(\frac{C-C_0}{C_{max}-C_0}\right)^a\right)}{a^2}}{k_a} \qquad 4.24$$

$$\frac{\partial \mathcal{L}}{\partial k_a} = -\frac{ln\left(\frac{1}{\left(1-\left(\frac{C-C_0}{C_{max}-C_0}\right)^a\right)^{\frac{1}{a}}\mu_{max}}\right)}{k_a^2} \qquad 4.25$$

The uncertainties in travel distance estimates arising from the uncertainty in each parameter were computed as: $\Delta\mathcal{L}(a) = \frac{\partial \mathcal{L}}{\partial a}\Delta a$ and $\Delta\mathcal{L}(k_a) = \frac{\partial \mathcal{L}}{\partial k_a}\Delta k_a$. The overall variability of $\mathcal{L}$, due to the combined uncertainties of both parameters was then calculated as:

$$\Delta\mathcal{L} = \sqrt{\left(\frac{\partial \mathcal{L}}{\partial a}\right)^2 + \left(\frac{\partial \mathcal{L}}{\partial k_a}\right)^2} \qquad 4.26$$

The results of this perturbation analysis are reported in Table 4.7 and Table 4.8, and show that a 10% uncertainty in both model parameters translates into an average relative deviation in estimated travel distances of approximately 65% for metabasalts and 45.5% for arenites. This demonstrates that the functional relationship is highly sensitive to the values of the model parameters.

When considering the contribution of each parameter separately, the effect of the rounding coefficient is, on average, around six times larger than that of the attrition coefficient for metabasalts and about four times larger for arenites.

This result may be interpreted positively for two reasons. Firstly, the relative variability of model parameters between lithologies was computed as the ratio between the absolute deviation of their values and the average value for the two lithologies. The three model parameters: C_0, a and k_a showed a relative variation of around 3%, 4% and 178% respectively. The different mechanical resistance of the two rock types suggests that the rounding coefficient varies less between lithologies than the attrition coefficient, which should make its estimation more accurate. Secondly, the rounding coefficient depends primarily on the mechanical properties of particles and on the types of impacts they undergo, which can be investigated under controlled laboratory conditions (Litwin Miller and Jerolmack, 2021). As a result, the rounding coefficient should be easier to constrain than the attrition coefficient, and doing so would substantially improve the precision of travel distance estimates.

Table 4.7. Sensitivity analysis of modelled travel distances as a function of the rounding and attrition coefficients for metabasalts. Parameter variations: $\Delta a = 0.594$, $\Delta k_a = 10^{-4}\ km^{-1}$.

$\mathcal{L}oc.\,i$	$\frac{\partial \mathcal{L}}{\partial a}$	$\Delta\mathcal{L}(a)$	$\frac{\partial \mathcal{L}}{\partial k_a}$	$\Delta\mathcal{L}(k_a)$	$\Delta\mathcal{L}$	$E_{\mathcal{L}}$	$\frac{\Delta\mathcal{L}(a)}{\Delta\mathcal{L}(k_a)}$
	$[km]$	$[-]$	$[km^2]$	$[km^{-1}]$	$[km]$	[%]	$[km]$
4	0.000	0.000	0.000	0.000	0.000		
5	-0.024	0.014	-13.771	0.001	0.014	104.6%	1041%
9	-0.194	0.115	-142.753	0.014	0.116	81.4%	808%
10	-1.038	0.617	-1004.656	0.100	0.625	62.2%	614%
11	-0.970	0.576	-926.748	0.093	0.584	63.0%	622%
12	-2.543	1.511	-2972.750	0.297	1.540	51.8%	508%
14	-0.909	0.540	-857.288	0.086	0.547	63.7%	630%
15	-1.957	1.162	-2155.297	0.216	1.182	54.8%	539%
18	-1.674	0.994	-1782.639	0.178	1.010	56.7%	558%
19	-3.753	2.229	-4827.375	0.483	2.281	47.2%	462%
Average		0.776		0.147	0.790	65.1%	642%

Table 4.8. Sensitivity analysis of modelled travel distances as a function of the rounding and attrition coefficients for arenites. Parameters variation: $\Delta a = 0.571$, $\Delta k_a = 0.0017\ km^{-1}$.

Location	$\frac{\partial \mathcal{L}}{\partial a}$	$\Delta\mathcal{L}(a)$	$\frac{\partial \mathcal{L}}{\partial k a}$	$\Delta\mathcal{L}(k_a)$	$\Delta\mathcal{L}$	$E_{\mathcal{L}}$	$\frac{\Delta\mathcal{L}(a)}{\Delta\mathcal{L}(k_a)}$
	$[km]$	$[-]$	$[km^2]$	$[km^{-1}]$	$[km]$	[%]	$[km]$
1	0.000	0.000	0.000	0.000	0.000		
2	-0.102	0.006	-6.064	0.001	0.006	5.7%	563%
3	-0.227	0.013	-16.348	0.003	0.013	4.8%	468%
12	-0.963	0.055	-108.545	0.018	0.058	3.1%	298%
Average		0.184		0.056	0.193	45.5%	443%

4.5 DISCUSSION

4.5.1 Deterministic method

A number of practical limitations exist in the application of the equation estimating the average travel distance of an ensemble of particles based on average circularity (equation 4.8) to a generic case study. The rounding coefficient, a, is lithology-specific, while the attrition coefficient (k_a) depends both on the lithology, through mechanical properties, and on the transport environment, through the energy imparted to particles in motion. Consequently, the application of equation 4.8 requires knowledge of three parameters: C_0, a, k_a. At present, these parameters can only be estimated through calibration, using field measurements. Nonetheless, as understanding of the relationships between rock mechanical properties and the associated rounding and attrition processes improves, constraining the values of these parameters should become easier (Bodek and Jerolmack, 2021; Litwin Miller and Jerolmack, 2021; Bray et al., 2024).

Another limitation is that the method assumes an invariant transformation function: the parameters a and k_a are treated as constant. However, results from Chapter 3 suggest that the rounding coefficient depends on the initial circularity of the particles at the source (C_0).

Most importantly, the method relies on ensemble averages of circularity, derived from multiple particles, to provide a deterministic estimate of travel distance. In doing so, it does not take full advantage of the distribution of circularity measured at a given location, nor of the knowledge of where particles were sampled. Both these sources of information can instead be incorporated into the proposed probabilistic method.

4.5.2 Probabilistic method

The accuracy and precision of this method have not been tested yet; however, some advantages and disadvantages can already be discussed, as they are inherent to its probabilistic formulation.

The Bayesian approach provides a probabilistic characterisation of travel distances, offering more nuanced insights than the deterministic estimates of the mean travel distance. Knowledge of $P_{\mathcal{L}}(\mathcal{L})$ would allow, for example, estimation of the distance from the sampling location beyond which only a certain percentage of particles originate, or the assignment of probabilities of provenance to reaches located within defined travel distance boundaries.

Another advantage of the Bayesian approach is that, through an appropriate selection of the prior distribution, it enables the integration of existing information on potential sediment sources. For instance, in the previously discussed case of two sources for the tracer lithology, a probabilistic method would assign a probability to each source rather than providing a single average travel distance, which is unlikely to correspond precisely to either.

On the other hand, a limitation of the current Bayesian formulation is that it does not account for the longitudinal dispersion of coarse particles along a river. Because of this phenomenon, sources located at different distances contribute unequally, and accounting for this effect has been shown to be crucial when modelling the evolution of circularity from multiple sources (Chapter 3). Future formulations may address this by incorporating such effects, raising new research questions, for example, whether the weighting function proposed there could also be applied to assign weights to travel distances, and whether this function is lithology-specific or exhibits universal scaling across different rock types.

4.6 Conclusions

This chapter has presented two methods for estimating the travel distance of coarse sediments based on their shape.

The first method provides the average distance travelled by an ensemble of particles and was applied to reproduce the distance travelled from a single source. Using the available data, it achieved an accuracy of approximately 6% for arenites and 21% for metabasalts.

The relative error is expected to decrease with increasing distance from the source. However, the precision of the method improves only very slowly with increasing travel distances. This behaviour reflects two key factors: the form of the relationship between average circularity and travel distance, and the inherent variability of sediment shapes at each location. Overall, the method offers an approximation of average travel distance but is highly sensitive to input values of circularity and other parameters. Consequently, a sufficiently large sample size is required. Furthermore, because the method does not incorporate prior information on possible source areas, it lacks any form of weighing function, representing a major limitation in settings with multiple sources.

The second method is a Bayesian approach that integrates available information on potential source locations to construct a prior distribution of travel distances. Sediment shape is then incorporated as an additional variable to refine this estimate. This probabilistic formulation provides more nuanced insights and can, in principle, be extended to settings with multiple sources through the introduction of a weighing function. Although the method has not yet been tested, its theoretical basis suggests a substantial improvement over the deterministic approach, warranting further investigation.

5

DISCUSSION AND CONCLUSIONS

This chapter summarises the main findings and discusses them within the broader context of landscape and river geomorphology and river engineering. Specific research questions are answered, methodological limitations are highlighted, and suggestions for areas for further research are provided.

5.1 GENERAL DISCUSSION

This thesis presents a series of contributions to the overarching question of how sediment shape can provide information on travel distance in mountainous rivers. The study is motivated by the potential for multiple applications to benefit from the use of an easily measurable property to infer sediment transport environments and pathways. Examples include restoration projects, infrastructure planning and development, and hazard assessments.

Within this broader objective, three key knowledge gaps were addressed. The first gap concerns the accuracy and reproducibility of sediment shape measurements obtained from field-collected images. As circularity, or isoperimetric ratio, is the parameter used to link shape to travel distance, the discussion and conclusions focus on this. The accuracy of circularity estimates was relatively high, with an absolute error of around 0.013. However, results showed that estimates depend on the segmentation method and the algorithm used to describe the geometry of particle outlines, producing relative errors of approximately 1.5% and 3.9%, respectively. This has implications for comparing results from different studies, where varying methodologies may make direct comparisons difficult. Although circularity is theoretically bounded between zero and one, values for natural sediments typically range between 0.4 and 0.99, further limiting inherent variability (Joo et al., 2018). As demonstrated in Chapter 2 results from different, potentially biased methods may therefore be difficult to reconcile. In this respect, the proposed segmentation method offers an advantage: unlike machine-learning algorithms, which depend on training datasets (Hassan et al., 2024), it is based on parameters that can be explicitly chosen by the user, ensuring reproducibility. Moreover, since its parameters have a physical meaning, the user could adapt them to keep a constant dimension when working with images with different resolutions. Finally, the method is operator independent, meaning that it does not require the refinement of the segmentation, even in the case of shadows, unlike existing tools, e.g., the “Quick Selection tool” available in Adobe Photoshop CC.

The data collection method should therefore be tested at the beginning of a field campaign and kept as consistent as possible throughout. When comparing results, potential biases between methods should be assessed, for example, by applying alternative methods to a subset of the dataset. Overall, however, the proposed method proved capable of producing reliable and repeatable measures of sediment size and shape, even when images were collected under field conditions with limited control over lighting. This demonstrates the feasibility of using low-cost measurement techniques to obtain sediment size and shape data. A possible improvement to facilitate the adoption of the proposed algorithm consists of its translation into an open-source language. Nonetheless, such effort should also envision the translation of the algorithm by Zheng and Hryciw (2015) to obtain results comparable with the ones presented in this work.

Opportunities for further exploration include drone-based imaging (Miazza et al., 2024). Preliminary tests during this research indicated that while drone images can be used to estimate sediment size statistics, lower resolution, imbrication, and partial coverage make them less suitable for precise shape analysis. Some research groups are exploring the possibility of using point clouds to provide a quasi-3D characterisation of sediment shape (Woodget and Austrums, 2017). Combining such methods with drone technology could allow rapid collection of large datasets. Advances in point cloud filtering and object identification suggest that automated removal of vegetation and other cover may soon be feasible, further contributing to the aims of this thesis. As explained in Chapter 4, improving the precision of travel distance estimates requires large sample sizes. Another promising development would be the automatic identification of sediment lithology. While AI-based tools already exist, unlike methods based on image thresholding, they depend on the training dataset. Nonetheless, recent comparisons suggest that in the future they could become a standard for optical granulometry (Miazza et al., 2024). Therefore, as these methods improve, the potential to combine quasi-3D shape metrics with lithology tagging could significantly enhance estimates of travel distance.

The second gap addressed relates to modelling the shape evolution of fragments originating from parent sediment rock outcrops. A new conceptual yet physically based model for sediment circularity was proposed. Importantly, the sampling methodology allowed, for the first time, assessment of the heterogeneity of the shapes produced by outcrops of different lithologies. Based on curvature-driven flow assumptions, which imply that chipping is the dominant attrition mechanism, the model successfully reproduced the shape evolution of fragments in alpine streams, where fragmentation cannot be *a priori* neglected. It is also performed well for lithologies with differing mechanical properties (arenites and metabasalts). Field data on spatial variation in sediment shape confirmed that a particle's shape at a given distance depends not only on transport but also on its initial form. Thus, measuring the shape of an individual particle at a given location does not allow deterministic estimation of travel distance. The data presented here, therefore, suggest that the models presented in the literature for the estimation of travel distance based on sediment shape (Szabó et al., 2015; Maue et al., 2022; Pokhrel et al., 2024; Takahashi et al., 2025a; Gehringer et al., 2025), which use a single relationship for all particles, regardless of their initial shape, are unlikely to provide accurate results. This is because they are inherently associating the full range of sediment shapes with their travel distance, without considering the fact that particles that have travelled the same distance might have different circularity, due to a different initial shape, and particles with the same shape might have travelled different distances for the same reason.

The proposed model was further applied to reproduce the overall shape evolution resulting from multiple arenite inputs, which was the lithology of interest in this case. Results indicate that two contrasting processes control sediment shape: attrition, which increases circularity rapidly with distance, and bedload dispersion, which reduces the influence of distant sources while enhancing the contribution of nearby ones. The combined effect is that the longitudinal evolution of circularity is characterised by sharp decreases where near outcrops supply fresh fragments, and a nonlinear increase with distance. The rate of circularity increase is controlled by rounding and attrition coefficients, highlighting the need for further research to assess how different values affect spatial dynamics under varying source distributions. Laboratory experiments could help identify measurable metrics to estimate such coefficients across rock types and transport settings, and thereby determine which lithologies are best suited as tracers in practical applications.

The third gap concerns the accuracy and precision of travel distance estimates from shape measurements. Deterministic estimates of average travel distance showed relative errors of about 63.5% for metabasalts and 31% for arenites, decreasing with increasing distance. The high error for metabasalts is likely due to a combination of factors: the presence of small contributions of metabasalts from unidentified sources, possibly small creeks which were not mapped in the available lithological map, and the relatively small sample size in some locations, which might have led to an imprecise measure of the average circularity. For metabasalts, constraining precision within 20% would require more than 1,000 samples in some cases, making the method impractical. For arenites, however, only about 40 samples were needed, making the approach more attractive.

The mechanical properties of a rock determine its rounding and attrition coefficients in a given transport environment and play a critical role in its suitability as a tracer (Litwin Miller and Jerolmack, 2021; Bray et al., 2024). According to the available data, “harder” rocks require longer distances to become rounded (Pfeiffer et al., 2022); hence, the sensitivity of travel distance estimates to changes in circularity, expressed by $\partial \mathcal{L}/\partial C$, is higher, making such estimates more uncertain. By contrast, “softer” rocks round more quickly, enabling more accurate estimates over shorter distances.

Nevertheless, estimating average travel distance from an ensemble of sediment shapes only captures a “mean” behaviour, which may be far more complex in systems with multiple sources and pathways. For this reason, a probabilistic approach offers clear advantages, as it can incorporate prior knowledge of travel distance distributions and address some of the limitations inherent in deterministic methods.

Although the proposed Bayesian framework has not yet been applied to the Sarzana Stream, it has one advantage over the deterministic approach. If information on the existing outcrops of the lithology of interest is available, this could be integrated to constrain the domain of all possible travel distances. Once its performance is assessed, it may be valuable to explore combining sediment shape with other properties, such as lithology, mineral content, radionuclides, or isotopes, to further refine travel distance estimates.

In conclusion, this work demonstrates that sediment shape has significant potential to provide information on travel distances, but the accuracy and precision of such estimates depend on a number of factors: the spatial distribution of sediment sources within the river network, the mechanical properties of the rock, and the size of the available sample.

5.2 Specific Conclusions

The following answers were provided to the specific research questions:

1. How can repeatable measurements of pebble shape be obtained from field images when lighting conditions cannot be controlled?

The proposed segmentation method, combined with the shape analysis algorithm developed by Zheng and Hryciw (2015), provides repeatable measurements of pebble shape with errors below 8% for all shape parameters considered, even when images are collected in uncontrolled field lighting conditions [Chapter 2.5].

2. What is the relative importance of the segmentation method and the shape characterisation algorithm in the accuracy of estimates of sediment shape from field-collected images?

Both steps contribute errors of the same order of magnitude. For circularity, segmentation introduced a relative error of approximately 1.5%, while the shape characterisation algorithm contributed around 3.9% [Chapter 2.5].

With respect to the estimation of sediment shape as a function of travel distance:

1. How can the spatial evolution of sediment shape in mountainous streams be modelled, starting from a localised point source?

The spatial evolution of the normalised isoperimetric ratio can be modelled by linking attrition-related mass loss to shape change through a superelliptical relationship and exponential decay of mass with distance. The model depends on three parameters: the initial shape of a particle, the rounding coefficient, and the attrition coefficient [Chapter 3.2].

2. What is the relative importance of the parameters associated with rounding rates and the spatial scaling of mass loss in controlling the rate of shape evolution?

Calibration against field data indicated that rounding coefficients were relatively similar across lithologies, whereas attrition coefficients varied by an order of magnitude. Thus, attrition plays the dominant role in controlling shape evolution [Chapter 3.4].

3. How can the contributions of multiple sediment sources be incorporated when modelling shape evolution in mountainous streams?

Field evidence showed that closer sources exert a disproportionate influence on circularity values. This was attributed to particle dispersion, which reduces contributions from more distant sources. An exponential probability distribution was used to represent this effect and performed well after calibration [Chapter 3.4].

4. Do outcrops exhibit lithology-specific shape properties?

The field data indicated that fragments produced by different lithologies exhibit distinct shape properties, and that these differ from the shapes of sediments derived from the same lithology even after short transport distances. This result merits further study across additional lithologies and transport environments [Chapter 3.4].

With respect to the estimation of sediment travel distance based on shape:

1. What is the accuracy and precision of travel distance estimates derived from sediment shape?

Deterministic estimates yielded mean absolute percentage errors of 63.5% for metabasalts and 31% for arenites. The relative standard deviations were around 4.3 and 2.4, respectively [Chapter 4.3].

2. How can sediment shape be used to update prior estimates of the probability distribution of sediment travel distances?

A Bayesian framework allows prior knowledge of travel distance distributions to be updated with shape data and enables integration of additional information (e.g., lithology) into source identification and distance estimation. Although not yet quantitatively assessed, this approach has clear advantages over purely deterministic methods [Chapter 4.4].

5.3 LIMITATIONS AND OPPORTUNITIES

The study of sediment attrition is important for scientific and practical implications that extend beyond the estimation of travel distance, which represents the primary motivation of this work. The results presented here are consistent with field observation: sediment shape evolves rapidly in lower-order streams, whereas as the contributing area increases, rivers become progressively saturated with pebbles exhibiting similar shapes. This impacts travel distance estimations because, as discussed in Chapter 4, for highly circular pebbles, these estimates become very sensitive to small variations in shape. Consequently, the precision of the deterministic method decreases, and large sample sizes are necessary to produce robust estimates of the average travel distance.

This natural limit could be addressed in different ways, depending on the scope of the research. One relatively drastic approach would consist of truncating the sampled population, excluding particles with a circularity higher than a given threshold, because the uncertainty in the estimation of their travel distance might be too large. In practice, this approach corresponds to choosing a window of travel distances associated with the contributing reaches under consideration and progressively moving this window downstream across different sampling locations.

Another, possibly complementary approach could be based on the development of new segmentation techniques to improve the accuracy of shape estimates from UAV imagery. This would produce significantly larger datasets, potentially leading to more robust estimates of the mean travel distance.

In cases such as the one presented here, where the outcrops of the tracer lithologies cover a limited area of the overall catchment, their contribution to the volume of sediments composing the riverbed is also relatively limited. Consequently, finding samples of these lithologies is time-consuming and labour-intensive. Moreover, assessing the lithology of sampled particles, which required scrutiny and comparison with known samples, was also time-consuming.

The methodology adopted in this work does not allow the tracking of individual particles as they are transported and undergo attrition. Consequently, the analyses were based on different statistics of the shape distribution, rather than on the evolution of the shape of individual particles. Tracking individual bedload particles in rivers is possible with multiple methods. Radio Frequency Identification tags (RFID) became the most adopted technology for this purpose, with more than 30,000 RFID tags injected in gravel-bed rivers around the world in the last 20 years (Liébault et al., 2023). This technology, although usually characterised by small recovery rates, has recently been coupled with UAV detectors to speed up the collection of tracers' positions.

Regardless of the chosen approach, the application of a probabilistic method, as the one described in Chapter 4 would allow the estimation of richer statistics of travel distances, compared to the deterministic method.

The author acknowledges that field campaigns require substantial effort and that sampling tracers to collect images and measure their shape introduces a disturbance to the pebble, which might modify its resting times and threshold for motion. Nonetheless, since tracer experiments are usually expensive and collecting multiple motion events might require several years, the author envisions the possibility of collaboration between scientists working with this methodology. Even when attrition might not be the primary focus of a given study, a subset of the injected tracers could be allocated to the collection of size and shape data. This would allow the creation of a vast dataset of particles' motion, and resting times, threshold conditions, and size and shape evolution. The additional cost would be limited to imaging tracer particles, while the benefit would be significant, because this would allow for the first time to link processes at the scale of the individual particle, such as jump lengths and threshold for motion conditions, to processes at the river scale, like size and shape changes of the riverbed, sorting, and, potentially, the gravel-sand transition.

Regarding the attrition of river sediment, this work assumes that particles lose mass solely due to their impact with the sediment on the riverbed. Their attrition is assumed to stop when particles are immobile, even though they might be subject to impacts from moving particles. This assumption is needed to make the process of mass loss independent of transport dynamics and of time. This, in turn, allows one to assume that the relative mass loss of a particle only depends on its properties, and not on those of the rest of the riverbed. In other words, interactions between particles of different lithologies are not considered.

The abrasion of bedrock rivers proves that moving particles produce attrition on a stationary rock surface. The relative importance of "in motion" and "in place" attrition is still poorly constrained, with considerably less research covering the latter process. In fluvial settings, the cumulative mass loss of a particle depends on the sequence of impacts it has been subject to. These impacts can be broadly classified into two categories: impacts experienced by the moving particle hitting the riverbed, and impacts experienced while the particle remains stationary. Mass loss due to "in-motion" impacts depends primarily on particle size, which controls both kinetic energy and the frequency of transport events, as well as on the mechanical properties of the material with which the particle collides. By contrast, mass loss due to "in-place" impacts can be viewed as a stochastic process governed by the probability distribution of sizes and mechanical properties of the moving particles.

The work by Sipos et al. (2020) provides a framework to model the evolution of the probability distribution of the size of colliding bedload particles, which depends on a single scalar parameter representing the energy level of the collective evolution process. Their results show that for low energy regimes, the probability distribution of particle size tends to focus, while it tends to disperse in high energy regimes. In both regimes, the particle mass decays exponentially with the number of impacts, in agreement with Sternberg's law. These results suggest the possibility of combining the energetic effects of all impacts in a single parameter, which could lead to a similar framework for the evolution of the probability of shape.

A key difference between size and shape metrics must be highlighted. While the size of a particle can only decrease due to attrition, its isoperimetric ratio might increase or decrease, for example in the case of fragmentation or eikonal flow. This might lead to more nuanced dynamics of the shape evolution. For this reason, some authors have suggested alternative descriptors of particle shape based on the number of stable (S) and unstable (U) equilibrium points, which are related by the Poincaré-Hopf Theorem: $S + U - H = 2$, where H is the number of saddle-type equilibrium points. The number of equilibrium points is expected to monotonically decrease, on average, due to attrition (Domokos, 2015), making it a potentially suitable descriptor for linking particle shape to transport history, even outside the strict applicability of curvature-driven abrasion models. While methods to estimate equilibrium points from 3D laser scans of pebbles exist, their adoption in the geophysical community is still limited. Nevertheless, given their theoretical robustness, further exploration of these metrics may prove valuable.

Addressing these questions will likely require a combination of approaches. On the one hand, the development of simplified theoretical frameworks capable of capturing the essential dynamics of particle evolution would allow numerical exploration of the parameter regimes governing different patterns of size and shape change. On the other hand, controlled laboratory experiments could provide the empirical data necessary to validate these models and inform the choice of functional relationships used in their formulation.

Ultimately, progress in understanding sediment attrition will require collaboration among researchers with complementary expertise and approaches.

ANNEXES

Annex to Chapter 3

The graphs presented in Figure A1 show the difference in distribution of normalised isoperimetric ratio between source locations and non-source ones. Highlighting the fact that, even after a very small travel distance, the shape of particles changes enough to be captured by a statistical test for equality of distributions.

This file provides the results of the Anderson-Darling test performed to assess whether the distributions of normalised isoperimetric ratios of sediment fragments at source locations can be considered the same as those in non-source locations, for each lithology. A significance level p=0.01 was assumed. Values were rounded to the fourth significant digit.

A separate file containing the overview of the sediment data collected in the field and used is provided as a separate file. These data include, the identifier of each sampling location, its coordinates, the sample size, for each lithology and mean and standard deviations of a series of size and shape parameters, which would allow the repetition of the analysis performed here.

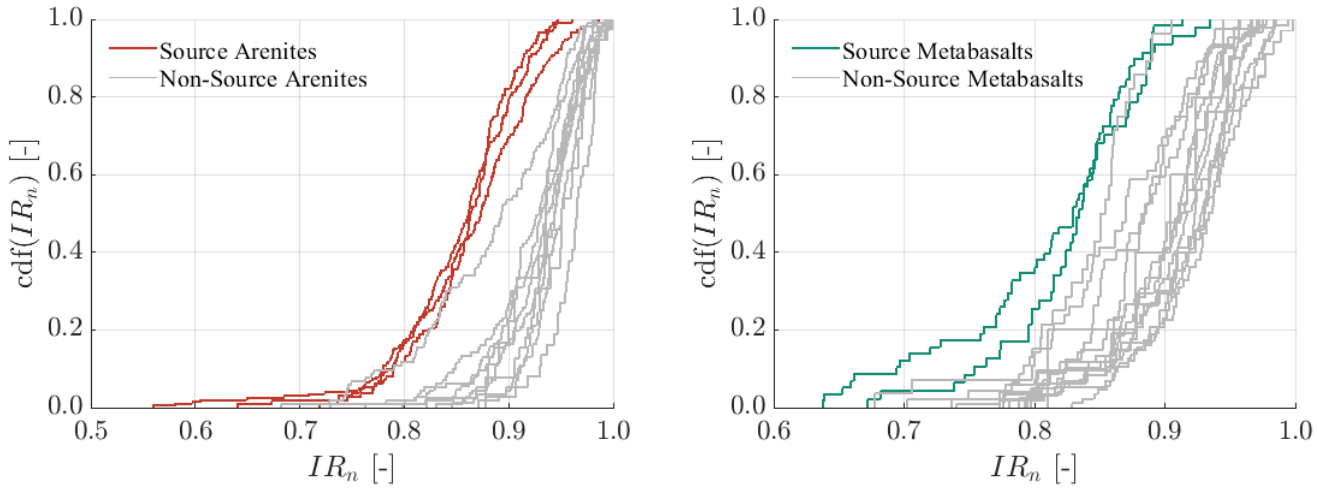

Figure A1. Cumulative distribution functions of normalised isoperimetric ratios for arenites and metabasalts. Source locations are coloured to highlight their different distribution with respect to other locations.

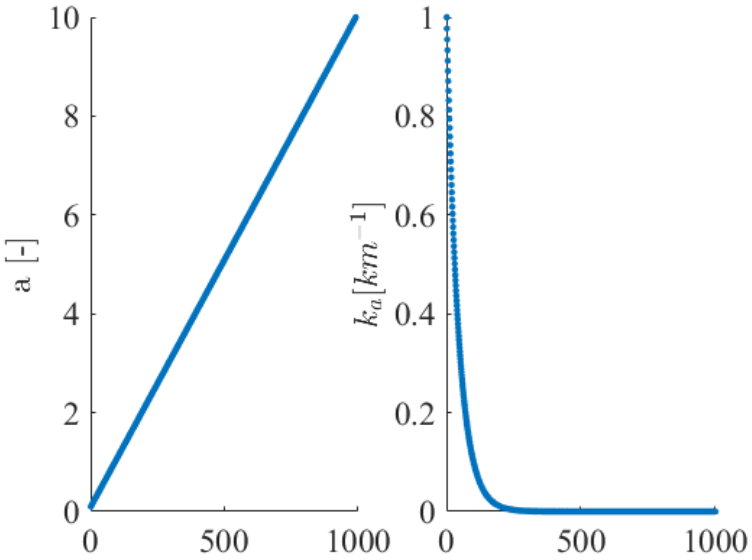

Figure A2. Set of parameters a and k_a used in the model calibration.

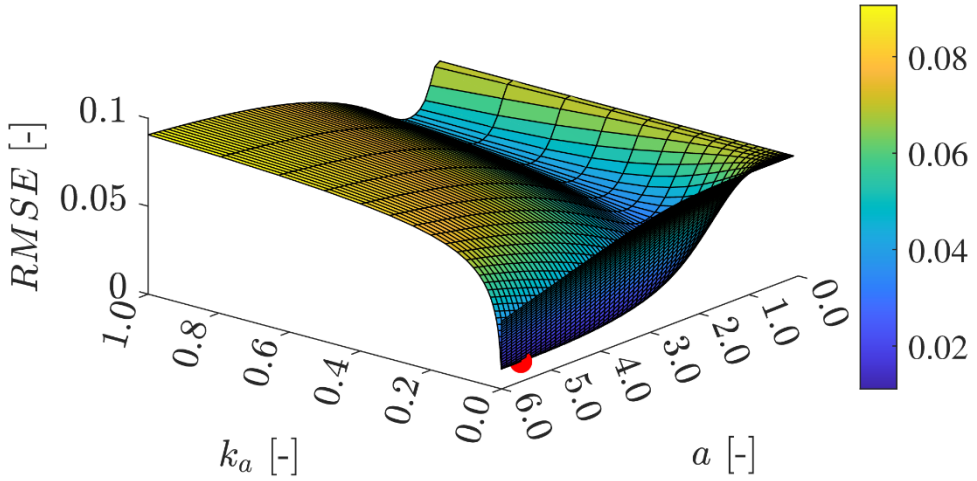

Figure A3. Minimisation of the root mean square error of the average circularity of metabasalts. The red dot represents the set of optimum model parameters.

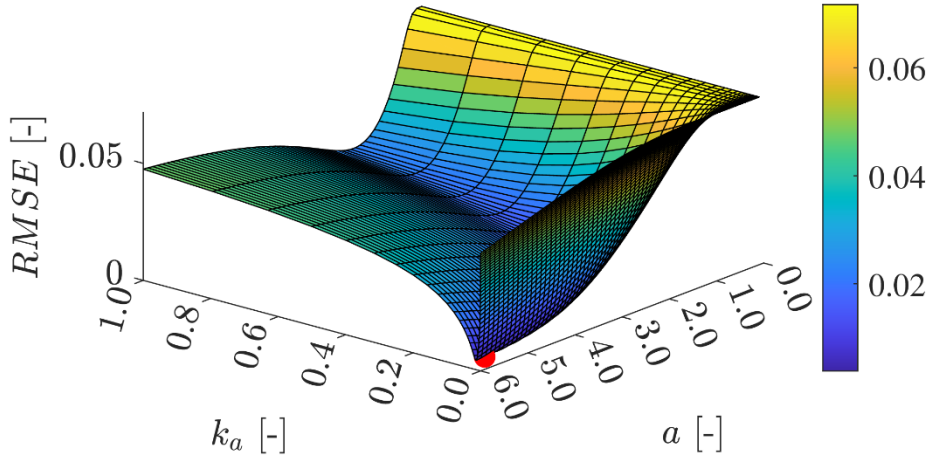

Figure A4. Minimisation of the root mean square error of the average circularity of arenites. The red dot represents the set of optimum model parameters.

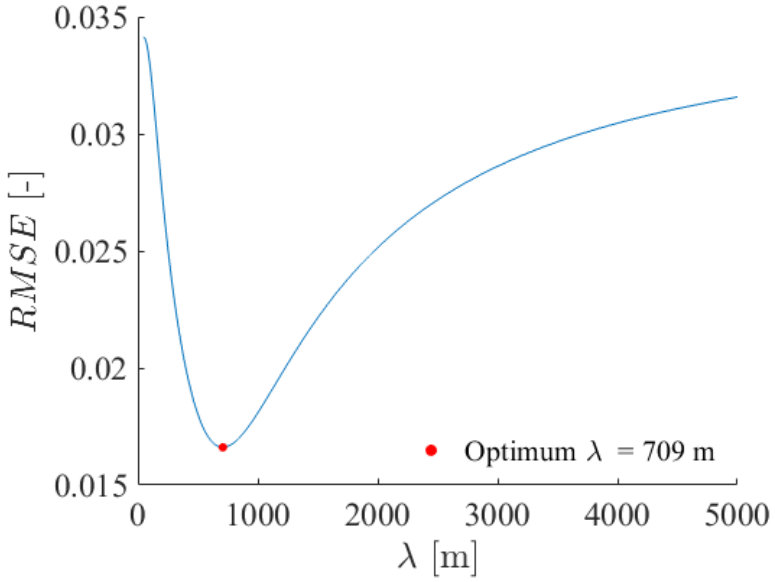

Figure A5. Minimisation of the root mean square error of multiple sources of arenites. Optimum value of the parameter of the exponential distribution weighing function for sources located at different distances.

Table A1a. Summary of sampling locations and sediment size.

Location	Lithology	Origin	Latitude [°]	Longitude [°]	Elevation [m a.s.l.]	Drainage Area [km^2]	Distance [km]	Sample Size
1	Arenites	Source	46.245755	11.98058	1126.4	0.03	6.73	112
2	Arenites	Creek	46.245891	11.981488	1108	0.03	6.65	109
3	Arenites	River	46.246834	11.984985	1055.8	2.19	6.29	18
12	Arenites	River	46.253362	11.990762	983.8	9.41	5.21	37
13	Arenites	Creek	46.254931	11.992186	975.7	3.02	4.97	39
14	Arenites	River	46.255349	11.992921	969	9.82	4.88	57
15	Arenites	River	46.259202	11.999316	897.5	14.62	4.01	103
15	Arenites	Source	46.259202	11.999316	897.5	14.62	4.01	133
16	Arenites	Source	46.27198	11.998473	975.3	1.12	3.08	204
17	Arenites	Creek	46.272289	11.999252	958.3	1.14	3.00	113
18	Arenites	River	46.267751	12.006646	824.4	19.38	2.57	116
19	Arenites	River	46.271622	12.015076	692.5	23.33	1.57	113
4	Metabasalts	Source	46.248233	11.990253	1124.6	0.15	6.14	47
5	Metabasalts	Creek	46.248494	11.989842	1103.2	0.16	6.10	46
6	Metabasalts	Source	46.24913	11.9916	1128.6	0.03	6.01	58
7	Metabasalts	Creek	46.249446	11.991154	1107.7	0.04	5.96	28
8	Metabasalts	River	46.249877	11.987362	1037.1	2.70	5.86	40

Table A1b. Summary of sampling locations and sediment size.

Location	Lithology	Origin	Latitude [°]	Longitude [°]	Elevation [m a.s.l.]	Drainage Area [km^2]	Distance [km]	Sample Size
9	Metabasalts	Creek	46.249803	11.988163	1040.9	0.18	5.85	42
10	Metabasalts	River	46.251105	11.989137	1026.2	2.98	5.64	21
11	Metabasalts	River	46.252051	11.990173	1009.3	3.02	5.48	59
12	Metabasalts	River	46.253362	11.990762	983.8	9.41	5.21	34
14	Metabasalts	River	46.255349	11.992921	969	9.82	4.88	68
15	Metabasalts	River	46.259202	11.999316	897.5	14.62	4.01	30
18	Metabasalts	River	46.267751	12.006646	824.4	19.38	2.57	97
19	Metabasalts	River	46.271622	12.015076	692.5	23.33	1.57	88
20	Metabasalts	River	46.271167	12.022084	626.1	23.99	0.67	48
21	Metabasalts	River	46.272602	12.02853	570.1	25.24	0.00	58
11	Mixed Sample	River	46.252051	11.990173	1009.3	3.02	5.48	123
12	Mixed Sample	River	46.253362	11.990762	983.8	9.41	5.21	126
15	Mixed Sample	River	46.259202	11.999316	897.5	14.62	4.01	132
17	Mixed Sample	Creek	46.272289	11.999252	958.3	1.14	3.00	150
18	Mixed Sample	River	46.267751	12.006646	824.4	19.38	2.57	124
19	Mixed Sample	River	46.271622	12.015076	692.5	23.33	1.57	111
20	Mixed Sample	River	46.271167	12.022084	626.1	23.99	0.67	106

Table A1c. Summary of shape parameters (averages on the left, standard deviation on the right).

Location	b [mm]		elongation [-]		Area [mm^2]		Roundness [-]		IR [-]		Normalised IR [-]	
1	47.55	20.53	0.67	0.13	3034.57	2714.96	0.51	0.08	0.79	0.06	0.86	0.05
2	29.81	12.90	0.70	0.12	1165.60	1063.77	0.59	0.08	0.86	0.06	0.92	0.04
3	27.55	15.73	0.70	0.11	1159.37	1428.95	0.62	0.07	0.88	0.05	0.93	0.03
12	43.32	27.38	0.73	0.12	2786.83	3890.90	0.73	0.08	0.91	0.05	0.96	0.03
13	49.99	39.55	0.75	0.10	4146.31	8085.38	0.66	0.10	0.91	0.04	0.95	0.04
14	52.77	31.67	0.73	0.11	3956.73	4923.47	0.69	0.08	0.90	0.04	0.94	0.02
15	41.24	24.54	0.64	0.16	2798.79	4026.34	0.55	0.11	0.80	0.10	0.88	0.07
15	36.18	16.38	0.61	0.15	2000.71	1809.04	0.49	0.06	0.76	0.08	0.86	0.05
16	30.82	13.44	0.64	0.15	1345.01	1175.46	0.50	0.09	0.78	0.10	0.86	0.07
17	24.99	23.05	0.66	0.15	1292.68	4305.87	0.57	0.09	0.85	0.08	0.92	0.05
18	34.16	29.81	0.68	0.13	2231.33	4293.26	0.65	0.10	0.87	0.07	0.93	0.04
19	49.45	27.95	0.68	0.14	3645.31	4329.38	0.68	0.09	0.87	0.07	0.93	0.03
4	61.92	32.99	0.64	0.14	5625.91	5710.73	0.50	0.08	0.76	0.08	0.83	0.06
5	89.68	56.77	0.73	0.12	11356.71	13442.97	0.56	0.08	0.82	0.07	0.86	0.06
6	69.00	32.08	0.66	0.14	6497.32	6696.76	0.49	0.06	0.74	0.07	0.81	0.07
7	113.12	36.19	0.73	0.14	14789.94	9026.77	0.52	0.07	0.79	0.06	0.84	0.05
8	105.24	44.60	0.67	0.13	14806.21	11708.14	0.63	0.08	0.82	0.06	0.88	0.04

Table A1d. Summary of shape parameters (averages on the left, standard deviation on the right).

Location	b [mm]		elongation [-]		Area [mm^2]		Roundness [-]		IR [-]		Normalised IR [-]	
9	100.20	57.44	0.67	0.16	14370.04	15230.88	0.59	0.09	0.81	0.08	0.88	0.04
10	82.64	61.98	0.63	0.19	14925.68	20595.54	0.61	0.07	0.80	0.10	0.90	0.04
11	122.61	55.70	0.71	0.14	20535.04	17096.65	0.64	0.09	0.85	0.07	0.90	0.04
12	76.59	66.09	0.69	0.16	11045.47	19830.60	0.66	0.10	0.85	0.09	0.92	0.05
14	68.95	40.12	0.68	0.13	6932.47	7911.29	0.62	0.09	0.84	0.08	0.90	0.05
15	103.37	49.71	0.70	0.14	14684.31	15003.52	0.64	0.08	0.85	0.08	0.91	0.05
18	71.86	36.49	0.68	0.13	7161.49	6943.01	0.65	0.09	0.85	0.07	0.91	0.04
19	62.88	33.99	0.69	0.14	5840.07	6474.65	0.67	0.08	0.86	0.07	0.92	0.04
20	71.81	43.13	0.68	0.13	7720.94	9290.66	0.65	0.10	0.85	0.07	0.92	0.05
21	95.81	40.52	0.68	0.14	11988.85	9617.88	0.68	0.09	0.86	0.07	0.93	0.04
11	48.72	19.31	0.67	0.14	3314.54	3078.75	0.60	0.10	0.84	0.07	0.91	0.04
12	50.75	24.03	0.69	0.14	3595.99	3786.43	0.62	0.08	0.85	0.07	0.91	0.04
15	49.31	25.19	0.68	0.13	3363.47	3773.99	0.60	0.09	0.84	0.07	0.90	0.05
17	41.21	24.26	0.70	0.13	2412.97	2834.60	0.59	0.09	0.85	0.07	0.90	0.05
18	49.47	25.16	0.70	0.13	3418.92	4304.60	0.60	0.10	0.85	0.06	0.91	0.04
19	59.31	31.05	0.71	0.13	4769.85	5736.13	0.65	0.09	0.86	0.06	0.92	0.04
20	47.41	21.45	0.71	0.13	2971.22	2784.10	0.64	0.10	0.88	0.06	0.94	0.04

Table A2. p values of Anderson-Darling test for same distributions of arenites normalised isoperimetric ratios.

Location		**3**	**4**	**5**	**15**	**16**	**17**	**18**	**18**	**19**	**20**	**21**	**22**
	Origin	**Source**	Creek	River	River	Creek	River	River	**Source**	**Source**	Creek	River	River
3	**Source**	0.8690	0.0000	0.0000	0.0000	0.0000	0.0000	0.0000	0.4057	0.0209	0.0000	0.0000	0.0000
4	Creek		0.8690	0.4015	0.0000	0.0000	0.0003	0.0000	0.0000	0.0000	0.0771	0.0010	0.0142
5	River			0.8835	0.0013	0.1643	0.1192	0.0031	0.0000	0.0000	0.5989	0.6477	0.7408
15	River				0.8748	0.0807	0.0000	0.0000	0.0000	0.0000	0.0000	0.0000	0.0000
16	Creek					0.8743	0.0237	0.0000	0.0000	0.0000	0.0074	0.0811	0.0230
17	River						0.8718	0.0000	0.0000	0.0000	0.0054	0.1566	0.0842
18	River							0.8692	0.0000	0.0021	0.0000	0.0000	0.0000
18	**Source**								0.8685	0.0632	0.0000	0.0000	0.0000
19	**Source**									0.8676	0.0000	0.0000	0.0000
20	Creek										0.8689	0.0921	0.0744
21	River											0.8689	0.3455
22	River												0.8689

Table A3. p values of Anderson-Darling test for same distributions of metabasalts normalised isoperimetric ratios.

Location		**4**	**5**	**6**	**7**	**8**	**9**	**10**	**11**	**12**	**14**	**15**	**18**	**19**	**20**	**21**
	Origin	**Source**	Creek	**Source**	Creek	River	Creek	River	River	River	River	River	River	River	River	River
4	**Source**	0.8730	0.0032	0.2524	0.2612	0.0000	0.0000	0.0000	0.0000	0.0000	0.0000	0.0000	0.0000	0.0000	0.0000	0.0000
5	Creek		0.8731	0.0000	0.0211	0.1260	0.2289	0.0114	0.0004	0.0000	0.0004	0.0002	0.0000	0.0000	0.0000	0.0000
6	**Source**			0.8717	0.0482	0.0000	0.0000	0.0000	0.0000	0.0000	0.0000	0.0000	0.0000	0.0000	0.0000	0.0000
7	Creek				0.8775	0.0000	0.0010	0.0000	0.0000	0.0000	0.0000	0.0000	0.0000	0.0000	0.0000	0.0000
8	River					0.8741	0.5532	0.0803	0.0363	0.0006	0.0142	0.0011	0.0002	0.0000	0.0000	0.0000
9	Creek						0.8738	0.1078	0.0334	0.0015	0.0139	0.0023	0.0003	0.0000	0.0000	0.0000
10	River							0.8811	0.6828	0.2890	0.6813	0.4074	0.6462	0.0632	0.1663	0.0259
11	River								0.8716	0.0283	0.5114	0.0425	0.1418	0.0007	0.0056	0.0001
12	River									0.8755	0.0506	0.5116	0.1288	0.3937	0.5038	0.4550
14	River										0.8709	0.0904	0.2569	0.0026	0.0111	0.0003
15	River											0.8768	0.4349	0.3809	0.6603	0.2436
18	River												0.8694	0.0388	0.1206	0.0035
19	River													0.8698	0.5572	0.4719
20	River														0.8728	0.3156
21	River															0.8717

REFERENCES

Adams, J.: Gravel Size Analysis from Photographs, J. Hydraul. Div., 105, 1247–1255, https://doi.org/10.1061/JYCEAJ.0005283, 1979a.

Adams, J.: Wear of Unsound Pebbles in River Headwaters, Science, 203, 171–172, 1979b.

Al-Najdawi, N., Bez, H. E., Singhai, J., and Edirisinghe, Eran. A.: A survey of cast shadow detection algorithms, Pattern Recognit. Lett., 33, 752–764, https://doi.org/10.1016/j.patrec.2011.12.013, 2012.

Ancey, C., Davison, A. C., Böhm, T., Jodeau, M., and Frey, P.: Entrainment and motion of coarse particles in a shallow water stream down a steep slope, J. Fluid Mech., 595, 83–114, https://doi.org/10.1017/S0022112007008774, 2008.

Anon: Database of the different lithologies that make up the territory of the Veneto Region scale 1:250,000, 2016.

Atkinson, C. L., Allen, D. C., Davis, L., and Nickerson, Z. L.: Incorporating ecogeomorphic feedbacks to better understand resiliency in streams: A review and directions forward, Geomorphology, https://doi.org/10.1016/j.geomorph.2017.07.016, 2017.

Attal, M. and Lavé, J.: Pebble abrasion during fluvial transport: Experimental results and implications for the evolution of the sediment load along rivers, J. Geophys. Res. Earth Surf., 114, F04023, https://doi.org/10.1029/2009JF001328, 2009.

Barbi, A., Cagnati, A., Cola, G., Checchetto, F., Chiaudani, A., Crepaz, A., Delillo, I., Mariani, L., Marigo, G., Meneghin, P., Parsi, S. G., Rech, F., Renon, B., and Robert-Luciani, T.: Atlante climatico del Veneto. Precipitazioni - Basi informative per l'analisi delle correlazioni tra cambiamenti climatici e dinamiche forestali nel Veneto., ARPAV – Agenzia Regionale per la Prevenzione e la protezione Ambientale del Veneto, Mestre (Venezia), Italy, 2013.

Barrett, P. J.: The shape of rock particles, a critical review, Sedimentology, 27, 291–303, https://doi.org/10.1111/j.1365-3091.1980.tb01179.x, 1980.

Beven, K. and Binley, A.: The future of distributed models: Model calibration and uncertainty prediction, Hydrol. Process., 6, 279–298, https://doi.org/10.1002/hyp.3360060305, 1992.

Beveridge, C., Hossain, F., and Bonnema, M.: Estimating Impacts of Dam Development and Landscape Changes on Suspended Sediment Concentrations in the Mekong River Basin's 3S Tributaries, J. Hydrol. Eng., 25, 05020014, https://doi.org/10.1061/(ASCE)HE.1943-5584.0001949, 2020.

Binh, D. V., Kantoush, S. A., Sumi, T., Mai, N. P., Ngoc, T. A., Trung, L. V., and An, T. D.: Effects of riverbed incision on the hydrology of the Vietnamese Mekong Delta, Hydrol. Process., 35, e14030, https://doi.org/10.1002/hyp.14030, 2021.

Bloore, F. J.: The shape of pebbles, J. Int. Assoc. Math. Geol., 9, 113–122, 1977.

Bodek, S. and Jerolmack, D. J.: Breaking down chipping and fragmentation in sediment transport: the control of material strength, Earth Surf. Dyn. Discuss., 1–21, https://doi.org/10.5194/esurf-2021-17, 2021.

Bradley, W. C.: Effect of Weathering on Abrasion of Granitic Gravel, Colorado River (Texas), Geol. Soc. Am. Bull., 81, 61, https://doi.org/10.1130/0016-7606(1970)81%255B61:EOWOAO%255D2.0.CO;2, 1970.

Bradley, W. C., Fahnestock, R. K., and Rowekamp, E. T.: Coarse Sediment Transport by Flood Flows on Knik River, Alaska, GSA Bull., 83, 1261–1284, https://doi.org/10.1130/0016-7606(1972)83%255B1261:CSTBFF%255D2.0.CO;2, 1972.

Bray, E. N., Litwin Miller, K., Cardona, M., Pettyjohn, S., and Sklar, L. S.: Influence of particle lithology, size and angularity on rates and products of bedload wear: An experimental study, Earth Surf. Process. Landf., n/a, https://doi.org/10.1002/esp.6007, 2024.

Bregoli, F., Crosato, A., Paron, P., and McClain, M. E.: Humans reshape wetlands: Unveiling the last 100 years of morphological changes of the Mara Wetland, Tanzania, Sci. Total Environ., 691, 896–907, https://doi.org/10.1016/j.scitotenv.2019.07.189, 2019.

Brenna, A. and Surian, N.: Coarse sediment mobility and fluxes in wide mountain streams: Insights using the virtual velocity approach, Geomorphology, 427, 108625, https://doi.org/10.1016/j.geomorph.2023.108625, 2023.

Brewer, P., Leeks, G., and Lewin, J.: Direct measurement of in-channel abrasion processes, in: Proceedings of the Oslo Symposium, Erosion and Sediment Transport Monitoring Programmes in River Basins, Oslo, Norway, 1992.

Buscombe, D., Rubin, D. M., and Warrick, J. A.: A universal approximation of grain size from images of noncohesive sediment, J. Geophys. Res. Earth Surf., 115, F02015, https://doi.org/10.1029/2009JF001477, 2010.

Butler, J. B., Lane, S. N., and Chandler, J. H.: Automated extraction of grain-size data from gravel surfaces using digital image processing, J. Hydraul. Res., 39, 519–529, https://doi.org/10.1080/00221686.2001.9628276, 2001.

Canny, J.: A Computational Approach to Edge Detection, IEEE Trans. Pattern Anal. Mach. Intell., PAMI-8, 679–698, https://doi.org/10.1109/TPAMI.1986.4767851, 1986.

Carbonneau, P. E., Lane, S. N., and Bergeron, N. E.: Catchment-scale mapping of surface grain size in gravel bed rivers using airborne digital imagery, Water Resour. Res., 40, W07202, https://doi.org/10.1029/2003WR002759, 2004.

Carbonneau, P. E., Bizzi, S., and Marchetti, G.: Robotic photosieving from low-cost multirotor sUAS: a proof-of-concept: Robotic photosieving, Earth Surf. Process. Landf., 43, 1160–1166, https://doi.org/10.1002/esp.4298, 2018.

Carretier, S. and Regard, V.: Is it possible to quantify pebble abrasion and velocity in rivers using terrestrial cosmogenic nuclides?, J. Geophys. Res. Earth Surf., 116, https://doi.org/10.1029/2011JF001968, 2011.

Cassel, M., Dépret, T., and Piégay, H.: Assessment of a new solution for tracking pebbles in rivers based on active RFID, Earth Surf. Process. Landf., 42, 1938–1951, https://doi.org/10.1002/esp.4152, 2017a.

Cassel, M., Piégay, H., and Lavé, J.: Effects of transport and insertion of radio frequency identification (RFID) transponders on resistance and shape of natural and synthetic pebbles: applications for riverine and coastal bedload tracking: Transport and Rfid-Insertion Effects on the Fragility of Pebbles, Earth Surf. Process. Landf., 42, 399–413, https://doi.org/10.1002/esp.3989, 2017b.

Cassel, M., Piégay, H., Lavé, J., Vaudor, L., Hadmoko Sri, D., Wibiwo Budi, S., and Lavigne, F.: Evaluating a 2D image-based computerized approach for measuring riverine pebble roundness, Geomorphology, 311, 143–157, https://doi.org/10.1016/j.geomorph.2018.03.020, 2018.

Cassel, M., Lavé, J., Recking, A., Malavoi, J.-R., and Piégay, H.: Bedload transport in rivers, size matters but so does shape, Sci. Rep., 11, 508, https://doi.org/10.1038/s41598-020-79930-7, 2021.

Cattapan, A., Paron, P., and Franca, M. J.: Deriving Grain Size Distributions From UAVs Images, in: The Future River, NCR Days 2018, Delft, The Netherlands, 90–91, 2018.

Cattapan, A., Gurini, A., Paron, P., Ballio, F., and Franca, M. J.: A method for segmentation of pebble images in the presence of shadows, Earth Surf. Process. Landf., 49, 5202–5212, https://doi.org/10.1002/esp.6027, 2024.

Chang, F.-J. and Chung, C.-H.: Estimation of riverbed grain-size distribution using image-processing techniques, J. Hydrol., 440–441, 102–112, https://doi.org/10.1016/j.jhydrol.2012.03.032, 2012.

Chapkanski, S., Ertlen, D., Rambeau, C., and Schmitt, L.: Provenance discrimination of fine sediments by mid-infrared spectroscopy: Calibration and application to fluvial palaeo-environmental reconstruction, Sedimentology, 67, 1114–1134, https://doi.org/10.1111/sed.12678, 2020.

Chen, X., Hassan, M. A., and Fu, X.: Convolutional neural networks for image-based sediment detection applied to a large terrestrial and airborne dataset, Earth Surf. Dyn., 10, 349–366, https://doi.org/10.5194/esurf-10-349-2022, 2022.

Chong, X. Y., Vericat, D., Batalla, R. J., Teo, F. Y., Lee, K. S. P., and Gibbins, C. N.: A review of the impacts of dams on the hydromorphology of tropical rivers, Sci. Total Environ., 794, 148686, https://doi.org/10.1016/j.scitotenv.2021.148686, 2021.

Collins, A. L., Pulley, S., Foster, I. D. L., Gellis, A., Porto, P., and Horowitz, A. J.: Sediment source fingerprinting as an aid to catchment management: A review of the current state of knowledge and a methodological decision-tree for end-users, J. Environ. Manage., 194, 86–108, https://doi.org/10.1016/j.jenvman.2016.09.075, 2017.

Collins, A. L., Blackwell, M., Boeckx, P., Chivers, C.-A., Emelko, M., Evrard, O., Foster, I., Gellis, A., Gholami, H., Granger, S., Harris, P., Horowitz, A. J., Laceby, J. P., Martinez-Carreras, N., Minella, J., Mol, L., Nosrati, K., Pulley, S., Silins, U., da Silva, Y. J., Stone, M., Tiecher, T., Upadhayay, H. R., and Zhang, Y.: Sediment source fingerprinting: benchmarking recent outputs, remaining challenges and emerging themes, J. Soils Sediments, 20, 4160–4193, https://doi.org/10.1007/s11368-020-02755-4, 2020.

Cooper, R. J. and Krueger, T.: An extended Bayesian sediment fingerprinting mixing model for the full Bayes treatment of geochemical uncertainties, Hydrol. Process., 31, 1900–1912, https://doi.org/10.1002/hyp.11154, 2017.

Czuba, J. A.: A Lagrangian framework for exploring complexities of mixed-size sediment transport in gravel-bedded river networks, Geomorphology, 321, 146–152, https://doi.org/10.1016/j.geomorph.2018.08.031, 2018.

Czuba, J. A. and Foufoula-Georgiou, E.: A network-based framework for identifying potential synchronizations and amplifications of sediment delivery in river basins, Water Resour. Res., 50, 3826–3851, https://doi.org/10.1002/2013WR014227, 2014.

Davies, J., Olley, J., Hawker, D., and McBroom, J.: Application of the Bayesian approach to sediment fingerprinting and source attribution, Hydrol. Process., 32, 3978–3995, https://doi.org/10.1002/hyp.13306, 2018.

Dawson, M.: Sediment size variation in a braided reach of the Sunwapta River, Alberta, Canada, Earth Surf. Process. Landf., 13, 599–618, https://doi.org/10.1002/esp.3290130705, 1988.

Deal, E., Venditti, J. G., Benavides, S. J., Bradley, R., Zhang, Q., Kamrin, K., and Perron, J. T.: Grain shape effects in bed load sediment transport, Nature, 613, 298–302, https://doi.org/10.1038/s41586-022-05564-6, 2023.

Detert, M. and Weitbrecht, V.: Automatic object detection to analyze the geometry of gravel grains – a free stand-alone tool, in: Proceedings of the International Conference on Fluvial Hydraulics, River flow 2012, San José, Costa Rica, 2012.

Dhont, B. and Ancey, C.: Are Bedload Transport Pulses in Gravel Bed Rivers Created by Bar Migration or Sediment Waves?, Geophys. Res. Lett., 45, 5501–5508, https://doi.org/10.1029/2018GL077792, 2018.

Domingo, J. P. T., Ngwenya, B. T., Attal, M., David, C. P. C., and Mudd, S. M.: Geochemical fingerprinting to determine sediment source contribution and improve contamination assessment in mining-impacted floodplains in the Philippines, Appl. Geochem., 159, 105808, https://doi.org/10.1016/j.apgeochem.2023.105808, 2023.

Domokos, G.: Monotonicity of Spatial Critical Points Evolving Under Curvature-Driven Flows, J. Nonlinear Sci., 25, 247–275, https://doi.org/10.1007/s00332-014-9228-3, 2015.

Domokos, G. and Gibbons, G. W.: The evolution of pebble size and shape in space and time, Proc. R. Soc. Lond. Math. Phys. Eng. Sci., 468, 3059–3079, https://doi.org/10.1098/rspa.2011.0562, 2012.

Domokos, G. and Gibbons, G. W.: The Geometry of Abrasion, in: New Trends in Intuitive Geometry, edited by: Ambrus, G., Bárány, I., Böröczky, K. J., Fejes Tóth, G., and Pach, J., Springer, Berlin, Heidelberg, 125–153, https://doi.org/10.1007/978-3-662-57413-3_6, 2018.

Domokos, G. and Lángi, Z.: The Evolution of Geological Shape Descriptors Under Distance-Driven Flows, Math. Geosci., 50, 337–363, https://doi.org/10.1007/s11004-017-9723-9, 2018.

Domokos, G., Jerolmack, D. J., Sipos, A. Á., and Török, Á.: How river rocks round: resolving the shape-size paradox, PloS One, 9, e88657, 2014.

Domokos, G., Kun, F., Sipos, A. Á., and Szabó, T.: Universality of fragment shapes, Sci. Rep., 5, https://doi.org/10.1038/srep09147, 2015.

Ecins, A., Fermüller, C., and Aloimonos, Y.: Shadow free segmentation in still images using local density measure, in: 2014 IEEE International Conference on Computational Photography (ICCP), 2014 IEEE International Conference on Computational Photography (ICCP), 1–8, https://doi.org/10.1109/ICCPHOT.2014.6831803, 2014.

Einstein, H. A.: The Bed-Load Function for Sediment Transportation in Open Channel Flows, Technical Bulletins, United States Department of Agriculture, Economic Research Service, 1950.

Engelund, F. and Hansen, E.: A monograph on sediment transport in alluvial streams, Tech. Univ. Den. 0stervoldgade 10 Cph. K, 1967.

European Union, Copernicus Land Monitoring Service: CORINE Land Cover 2018 (vector), Europe, 6-yearly (2018), https://doi.org/10.2909/71c95a07-e296-44fc-b22b-415f42acfdf0, 2018.

Feehan, S. A., McCoy, S. W., Scheingross, J. S., and Gardner, M. H.: Quantifying Variability of Incipient-Motion Thresholds in Gravel-Bedded Rivers Using a Grain-Scale Force-Balance Model, J. Geophys. Res. Earth Surf., 128, e2023JF007162, https://doi.org/10.1029/2023JF007162, 2023.

Ferguson, R., Hoey, T., Wathen, S., and Werritty, A.: Field evidence for rapid downstream fining of river gravels through selective transport, Geology, 24, 179–182, https://doi.org/10.1130/0091-7613(1996)024%253C0179:FEFRDF%253E2.3.CO;2, 1996.

Firey, W. J.: Shapes of worn stones, Mathematika, 21, 1–11, https://doi.org/10.1112/S0025579300005714, 1974.

Frings, R. M.: Downstream fining in large sand-bed rivers, Earth-Sci. Rev., 87, 39–60, https://doi.org/10.1016/j.earscirev.2007.10.001, 2008.

Gehringer, E. R., Ferrari, G., Morgan, A. M., and Palucis, M. C.: Using Clast Morphometry to Reconstruct Basaltic Sediment Transport History, J. Geophys. Res. Planets, 130, e2025JE009154, https://doi.org/10.1029/2025JE009154, 2025.

Gonzalez, R. C., Woods, R. E., and Eddins, S. L.: Digital Image processing using MATLAB, 2nd ed., Gatesmark Pub, S.I., 826 pp., 2009.

Hassan, R., Onyelowe, K. C., and Zamel, A. A.: Image processing and neural network technique for size characterization of gravel particles, Sci. Rep., 14, 22737, https://doi.org/10.1038/s41598-024-72700-9, 2024.

Havasi-Tóth, B. and Fehér, E.: A Geometrically Motivated Two-Dimensional Collisional Abrasion Model to Resolve the Evolution of Natural Fragment Shapes, Rock Mech. Rock Eng., 58, 1639–1649, https://doi.org/10.1007/s00603-024-04253-2, 2025.

Hayakawa, Y. and Oguchi, T.: Evaluation of gravel sphericity and roundness based on surface-area measurement with a laser scanner, Comput. Geosci., 31, 735–741, https://doi.org/10.1016/j.cageo.2005.01.004, 2005.

Heckmann, T. and Schwanghart, W.: Geomorphic coupling and sediment connectivity in an alpine catchment — Exploring sediment cascades using graph theory, Geomorphology, 182, 89–103, https://doi.org/10.1016/j.geomorph.2012.10.033, 2013.

Hodge, R., Brasington, J., and Richards, K.: In situ characterization of grain-scale fluvial morphology using Terrestrial Laser Scanning, Earth Surf. Process. Landf., 34, 954–968, https://doi.org/10.1002/esp.1780, 2009.

Houssais, M., Ortiz, C. P., Durian, D. J., and Jerolmack, D. J.: Onset of sediment transport is a continuous transition driven by fluid shear and granular creep, Nat. Commun., 6, 6527, https://doi.org/10.1038/ncomms7527, 2015.

Hryciw Roman D., Zheng Junxing, and Shetler Kristen: Particle Roundness and Sphericity from Images of Assemblies by Chart Estimates and Computer Methods, J. Geotech. Geoenvironmental Eng., 142, 04016038, https://doi.org/10.1061/(ASCE)GT.1943-5606.0001485, 2016.

Huang, G.-H., Atkinson, P. M., and Wang, C.-K.: Quantifying the scales of spatial variation in gravel beds using terrestrial and airborne laser scanning data, Open Geosci., 10, 607–617, https://doi.org/10.1515/geo-2018-0048, 2018.

Ito, K., Matsunaga, M., Itakiyo, T., Oishi, H., Nukazawa, K., Irie, M., and Suzuki, Y.: Tracing sediment transport history using mineralogical fingerprinting in a river basin with

dams utilizing sediment sluicing, Int. J. Sediment Res., 38, 469–480, https://doi.org/10.1016/j.ijsrc.2022.12.002, 2023.

Janku, A.: China: A hydrological history, Nature, 536, 28–29, https://doi.org/10.1038/536028a, 2016.

Jones, L. S. and Humphrey, N. F.: Weathering-controlled abrasion in a coarse-grained, meandering reach of the Rio Grande: Implications for the rock record, GSA Bull., 109, 1080–1088, https://doi.org/10.1130/0016-7606(1997)109%253C1080:WCAIAC%253E2.3.CO;2, 1997.

Joo, Y. J., Soreghan, A. M., Madden, M. E. E., and Soreghan, G. S.: Quantification of particle shape by an automated image analysis system: a case study in natural sediment samples from extreme climates, Geosci. J., 22, 525–532, https://doi.org/10.1007/s12303-018-0025-0, 2018.

Juez, C., Hassan, M. A., and Franca, M. J.: The origin of fine sediment determines the observations of suspended sediment fluxes under unsteady flow conditions, Water Resour. Res., 0, https://doi.org/10.1029/2018WR022982, 2018.

Khan, S., Fryirs, K., and Bizzi, S.: Modelling sediment (dis)connectivity across a river network to understand locational-transmission-filter sensitivity for identifying hotspots of potential geomorphic adjustment, Earth Surf. Process. Landf., n/a, https://doi.org/10.1002/esp.5213, 2021.

Kodama, Y.: Experimental study of abrasion and its role in producing downstream fining in gravel-bed rivers, J. Sediment. Res., 64, 76–85, https://doi.org/10.2110/jsr.64.76, 1994.

Koh, T. K., Miles, N., Morgan, S., and Hayes-Gill, B.: Image Segmentation of Overlapping Particles in Automatic Size Analysis Using Multi-Flash Imaging, in: 2007 IEEE Workshop on Applications of Computer Vision (WACV ’07), 2007 IEEE Workshop on Applications of Computer Vision (WACV ’07), 47–47, https://doi.org/10.1109/WACV.2007.37, 2007.

Krumbein, W. C.: The Effects of Abrasion on the Size, Shape and Roundness of Rock Fragments, J. Geol., 49, 482–520, https://doi.org/10.1086/624985, 1941.

Kuenen, Ph. H.: Experimental Abrasion of Pebbles: 2. Rolling by Current, J. Geol., 64, 336–368, https://doi.org/10.1086/626370, 1956.

Lajeunesse, E., Malverti, L., and Charru, F.: Bed load transport in turbulent flow at the grain scale: Experiments and modeling, J. Geophys. Res. Earth Surf., 115, F04001, https://doi.org/10.1029/2009JF001628, 2010.

Lamb, M. P., Dietrich, W. E., and Venditti, J. G.: Is the critical Shields stress for incipient sediment motion dependent on channel-bed slope?, J. Geophys. Res. Earth Surf., 113, https://doi.org/10.1029/2007JF000831, 2008.

Lamb, M. P., Brun, F., and Fuller, B. M.: Direct measurements of lift and drag on shallowly submerged cobbles in steep streams: Implications for flow resistance and sediment transport, Water Resour. Res., 53, 7607–7629, https://doi.org/10.1002/2017WR020883, 2017.

Lane, E. W. and Carlson, E. J.: Some observations on the effect of particle shape on the movement of coarse sediments, Eos Trans. Am. Geophys. Union, 35, 453–462, https://doi.org/10.1029/TR035i003p00453, 1954.

Langhammer, J., Lendzioch, T., Miřijovský, J., and Hartvich, F.: UAV-Based Optical Granulometry as Tool for Detecting Changes in Structure of Flood Depositions, Remote Sens., 9, 240, https://doi.org/10.3390/rs9030240, 2017.

Larimer, J. E., Yager, E. M., Yanites, B. J., and Witsil, A. J. C.: Flume Experiments on the Erosive Energy of Bed Load Impacts on Rough and Planar Beds, J. Geophys. Res. Earth Surf., 126, e2020JF005834, https://doi.org/10.1029/2020JF005834, 2021.

Larimer, J. E., Yanites, B. J., and Jung, S. J.: A Field Study on the Lithological Influence on the Interaction Between Weathering and Abrasion Processes in Bedrock Rivers, J. Geophys. Res. Earth Surf., 127, e2021JF006418, https://doi.org/10.1029/2021JF006418, 2022.

Le, H. and Samaras, D.: From Shadow Segmentation to Shadow Removal, ArXiv200800267 Cs, 2020.

Lewin, J. and Brewer, P. A.: Laboratory simulation of clast abrasion, Earth Surf. Process. Landf., 27, 145–164, https://doi.org/10.1002/esp.306, 2002.

Li, R., Lu, W., Chen, M., Wang, G., Xia, W., and Yan, P.: Quantitative analysis of shapes and specific surface area of blasted fragments using image analysis and three-dimensional laser scanning, Int. J. Rock Mech. Min. Sci., 141, 104710, https://doi.org/10.1016/j.ijrmms.2021.104710, 2021.

Liébault, F., Piégay, H., Cassel, M., and Arnaud, F.: Bedload tracing with RFID tags in gravel-bed rivers: Review and meta-analysis after 20 years of field and laboratory experiments, Earth Surf. Process. Landf., n/a, https://doi.org/10.1002/esp.5704, 2023.

Litty, C. and Schlunegger, F.: Controls on Pebbles' Size and Shape in Streams of the Swiss Alps, J. Geol., 125, 101–112, https://doi.org/10.1086/689183, 2017.

Litwin Miller, K. and Jerolmack, D.: Controls on the rates and products of particle attrition by bed-load collisions, Earth Surf. Dyn., 9, 755–770, https://doi.org/10.5194/esurf-9-755-2021, 2021.

Litwin Miller, K., Szabó, T., Jerolmack, D. J., and Domokos, G.: Quantifying the significance of abrasion and selective transport for downstream fluvial grain size evolution, J. Geophys. Res. Earth Surf., 119, 2014JF003156, https://doi.org/10.1002/2014JF003156, 2014.

Liu, H., Zhang, Z., Su, H., Zhang, X., and Hu, J.: Three-dimensional characterization of particle morphology in natural gravel and blasted rock fragments using SfM-MVS photogrammetry, River, 4, 70–83, https://doi.org/10.1002/rvr2.114, 2025.

Manga, M., Patel, A., and Dufek, J.: Rounding of pumice clasts during transport: field measurements and laboratory studies, Bull. Volcanol., 73, 321–333, https://doi.org/10.1007/s00445-010-0411-6, 2011.

Maniatis, G., Hoey, T., Hodge, R., Rickenmann, D., and Badoux, A.: Inertial drag and lift forces for coarse grains on rough alluvial beds measured using in-grain accelerometers, Earth Surf. Dyn., 8, 1067–1099, https://doi.org/10.5194/esurf-8-1067-2020, 2020.

Maue, A. D., Levy, J. S., Burr, D. M., Matulka, P. R., and Nathan, E.: Rapid rounding of icy clasts during simulated fluvial transport in the Titan Tumbler, Icarus, 375, 114831, https://doi.org/10.1016/j.icarus.2021.114831, 2022.

McCallister, W. O. and Hung, C.-C.: Image segmentation using dynamic run-length coding technique, in: Proceedings of the 13th Scandinavian conference on Image analysis, Berlin, Heidelberg, 343–348, 2003.

McClain, M. E., Kashaigili, J. J., and Ndomba, P.: Environmental flow assessment as a tool for achieving environmental objectives of African water policy, with examples from East Africa, Int. J. Water Resour. Dev., 29, 650–665, https://doi.org/10.1080/07900627.2013.781913, 2013.

Menditto, A., Patriarca, M., and Magnusson, B.: Understanding the meaning of accuracy, trueness and precision, Accreditation Qual. Assur., 12, 45–47, https://doi.org/10.1007/s00769-006-0191-z, 2007.

Meyer-Peter, E. and Müller, R.: Formulas for bed-load transport, Rep 2nd Meet Int Assoc Hydraul Struct Res, 39–64, 1948.

Miazza, R., Pascal, I., and Ancey, C.: Automated grain sizing from uncrewed aerial vehicles imagery of a gravel-bed river: Benchmarking of three object-based methods, Earth Surf. Process. Landf., 49, 1503–1514, https://doi.org/10.1002/esp.5782, 2024.

Montenegro Ríos, A., Sarocchi, D., Nahmad-Molinari, Y., and Borselli, L.: Form From Projected Shadow (FFPS): An algorithm for 3D shape analysis of sedimentary particles, Comput. Geosci., 60, 98–108, https://doi.org/10.1016/j.cageo.2013.07.008, 2013.

Mörtl, C., Baratier, A., Berthet, J., Duvillard, P.-A., and De Cesare, G.: GALET: A deep learning image segmentation model for drone-based grain size analysis of gravel bars, in: Proceedings of the 39th IAHR World Congress, Proceedings of the 39th IAHR World Congress From Snow to Sea, 5326–5335, https://doi.org/10.3850/IAHR-39WC252171192022895, 2022.

Nguyen, M. T., Sebesvari, Z., Souvignet, M., Bachofer, F., Braun, A., Garschagen, M., Schinkel, U., Yang, L. E., Nguyen, L. H. K., Hochschild, V., Assmann, A., and Hagenlocher, M.: Understanding and assessing flood risk in Vietnam: Current status, persisting gaps, and future directions, J. Flood Risk Manag., 14, e12689, https://doi.org/10.1111/jfr3.12689, 2021.

Nicholas, A. P. and Quine, T. A.: Quantitative assessment of landform equifinality and palaeoenvironmental reconstruction using geomorphic models, Geomorphology, 121, 167–183, https://doi.org/10.1016/j.geomorph.2010.04.004, 2010.

Niu, B., Qu, J., Zhang, X. (John), Liu, B., Tan, L., and An, Z.: Quantifying provenance of reservoir sediment using multiple composite fingerprints in an arid region experiencing both wind and water erosion, Geomorphology, 332, 112–121, https://doi.org/10.1016/j.geomorph.2019.02.011, 2019.

Novák-Szabó, T., Sipos, A. Á., Shaw, S., Bertoni, D., Pozzebon, A., Grottoli, E., Sarti, G., Ciavola, P., Domokos, G., and Jerolmack, D. J.: Universal characteristics of particle shape evolution by bed-load chipping, Sci. Adv., 4, eaao4946, https://doi.org/10.1126/sciadv.aao4946, 2018.

Pacific Institute: Water Conflict – World Water, Water Confl. Chronol., 2024.

Pähtz, T., Clark, A. H., Valyrakis, M., and Durán, O.: The Physics of Sediment Transport Initiation, Cessation, and Entrainment Across Aeolian and Fluvial Environments, Rev. Geophys., 58, e2019RG000679, https://doi.org/10.1029/2019RG000679, 2020.

Pál, G., Domokos, G., and Kun, F.: Curvature flows, scaling laws and the geometry of attrition under impacts, Sci. Rep., 11, 20661, https://doi.org/10.1038/s41598-021-00030-1, 2021.

Parker Gary: Selective Sorting and Abrasion of River Gravel. I: Theory, J. Hydraul. Eng., 117, 131–147, https://doi.org/10.1061/(ASCE)0733-9429(1991)117:2(131), 1991.

Pfeiffer, A. M., Morey, S., Karlsson, H. M., Fordham, E. M., and Montgomery, D. R.: Survival of the Strong and Dense: Field Evidence for Rapid, Transport-Dependent Bed Material Abrasion of Heterogeneous Source Lithology, J. Geophys. Res. Earth Surf., 127, e2021JF006455, https://doi.org/10.1029/2021JF006455, 2022.

Phillips, J. D.: Evolutionary geomorphology: thresholds and nonlinearity in landform response to environmental change, Hydrol Earth Syst Sci, 10, 731–742, https://doi.org/10.5194/hess-10-731-2006, 2006.

Pierce, J. K., Hassan, M. A., and Ferreira, R. M. L.: Probabilistic description of bedload fluxes from the aggregate dynamics of individual grains, Earth Surf. Dyn., 10, 817–832, https://doi.org/10.5194/esurf-10-817-2022, 2022.

Pokhrel, P., Attal, M., Sinclair, H. D., Mudd, S. M., and Naylor, M.: Downstream rounding rate of pebbles in the Himalaya, Earth Surf. Dyn., 12, 515–536, https://doi.org/10.5194/esurf-12-515-2024, 2024.

Quick, L., Sinclair, H. D., Attal, M., and Singh, V.: Conglomerate recycling in the Himalayan foreland basin: Implications for grain size and provenance, GSA Bull., 132, 1639–1656, https://doi.org/10.1130/B35334.1, 2019.

Recking, A.: A comparison between flume and field bed load transport data and consequences for surface-based bed load transport prediction, Water Resour. Res., 46, https://doi.org/10.1029/2009WR008007, 2010.

Recking, A.: An analysis of nonlinearity effects on bed load transport prediction, J. Geophys. Res. Earth Surf., 118, 1264–1281, https://doi.org/10.1002/jgrf.20090, 2013.

Rhoads, B. L.: The natural and human structuring of rivers and other geomorphological systems: A tribute to William L. Graf, Geomorphology, 252, 1–4, https://doi.org/10.1016/j.geomorph.2015.08.016, 2016.

Rickenmann, D.: Bed-Load Transport Measurements with Geophones and Other Passive Acoustic Methods, J. Hydraul. Eng., 143, 03117004, https://doi.org/10.1061/(ASCE)HY.1943-7900.0001300, 2017.

Ross, W. D.: The Works of Aristotle, Oxford, UK, 1913.

Roussillon, T., Piégay, H., Sivignon, I., Tougne, L., and Lavigne, F.: Automatic computation of pebble roundness using digital imagery and discrete geometry, Comput. Geosci., 35, 1992–2000, https://doi.org/10.1016/j.cageo.2009.01.013, 2009.

Saltelli, A., Tarantola, S., Campolongo, F., and Ratto, M.: Sensitivity Analysis in Practice: A Guide to Assessing Scientific Models, 1st ed., Wiley, https://doi.org/10.1002/0470870958, 2002.

Schleiss, A. J., Franca, M. J., Juez, C., and Cesare, G. D.: Reservoir sedimentation, J. Hydraul. Res., 54, 595–614, https://doi.org/10.1080/00221686.2016.1225320, 2016.

Schmidt, K.-H. and Ergenzinger, P.: Bedload entrainment, travel lengths, step lengths, rest periods—studied with passive (iron, magnetic) and active (radio) tracer techniques, Earth Surf. Process. Landf., 17, 147–165, https://doi.org/10.1002/esp.3290170204, 1992.

Schmitt, R. J. P., Bizzi, S., and Castelletti, A.: Tracking multiple sediment cascades at the river network scale identifies controls and emerging patterns of sediment connectivity, Water Resour. Res., 52, 3941–3965, https://doi.org/10.1002/2015WR018097, 2016.

Schmitt, R. J. P., Morgenroth, E., and Larsen, T. A.: Robust planning of sanitation services in urban informal settlements: An analytical framework, Water Res., 110, 297–312, https://doi.org/10.1016/j.watres.2016.12.007, 2017.

Schmitt, R. J. P., Bizzi, S., Castelletti, A., and Kondolf, G. M.: Improved trade-offs of hydropower and sand connectivity by strategic dam planning in the Mekong, Nat. Sustain., 1, 96–104, https://doi.org/10.1038/s41893-018-0022-3, 2018a.

Schmitt, R. J. P., Bizzi, S., Castelletti, A. F., and Kondolf, G. M.: Stochastic Modeling of Sediment Connectivity for Reconstructing Sand Fluxes and Origins in the Unmonitored Se Kong, Se San, and Sre Pok Tributaries of the Mekong River: Stochastic connectivity modelling, J. Geophys. Res. Earth Surf., 123, 2–25, https://doi.org/10.1002/2016JF004105, 2018b.

Schmitt, R. J. P., Bizzi, S., Castelletti, A., Opperman, J. J., and Kondolf, G. M.: Planning dam portfolios for low sediment trapping shows limits for sustainable hydropower in the Mekong, Sci. Adv., 5, eaaw2175, https://doi.org/10.1126/sciadv.aaw2175, 2019.

Schneider, J. M., Rickenmann, D., Turowski, J. M., Schmid, B., and Kirchner, J. W.: Bed load transport in a very steep mountain stream (Riedbach, Switzerland): Measurement and prediction, Water Resour. Res., 52, 9522–9541, https://doi.org/10.1002/2016WR019308, 2016.

Schumm, S.: Geomorphic Thresholds: The Concept and Its Applications, Trans. Inst. Br. Geogr., 4, 485, https://doi.org/10.2307/622211, 1979.

Schumm, S. A. and Stevens, M. A.: Abrasion in Place: A Mechanism for Rounding and Size Reduction of Coarse Sediments in Rivers, Geology, 1, 37–40, https://doi.org/10.1130/0091-7613(1973)1%253C37:AIPAMF%253E2.0.CO;2, 1973.

Scorpio, V. and Piégay, H.: Is afforestation a driver of change in italian rivers within the Anthropocene era?, CATENA, 105031, https://doi.org/10.1016/j.catena.2020.105031, 2020.

Seal, R. and Paola, C.: Observations of Downstream Fining on the North Fork Toutle River Near Mount St. Helens, Washington, Water Resour. Res., 31, 1409–1419, https://doi.org/10.1029/94WR02976, 1995.

Shields, A.: Application of similarity principles and turbulence research to bed-load movement, PhD Thesis, Berlin, Germany, 1936.

Shrestha, B., Giri, S., Cattapan, A., and Franca, M. J.: Morphological Impact of Bridge Construction on Sunsari Morang Irrigation Intake, in: Proceedings of the 22nd IAHR-APD Congress 2020, Sapporo, Japan, IAHR-APD, Sapporo, Japan, 7, 2020.

Shrestha, J. P., Pahlow, M., and Cochrane, T. A.: Managing reservoir sedimentation through coordinated operation of a transboundary system of reservoirs in the Mekong, J. Hydrol., 610, 127930, https://doi.org/10.1016/j.jhydrol.2022.127930, 2022.

Sipos, A. A., Domokos, G., and Török, J.: Particle size dynamics in abrading pebble populations, Earth Surf. Dyn. Discuss., 1–21, https://doi.org/10.5194/esurf-2020-84, 2020.

Sklar, L. S., Riebe, C. S., Marshall, J. A., Genetti, J., Leclere, S., Lukens, C. L., and Merces, V.: The problem of predicting the size distribution of sediment supplied by hillslopes to rivers, Geomorphology, https://doi.org/10.1016/j.geomorph.2016.05.005, 2016.

Sobel, I.: An Isotropic 3x3 Image Gradient Operator, in: Presentation at Stanford A.I. Project 1968, 2014.

Steer, P., Guerit, L., Lague, D., Crave, A., and Gourdon, A.: Size, shape and orientation matter: fast and automatic measurement of grain geometries from 3D point clouds, EGUsphere, 1–31, https://doi.org/10.5194/egusphere-2022-75, 2022.

Sun, Q., Zheng, J., and Li, C.: Improved watershed analysis for segmenting contacting particles of coarse granular soils in volumetric images, Powder Technol., 356, 295–303, https://doi.org/10.1016/j.powtec.2019.08.028, 2019.

Surian, N.: Downstream variation in grain size along an Alpine river: analysis of controls and processes, Geomorphology, 43, 137–149, https://doi.org/10.1016/S0169-555X(01)00127-1, 2002.

Szabó, T., Fityus, S., and Domokos, G.: Abrasion model of downstream changes in grain shape and size along the Williams River, Australia, J. Geophys. Res. Earth Surf., 118, 2013JF002723, https://doi.org/10.1002/jgrf.20142, 2013.

Szabó, T., Domokos, G., Grotzinger, J. P., and Jerolmack, D. J.: Reconstructing the transport history of pebbles on Mars, Nat. Commun., 6, 8366, https://doi.org/10.1038/ncomms9366, 2015.

Takahashi, N. O., Ishimura, D., Yamada, K., Ohta, R. J., Arai, Y., and Yamane, Y.: Shape evolution of bulk sediment in headwater streams: effects of rock type and particle size, Earth Surf. Dyn., 13, 959–980, https://doi.org/10.5194/esurf-13-959-2025, 2025a.

Takahashi, N. O., Ishimura, D., Yamada, K., Ohta, R. J., Arai, Y., and Yamane, Y.: Three-stage evolution of particle shape in headwater streams, EGUsphere, 1–33, https://doi.org/10.5194/egusphere-2025-1080, 2025b.

Tangi, M.: Dynamic Sediment Connectivity Modelling for Strategic River Basin Planning, in: Special Topics in Information Technology, edited by: Riva, C. G., Springer International Publishing, Cham, 27–37, https://doi.org/10.1007/978-3-031-15374-7_3, 2023.

Tangi, M., Bizzi, S., Schmitt, R., and Castelletti, A.: Balancing Sediment Connectivity and Energy Production via Optimized Reservoir Sediment Management Strategies, Water Resour. Res., 59, e2022WR034033, https://doi.org/10.1029/2022WR034033, 2023.

Tarolli, P. and Sofia, G.: Human topographic signatures and derived geomorphic processes across landscapes, Geomorphology, 255, 140–161, https://doi.org/10.1016/j.geomorph.2015.12.007, 2016.

Tunwal, M. and Lim, A.: A Low-Cost, Repeatable Method for 3D Particle Analysis with SfM Photogrammetry, Geosciences, 13, 190, https://doi.org/10.3390/geosciences13070190, 2023.

Tunwal, M., Mulchrone, K. F., and Meere, P. A.: Image based Particle Shape Analysis Toolbox (IPSAT), Comput. Geosci., 135, 104391, https://doi.org/10.1016/j.cageo.2019.104391, 2020.

Turowski, J. M., Böckli, M., Rickenmann, D., and Beer, A. R.: Field measurements of the energy delivered to the channel bed by moving bed load and links to bedrock erosion,

J. Geophys. Res. Earth Surf., 118, 2438–2450, https://doi.org/10.1002/2013JF002765, 2013.

Turowski, J. M., Pruß, G., Voigtländer, A., Ludwig, A., Landgraf, A., Kober, F., and Bonnelye, A.: Geotechnical controls on erodibility in fluvial impact erosion, EGUsphere, 1–31, https://doi.org/10.5194/egusphere-2023-76, 2023.

van Rijn Leo C.: Sediment Transport, Part I: Bed Load Transport, J. Hydraul. Eng., 110, 1431–1456, https://doi.org/10.1061/(ASCE)0733-9429(1984)110:10(1431), 1984.

Vangla, P., Roy, N., and Gali, M. L.: Image based shape characterization of granular materials and its effect on kinematics of particle motion, Granul. Matter, 20, 6, https://doi.org/10.1007/s10035-017-0776-8, 2017.

Viollet, P.-L.: Water Engineering in Ancient Civilizations: 5,000 Years of History, CRC Press, London, 334 pp., https://doi.org/10.1201/b13113, 2017.

Wadell, H.: Volume, Shape, and Roundness of Rock Particles, J. Geol., 40, 443–451, https://doi.org/10.1086/623964, 1932.

Walling, D. E.: The evolution of sediment source fingerprinting investigations in fluvial systems, J. Soils Sediments, 13, 1658–1675, https://doi.org/10.1007/s11368-013-0767-2, 2013.

Wang, Y., Liang, X., Flener, C., Kukko, A., Kaartinen, H., Kurkela, M., Vaaja, M., Hyyppä, H., and Alho, P.: 3D Modeling of Coarse Fluvial Sediments Based on Mobile Laser Scanning Data, Remote Sens., 5, 4571–4592, https://doi.org/10.3390/rs5094571, 2013.

Warrick, J. A., Rubin, D. M., Ruggiero, P., Harney, J. N., Draut, A. E., and Buscombe, D.: Cobble cam: grain-size measurements of sand to boulder from digital photographs and autocorrelation analyses, Earth Surf. Process. Landf., 34, 1811–1821, https://doi.org/10.1002/esp.1877, 2009.

Wentworth, C. K.: A Laboratory and Field Study of Cobble Abrasion, J. Geol., 27, 507–521, 1919.

van Westen, B., de Schipper, M. A., Pearson, S. G., and Luijendijk, A. P.: Lagrangian modelling reveals sediment pathways at evolving coasts, Sci. Rep., 15, 8793, https://doi.org/10.1038/s41598-025-92910-z, 2025.

Wheeler, K. G., Hall, J. W., Abdo, G. M., Dadson, S. J., Kasprzyk, J. R., Smith, R., and Zagona, E. A.: Exploring Cooperative Transboundary River Management Strategies for

the Eastern Nile Basin, Water Resour. Res., 54, 9224–9254, https://doi.org/10.1029/2017WR022149, 2018.

Williamson, J. E., Jr, A. E. H., Stamm, J. F., Valder, J. F., and Prautzch, V. L.: Fluvial sediment fingerprinting: literature review and annotated bibliography, Open-File Report, U.S. Geological Survey, https://doi.org/10.3133/ofr20141216, 2014.

Woodget, A. S. and Austrums, R.: Subaerial gravel size measurement using topographic data derived from a UAV-SfM approach, Earth Surf. Process. Landf., 42, 1434–1443, https://doi.org/10.1002/esp.4139, 2017.

Wyss, C. R., Rickenmann, D., Fritschi, B., Turowski, J. M., Weitbrecht, V., and Boes, R. M.: Measuring Bed Load Transport Rates by Grain-Size Fraction Using the Swiss Plate Geophone Signal at the Erlenbach, J. Hydraul. Eng., 142, 04016003, https://doi.org/10.1061/(ASCE)HY.1943-7900.0001090, 2016.

Xu, Z., Belmont, P., Brahney, J., and Gellis, A. C.: Sediment source fingerprinting as an aid to large-scale landscape conservation and restoration: A review for the Mississippi River Basin, J. Environ. Manage., 324, 116260, https://doi.org/10.1016/j.jenvman.2022.116260, 2022.

Yager, E. M., Schmeeckle, M. W., and Badoux, A.: Resistance Is Not Futile: Grain Resistance Controls on Observed Critical Shields Stress Variations, J. Geophys. Res. Earth Surf., 123, 3308–3322, https://doi.org/10.1029/2018JF004817, 2018.

Yashima, S., Kanda, Y., and Sano, S.: Relationships between particle size and fracture energy or impact velocity required to fracture as estimated from single particle crushing, Powder Technol., 51, 277–282, https://doi.org/10.1016/0032-5910(87)80030-X, 1987.

Zheng, J. and Hryciw, R. D.: Traditional soil particle sphericity, roundness and surface roughness by computational geometry, Géotechnique, 65, 494–506, https://doi.org/10.1680/geot.14.P.192, 2015.

Zheng, J. and Hryciw, R. D.: Segmentation of contacting soil particles in images by modified watershed analysis, Comput. Geotech., 73, 142–152, https://doi.org/10.1016/j.compgeo.2015.11.025, 2016.

LIST OF TABLES

LIST OF FIGURES

ABOUT THE AUTHOR

Alessandro holds a bachelor's and a master's degree from the University of Padova, Italy. He is working as a lecturer in river engineering at IHE Delft in the Netherlands since 2014. His research interests include transport processes on networks and the study of rivers as dynamical systems.

Before joining IHE Delft, he worked in the design of hydropower plants. He has worked on several river engineering studies, focusing on the interactions between water infrastructures and natural systems.

The current thesis represents an attempt to identify a measurable variable that could help improve the understanding of sediment transport along river networks.

Journals publications

Magaju, D., Cattapan, A., Franca, M. (2020). Identification of run-of-river hydropower investments in data scarce regions using global data. *Energy for Sustainable Development*, *58*, 30–41. https://doi.org/10.1016/j.esd.2020.07.001

Cattapan, A., Gurini, A., Paron, P., Ballio, F., Franca, M. J. (2024). A method for segmentation of pebble images in the presence of shadows. *Earth Surface Processes and Landforms*, *49*(15), 5202–5212. https://doi.org/10.1002/esp.6027

Ahmed, G., Cattapan, A., Omer, A., Mohamed, Y. (2025). A hybrid approach to evaluate sedimentation in large dams: case study of the Grand Ethiopian Renaissance Dam and Roseires Dam across the Blue Nile. *Journal of Hydrology: Regional Studies*, *60*, 102585. https://doi.org/10.1016/j.ejrh.2025.102585

Trust, B., Katsanou, K., Cattapan, A., Venneker, R., Batsatsashvili, M., Bol, R., Wenninger, J. (2025). Quantifying Groundwater Contributions To Streamflow Using a Multi-method Hydrological Approach. *Environmental Processes*, *12*(2), 21. https://doi.org/10.1007/s40710-025-00764-4

Conference proceedings

Cattapan, A., Khan, U. A., Franca, M. J. (2018). Sediment connectivity in the Piave River basin: effects of reservoirs on long-term sediment transport dynamics. In *EGU General Assembly Conference Abstracts*. Vienna, Austria.

Cattapan, A., Paron, P., Franca, M. J. (2018). Deriving Grain Size Distributions from UAVs Images. In *The Future River* (Vol. 42, pp. 90-91). Delft, The Netherlands.

Khan, U. A., Cattapan, A., Franca, M. J. (2018). Analysis of sediment transport dynamics in the Piave River Basin to define hotspots of geomorphic change. In *The Future River* (Vol. 42, pp. 42–43). Delft, The Netherlands.

Cattapan, A., Paron, P., McClain, M., Franca, M. (2019). Estimating sediment travel distances in Alpine catchments through UAV-based sediment shape indices. In *Book of abstracts: Land of Rivers* (Vol. NCR publication 43-2019). Utrecht, The Netherlands.

Cattapan, A., Paron, P., McClain, M. E. (2019). On the correlation between sediment shape indices and distance travelled in Alpine catchments, a UAV-based analysis. In *Geophysical Research Abstracts* (Vol. 21). Vienna, Austria.

Cattapan, A., Paron, P., McClain, M. E., Piégay, H., Franca, M. J. (2020). Contribution on understanding sediment alteration in an Alpine catchment; lithology matters! In *River Flow 2020: Proceedings of the 10th Conference on Fluvial Hydraulics* (pp. 1741–1748). CRC Press / Balkema.

Shrestha, B., Giri, S., Cattapan, A., Franca, M. J. (2020). Morphological Impact of Bridge Construction on Sunsari Morang Irrigation Intake. In *Proceedings of the 22nd IAHR-APD Congress 2020, Sapporo, Japan* (p. 7). Sapporo, Japan.

Abi Aad, Zeina, Duro, G., Cattapan, A., Crosato, A. (2022). Geul River flooding reproduced with a Delft3D depth-averaged model. In NCR Days 2022. Delft, The Netherlands: NCR Publication.

Illangasingha, S., Cattapan, A., Franca, M. (2023). Prioritization of minor hydraulic structures for flood management in the Lower Limpopo river basin, Mozambique. In *The 9th International Conference on Flood Management (ICFM9)* (Vol. Publication No. 44, p. 164). Tsukuba, Japan: ICHARM.

Katsanou, K., Batsatsashvili, M., Cattapan, A., Venneker, R., Pütz, T., Bogena, H., Wenninger, J. (2023, September). *Seasonal and spatial variations of physicochemical parameters in headwater catchments to define groundwater input - Wüstebach Catchment, Germany*. Conference presentation presented at the TERENO-OZCAR International Conference 2023, Bonn, Germany.

Cattapan, A., McClain, M., Paron, P., Franca, M. J. (2024). Linking coarse sediment morphometry and transport: Insights from field data and curvature flow attrition. In *River Flow 2024*. Liverpool, UK: CRC Press.

Katsanou, K., Cattapan, A., Venneker, R., Bol, R., Wenninger, J. (2025). *Can high-resolution monitoring provide a better understanding of the hyporheic zone in Groundwater Dependent Ecosystems?* In ARPHA Conference Abstracts (Vol. 8, p. e155243).

Cattapan A, Vis G, Katsanou K, Venneker R, Bol R, Wenninger J (2026). *Filtering and Analysing Distributed Temperature Sensing Data: lessons learnt from the Wüstebach headwater stream, Germany.* EGU 2026. May 3-8, 2026. Vienna, Austria.

Netherlands Research School for the
Socio-Economic and Natural Sciences of the Environment

D I P L O M A

for specialised PhD training

The Netherlands research school for the
Socio-Economic and Natural Sciences of the Environment
(SENSE) declares that

Alessandro Cattapan

born on 17 January 1983 in Belluno, Italy

has successfully fulfilled all requirements of the
educational PhD programme of SENSE.

Delft,30 April 2026

SENSE coordinator PhD education

Dr Ir Peter Vermeulen

The SENSE Director

Dr Jampel Dell'Angelo

The SENSE Research School declares that **Alessandro Cattapan** has successfully fulfilled all requirements of the educational PhD programme of SENSE with a workload of 40.6 EC, including the following activities:

SENSE PhD Courses

- A2 Research in context activity: 'Co-organizing IHE PhD Symposium (1-2 October 2018) and preparing future research proposal following up on PhD research" (2018)

Other PhD and Advanced MSc Courses

Sustainability of Water Reservoirs: from an exhaustible into a renewable resource, IHE Delft (2018)

- Fluvial Biogeomorphology Summer School, Universitá di Trento (2025)
- Introduction to Programming with MATLAB, Coursera (2025)
- Mastering Programming with MATLAB, Coursera (2025)

Management and Organisational activities

- Coordination of the Hydraulic Engineering and River Basin Development specialization within the WSE department (2014-2025)

Teaching and supervision

- Supervision of six MSc student with thesis (2018-2019)
- Academic Coaching Training for the Coaches in IHE W&SD (2020)
- PhD supervision course (2025)

Oral Presentations

- *On the correlation between sediment shape indices and distance travelled in Alpine catchments, a UAV based analysis.* EGU 2019, 7-12 April 2019, Vienna, Austria
- *On the evolution of sediment shape indices along the river network of an Alpine catchment.* IHE PhD Symposium, 10-11 October 2019, Delft, The Netherlands
- *Contribution on understanding sediment degradation in an Alpine catchment; lithology matters!,* Regionalized Fluvial Geomorphology Workshop Lyon 2019, 18-19/12/2019 2019, Lyon, France
- *Contribution on understanding sediment degradation in an Alpine catchment; lithology matters!* River Flow 2020, 6-10/7/2020 2020, Online, Online

IHE DELFT
Institute for Water Education
under the auspices of UNESCO

TU Delft Delft University of Technology

This work is motivated by a simple yet profound curiosity: the desire to pick up a stone from a riverbed and tell how far it has travelled, just by examining its shape. Addressing this overarching question, three main contributions are provided. First, a new image segmentation algorithm is developed to extract the outline of pebbles from photographs collected in the field, even in challenging lighting conditions, with shadows. This enables the reliable collection of sediment shape data directly from natural environments. Secondly, a physically based model is introduced to estimate the evolution of sediment shape along river courses. The model takes into account the natural variability of fragment shapes originating from outcrops of specific lithologies, which were monitored and analyzed for the first time. The third contribution involves the estimation of travel distances based on sediment shape. A direct method is presented, and its accuracy and precision are discussed, alongside a probabilistic method, based on a Bayesian framework, providing the opportunity to include multiple information sources in the estimates of travel distances.

This book is printed on paper from sustainably managed forests and controlled sources

9 789073 445826